ANL-NSE-3

METALLIC FUELS HANDBOOK

Nuclear Science and Engineering Division

DOES NOT CONTAIN OFFICIAL USE ONLY INFORMATION

About Argonne National Laboratory
Argonne is a U.S. Department of Energy laboratory managed by UChicago Argonne, LLC under contract DE-AC02-06CH11357. The Laboratory's main facility is outside Chicago, at 9700 South Cass Avenue, Argonne, Illinois 60439. For information about Argonne and its pioneering science and technology programs, see www.anl.gov.

DOCUMENT AVAILABILITY

Online Access: U.S. Department of Energy (DOE) reports produced after 1991 and a growing number of pre-1991 documents are available free via DOE's SciTech Connect (http://www.osti.gov/scitech/)

Reports not in digital format may be purchased by the public from the National Technical Information Service (NTIS):
U.S. Department of Commerce
National Technical Information Service
5301 Shawnee Rd
Alexandria, VA 22312
www.ntis.gov
Phone: (800) 553-NTIS (6847) or (703) 605-6000
Fax: (703) 605-6900
Email: **orders@ntis.gov**

Reports not in digital format are available to DOE and DOE contractors from the Office of Scientific and Technical Information (OSTI):
U.S. Department of Energy
Office of Scientific and Technical Information
P.O. Box 62
Oak Ridge, TN 37831-0062
www.osti.gov
Phone: (865) 576-8401
Fax: (865) 576-5728
Email: **reports@osti.gov**

Disclaimer
This report was prepared as an account of work sponsored by CRADA No. 1201201. Neither the United States Government nor any agency thereof, nor UChicago Argonne, LLC, nor any of their employees or officers, makes any warranty, express or implied, or assumes any legal liability or responsibility for the accuracy, completeness, or usefulness of any information, apparatus, product, or process disclosed, or represents that its use would not infringe privately owned rights. Reference herein to any specific commercial product, process, or service by trade name, trademark, manufacturer, or otherwise, does not necessarily constitute or imply its endorsement, recommendation, or favoring by the United States Government or any agency thereof. The views and opinions of document authors expressed herein do not necessarily state or reflect those of the United States Government or any agency thereof, Argonne National Laboratory, or UChicago Argonne, LLC.

ANL-NSE-3

METALLIC FUELS HANDBOOK

Compiled by
G. L. Hofman[1], M. C. Billone[2], J. F. Koenig[1], J. M. Kramer[3], J. D. B. Lambert[1],
L. Leibowitz[4], Y. Orechwa[5], D. R. Pedersen[3], D. L. Porter[1], H. Tsai[2], and A. E. Wright[3]

[1] EBR-II Division, Argonne National Laboratory
[2]Materials and Components Technology Division, Argonne National Laboratory
[3]Reactor Analysis and Safety Division, Argonne National Laboratory
[4]Chemical Technology Division, Argonne National Laboratory
[5]Engineering Physics Division, Argonne National Laboratory

April 28, 1989 (Compilation)
April 10, 2019 (Publication)

PREFACE

This compilation of thermophyical and mechanical properties of certain metallic fuels is meant to be used as a common source of data in work related to the Integral Fast Reactor. Because research on these properties is an ongoing effort, this handbook must be continuously updated in order to provide the best data set to all involved in the IFR program. The use of common source of properties will facilitate comparison of various analyses of fuel behavior performed within the program. It also will facilitate uncovering gaps and weaknesses in the data base, and thus enable better direction for future work on experimental properties work.

This handbook focuses on the two fuel compositions chosen for the IFR, namely, uranium-zirconium and uranium-plutonium-zirconium.

Because of the paucity of data in some areas on these specific alloys, data on the elements as well as related alloys are presented to aid the user in estimating property values that are not available.

The selection of properties to be included in the handbook was based on a survey of all IFR participants.

The Properties Evaluation Working Group will consider any requests for inclusion of additional properties, and solicits critiques of the present work as well as submittal of additional data that the user may encounter.

IFR Property Evaluation Working Group

Chairman: G. L. Hofman, EBR-II
Members: M. C. Billone, MCT
J. F. Koenig, EBR-II
J. M. Kramer, RAS
J.D.B. Lambert, EBR-II
L. Leibowitz, CT
Y. Orechwa, EP
D. R. Pedersen, RAS
D. L. Porter, EBR-II
H. Tsai, MCT
A. E. Wright, RAS

Metallic Fuels Handbook Coordinator: N. J. Picker
Text Processing: J. E. Ramos and C. F. Walton

CONTENTS

CONTENTS (cont'd)

LIST OF FIGURES

LIST OF FIGURES (cont'd)

Fig. No. Title Page

Section B.2.3 - Others

Section B.3.1 - Uranium-Zirconium Alloys

Section B.3.2 - Uranium-Plutonium-Zirconium Alloys

Section B.3.3 - Others

Section C.1.1 - Uranium-Zirconium Alloys

LIST OF FIGURES (cont'd)

LIST OF FIGURES (cont'd)

Fig. No. Title Page

Section D.1.1 - Uranium-Zirconium Alloys

Section D.2.3 - Others

Section E.1.1 - Mechanical Properties

Section E.1.2 - Physical Properties

LIST OF FIGURES (cont'd)

LIST OF TABLES

Section A

Section B.1.1 - Uranium-Zirconium Alloys

Section B.1.2 - Uranium-Plutonium-Zirconium Alloys

LIST OF TABLES (cont'd)

No. Title Page

Section B.1.3 - Others

Section B.2.3 - Others

Section B.3.1 - Uranium-Zirconium Alloys

Section B.3.2 - Uranium-Plutonium-Zirconium Alloys

LIST OF TABLES (cont'd)

Section B.3.3 - Others

Section C.1.1 - Uranium-Zirconium Alloys

Section C.1.2 - Uranium-Plutonium-Zirconium Alloys

Section C.1.3 - Others

Section C.3.1 - Uranium-Zirconium Alloys

LIST OF TABLES (cont'd)

CONVERSION FACTORS FOR THE U.S. CUSTOMARY SYSTEM, METRIC SYSTEM, AND INTERNATIONAL SYSTEM

A. UNITS OF LENGTH

Units	cm	m	in.	ft	yd	mile
1 cm	= 1	0.01*	0.3937008	0.03280840	0.01093613	6.213712×10^{-6}
1 m	= 100.	1	39.37008	3.280840	1.093613	6.213712×10^{-4}
1 in.	= 2.54*	0.0254	1	0.08333333...	0.02777777...	1.578283×10^{-5}
1 ft	= 30.48	0.3048	12.*	1	0.3333333...	1.893939×10^{-4}
1 yd	= 91.44	0.9144	36.	3.*	1	5.681818×10^{-4}
1 mile	= 1.609344×10^{5}	1.609344×10^{3}	6.336×10^{4}	5280.*	1760.	1

B. UNITS OF AREA

Units	cm^2	m^2	$in.^2$	ft^2	yd^2	$mile^2$
1 cm^2	= 1	10^{-4}*	0.1550003	1.076391×10^{-3}	1.195990×10^{-4}	3.861022×10^{-11}
1 m^2	= 10^{4}	1	1550.003	10.76391	1.195990	3.861022×10^{-7}
1 $in.^2$	= 6.4516*	6.4516×10^{-4}	1	6.944444×10^{-3}	7.716049×10^{-4}	2.490977×10^{-10}
1 ft^2	= 929.0304	0.09290304	144.*	1	0.1111111...	3.587007×10^{-8}
1 yd^2	= 8361.273	0.8361273	1296.	9.*	1	3.228306×10^{-7}
1 $mile^2$	= 2.589988×10^{10}	2.589988×10^{6}	4.014490×10^{9}	2.78784×10^{7}*	3.0976×10^{6}	1

C. UNITS OF VOLUME

Units	cm^3	liter	$in.^3$	ft^3	qt	gal
1 cm^3	= 1	10^{-3}	0.06102374	3.531467×10^{-5}	1.056688×10^{-3}	2.641721×10^{-4}
1 liter	= 1000.*	1	61.02374	0.03531467	1.056688	0.2641721
1 $in.^3$	= 16.38706*	0.01638706	1	5.787037×10^{-4}	0.01731602	4.329004×10^{-3}
1 ft^3	= 28316.85	28.31685	1728.*	1	2.992208	7.480520
1 qt	= 946.353	0.946353	57.75	0.0342014	1	0.25
1 gal (U.S.)	= 3785.412	3.785412	231.*	0.1336806	4.*	1

CONVERSION FACTORS FOR THE U.S. CUSTOMARY SYSTEM, METRIC SYSTEM, AND INTERNATIONAL SYSTEM (contd)

D. UNITS OF MASS

Units	g	kg	oz	lb	metric ton	ton
1 g	= 1	10^{-3}	0.03527396	2.204623×10^{-3}	10^{-6}	1.102311×10^{-6}
1 kg	= 1000.	1	35.27396	2.204623	10^{-3}	1.102311×10^{-3}
1 oz (avdp)	= 28.34952	0.02834952	1	0.0625	2.834952×10^{-5}	$5.\times10^{-4}$
1 lb (avdp)	= 453.5924	0.4535924	16.*	1	4.535924×10^{-4}	0.0005
1 metric ton	= 10^{6}	1000.*	35273.96	2204.623	1	1.102311
1 ton	= 907184.7	907.1847	32000.	2000.*	0.9071847	1

E. UNITS OF DENSITY

Units	g cm^{-3}	g $l.^{-1}$	oz $in.^{-3}$	lb $in.^{-3}$	lb ft^{-3}	lb gal^{-1}
1 g cm^{-3}	= 1	1000.	0.5780365	0.03612728	62.42795	8.345403
1 g $l.^{-1}$	= 10^{-3}	1	5.780365×10^{-4}	3.612728×10^{-5}	0.06242795	8.345403×10^{-3}
1 oz $in.^{-3}$	= 1.729994	1729.994	1	0.0625	108.	14.4375
1 lb $in.^{-3}$	= 27.67991	27679.91	16.	1	1728.	231.
1 lb ft^{-3}	= 0.01601847	16.01847	9.259259×10^{-3}	5.7870370×10^{-4}	1	0.1336806
1 lb gal^{-1}	= 0.1198264	119.8264	4.749536×10^{-3}	4.3290043×10^{-3}	7.480519	1

F. UNITS OF PRESSURE

Units	dyn cm^{-2}	bar	atm	kg(wt) cm^{-2}	mmHg (Torr)	in. Hg	lb(wt) $in.^{-2}$
1 dyn cm^{-2}	= 1	10^{-6}	9.869233×10^{-7}	1.019716×10^{-6}	7.500617×10^{-4}	2.952999×10^{-5}	1.450377×10^{-5}
1 bar	= 10^{6*}	1	0.9869233	1.019716	750.0617	29.52999	14.50377
1 atm	= 1013250.*	1.013250	1	1.033227	760.	29.92126	14.69595
1 kg(wt) cm^{-2}	= 980665.	0.980665	0.9678411	1	735.5592	28.95903	14.22334
1 mmHg (Torr)	= 1333.224	1.333224×10^{3}	1.3157895×10^{3}	1.8595099×10^{3}	1	0.03937008	0.01933678
1 in. Hg	= 33863.88	0.03386388	0.03342105	0.03453155	25.4	1	0.4911541
1 lb(wt) $in.^{-2}$	= 68947.57	0.06894757	0.06804596	0.07030696	51.71493	2.036021	1

CONVERSION FACTORS FOR THE U.S. CUSTOMARY SYSTEM,
METRIC SYSTEM, AND INTERNATIONAL SYSTEM (contd)

G. UNITS OF ENERGY

Units	g mass (energy equiv)	J	IntJ	cal	calIT	Btu$_{IT}$	kW hr	hp hr	ft-lb (wt)	cu ft-lb (wt) in.^{2}	1 atm
1 g mass (energy equiv)	=1	8.987554×10^{13}	8.986071×10^{13}	2.148077×10^{13}	2.146640×10^{13}	8.518558×10^{10}	2.496543×10^{7}	3.347919×10^{7}	6.628880×10^{13}	4.603399×10^{11}	8.870026×10^{11}
1J	$=1.112650 \times 10^{14}$	1	0.999835	0.2390057	0.2388459	9.478172×10^{4}	$2.777777... \times 10^{7}$	3.725062	0.7375622	5.121960×10^{3}	9.869233×10^{3}
1 int J	$=1.112833 \times 10^{14}$	1.000165	1	0.2390452	0.2388853	9.479735×10^{4}	2.778236×10^{7}	3.725676×10^{7}	0.7376839	5.122805×10^{3}	9.870862×10^{3}
1 cal	$=4.655327 \times 10^{14}$	4.184	4.183310	1	0.9993312	3.965667×10^{3}	$1.1622222... \times 10^{6}$	1.558562×10^{6}	3.085960	2.143028×10^{2}	0.04129287
1 calIT	$=4.658442 \times 10^{14}$	4.1868	4.186109	1.000669	1	3.968321×10^{3}	1.163000×10^{6}	1.559609×10^{6}	3.088025	2.144462×10^{2}	0.04132050
1 BtuIT	$=1.173908 \times 10^{11}$	1055.056	1054.882	252.1644	251.9958*	1	2.930711×10^{4}	3.930148×10^{4}	778.1693	5.403953	10.41259
1 kW hr	$=4.005539 \times 10^{8}$	3600000.*	3599406.	860420.7	859845.2	3412.142	1	1.341022	2655224.	18439.06	35529.24
1 hp hr	$=2.986930 \times 10^{8}$	2684519.	2684077.	641615.6	641186.5	2544.33	0.7456998	1	1980000.*	13750.	26494.15
1 ft-lb (wt)	$=1.508550 \times 10^{14}$	1.355818	1.355594	0.3240483	0.3238315	1.285067×10^{3}	3.766161×10^{7}	$5.050505... \times 10^{7}$	1	$6.944444.. \times 10^{3}$	0.0133805
1 cu ft-lb (wt) in.^{2}	$=2.172313 \times 10^{12}$	195.2378	195.2056	46.66295	46.63174	0.1850497	5.423272×10^{5}	$7.272727... \times 10^{5}$	144.*	1	1.926847
11 atm	$=1.1127392 \times 10^{12}$	101.3250	101.3083	24.21726	24.20106	0.09603757	2.814583×10^{5}	3.774419×10^{5}	74.73349	0.5189825	1

TEMPERATURES, CELSIUS TO FAHRENHEIT
Conversion Table

The values in the body of this table give, in degrees Fahrenheit, the temperatures indicated in degrees Celsius at the top and side.

1°C = 1.8°F
For temperatures below 0°C

Temp. °C	0	1	2	3	4	5	6	7	8	9
0	+32.0	30.2	28.4	26.6	24.8	23.0	21.2	19.4	17.6	15.8
-10	+14.0	12.2	10.4	8.6	6.8	5.0	3.2	+1.4	-0.4	-2.2
-20	-4.0	5.8	7.6	9.4	11.2	13.0	14.8	16.6	18.4	20.2
-30	-22.0	23.8	25.6	27.4	29.2	31.0	32.8	34.6	36.4	38.2
-40	-40.0	41.8	43.6	45.4	47.2	49.0	50.8	52.6	54.4	56.2
-50	-58.0	59.8	61.6	63.4	65.2	67.0	68.8	70.6	72.4	74.2
-60	-76.0	77.8	79.6	81.4	83.2	85.0	86.8	88.6	90.4	92.2
-70	-94.0	95.8	97.6	99.4	101.2	103.0	104.8	106.6	108.4	110.2
-80	-112.0	113.8	115.6	117.4	119.2	121.0	122.8	124.6	126.4	128.2
-90	-130.0	131.8	133.6	135.4	137.2	139.0	140.8	142.6	144.4	146.2
-100	-148.0	149.8	151.6	153.4	155.2	157.0	158.8	160.6	162.4	164.2
-110	-166.0	167.8	169.6	171.4	173.2	175.0	176.8	178.6	180.4	182.2
-120	-184.0	185.8	187.6	189.4	191.2	193.0	194.8	196.6	198.4	200.2
-130	-202.0	203.8	205.6	207.4	209.2	211.0	212.8	214.6	216.4	218.2
-140	-220.0	221.8	223.6	225.4	227.2	229.0	230.8	232.6	234.4	236.2
-150	-238.0	239.8	241.6	243.4	245.2	247.0	248.8	250.6	252.4	254.2
-160	-256.0	257.8	259.6	261.4	263.2	265.0	266.8	268.6	270.4	272.2
-170	-274.0	275.8	277.6	279.4	281.2	283.0	284.8	286.6	288.4	290.2
-180	-292.0	293.8	295.6	297.4	299.2	301.0	302.8	304.6	306.4	308.2
-190	-310.0	311.8	313.6	315.4	317.2	319.0	320.8	322.6	324.4	326.2
-200	-328.0	329.8	331.6	333.4	335.2	337.0	338.8	340.6	342.4	344.2
-210	-346.0	347.8	349.6	351.4	353.2	355.0	356.8	358.6	360.4	362.2
-220	-364.0	365.8	367.6	369.4	371.2	373.0	374.8	376.6	378.4	380.2
-230	-382.0	383.8	385.6	387.4	389.2	391.0	392.8	394.6	396.4	398.2
-240	-400.0	401.8	403.6	405.4	407.2	409.0	410.8	412.6	414.4	416.2
-250	-418.0	419.8	421.6	423.4	425.2	427.0	428.8	430.6	432.4	434.2
-260	-436.0	437.8	439.6	441.4	443.2	445.0	446.8	448.6	450.4	452.2
-270	-454.0	455.8	457.6	459.4	----	----	----	----	----	----

TEMPERATURES, CELSIUS TO FAHRENHEIT (contd)
For temperatures above 0°C

Temp. °C	0	1	2	3	4	5	6	7	8	9
0	32.0	33.8	35.6	37.4	39.2	41.0	42.8	44.6	46.4	48.2
10	50.0	51.8	53.6	55.4	57.2	59.0	60.8	62.6	64.4	66.2
20	68.0	69.8	71.6	73.4	75.2	77.0	78.8	80.6	82.4	84.2
30	86.0	87.8	89.6	91.4	93.2	95.0	96.8	98.6	100.4	102.2
40	104.0	105.8	107.6	109.4	111.2	113.0	114.8	116.6	118.4	120.2
50	122.0	123.8	125.6	127.4	129.2	131.0	132.8	134.6	136.4	138.2
60	140.0	141.8	143.6	145.4	147.2	149.0	150.8	152.6	154.4	156.2
70	158.0	159.8	161.6	163.4	165.2	167.0	168.8	170.6	172.4	174.2
80	176.0	177.8	179.6	181.4	183.2	185.0	186.8	188.6	190.4	192.2
90	194.0	195.8	197.6	199.4	201.2	203.0	204.8	206.6	208.4	210.2
100	212.0	213.8	215.6	217.4	219.2	221.0	222.8	224.6	226.4	228.2
110	230.0	231.8	233.6	235.4	237.2	239.0	240.8	242.6	244.4	246.2
120	248.0	249.8	251.6	253.4	255.2	257.0	258.8	260.6	262.4	264.2
130	266.0	267.8	269.6	271.4	273.2	275.0	276.8	278.6	280.4	282.2
140	284.0	285.8	287.6	289.4	291.2	293.0	294.8	296.6	298.4	300.2
150	302.0	303.8	305.6	307.4	309.2	311.0	312.8	314.6	316.4	318.2
160	320.0	321.8	323.6	325.4	327.2	329.0	330.8	332.6	334.4	336.2
170	338.0	339.8	341.6	343.4	345.2	347.0	348.8	350.6	352.4	354.2
180	356.0	357.8	359.6	361.4	363.2	365.0	366.8	368.6	370.4	372.2
190	374.0	375.8	377.6	379.4	381.2	383.0	384.8	386.6	388.4	390.2
200	392.0	393.8	395.6	397.4	399.2	401.0	402.8	404.6	406.4	408.2
210	410.0	411.8	413.6	415.4	417.2	419.0	420.8	422.6	424.4	426.2
220	428.0	429.8	431.6	433.4	435.2	437.0	438.8	440.6	442.4	444.2
230	446.0	447.8	449.6	451.4	453.2	455.0	456.8	458.6	460.4	462.2
240	464.0	465.8	467.6	469.4	471.2	473.0	474.8	476.6	478.4	480.2
250	482.0	483.8	485.6	487.4	489.2	491.0	492.8	494.6	496.4	498.2
260	500.0	501.8	503.6	505.4	507.2	509.0	510.8	512.6	514.4	516.2
270	518.0	519.8	521.6	523.4	525.2	527.0	528.8	530.6	532.4	534.2
280	536.0	537.8	539.6	541.4	543.2	545.0	546.8	548.6	550.4	552.2
290	554.0	555.8	557.6	559.4	561.2	563.0	564.8	566.6	568.4	570.2
300	572.0	573.8	575.6	577.4	579.2	581.0	582.8	584.6	586.4	588.2
310	590.0	591.8	593.6	595.4	597.2	599.0	600.8	602.6	604.4	606.2
320	608.0	609.8	611.6	613.4	615.2	617.0	618.8	620.6	622.4	624.2
330	626.0	627.8	629.6	631.4	633.2	635.0	636.8	638.6	640.4	642.2
340	644.0	645.8	647.6	649.4	651.2	653.0	654.8	656.6	658.4	660.2
350	662.0	663.8	665.6	667.4	669.2	671.0	672.8	674.6	676.4	678.2
360	680.0	681.8	683.6	685.4	687.2	689.0	690.8	692.6	694.4	696.2
370	698.0	699.8	701.6	703.4	705.2	707.0	708.8	710.6	712.4	714.2
380	716.0	717.8	719.6	721.4	723.2	725.0	726.8	728.6	730.4	732.2
390	734.0	735.8	737.6	739.4	741.2	743.0	744.8	746.6	748.4	750.2

-273.10°C = -450.72°F = absolute zero

For interpolation										
°C	0.1	0.2	0.3	0.4	0.5	0.6	0.7	0.8	0.9	0.10
°F	0.18	0.36	0.54	0.72	0.90	1.08	1.26	1.44	1.62	1.80

TEMPERATURES, CELSIUS TO FAHRENHEIT (contd)
For temperatures above 0°C.

Temp. °C	0	1	2	3	4	5	6	7	8	9
400	752.0	753.8	755.6	757.4	759.2	761.0	762.8	764.6	766.4	768.2
410	770.0	771.8	773.6	775.4	777.2	779.0	780.8	782.6	784.4	786.2
420	788.0	789.8	791.6	793.4	795.2	797.0	798.8	800.6	802.4	804.2
430	806.0	807.8	809.6	811.4	813.2	815.0	816.8	818.6	820.4	822.2
440	824.0	825.8	827.6	829.4	831.2	833.0	834.8	836.6	838.4	840.2
450	842.0	843.8	845.6	847.4	849.2	851.0	852.8	854.6	856.4	858.2
460	860.0	861.8	863.6	865.4	867.2	869.0	870.8	872.6	874.4	876.2
470	878.0	879.8	881.6	883.4	885.2	887.0	888.8	890.6	892.4	894.2
480	896.0	897.8	899.6	901.4	903.2	905.0	906.8	908.6	910.4	912.2
490	914.0	915.8	917.6	919.4	921.2	923.0	924.8	926.6	928.4	930.2
500	932.0	933.8	935.6	937.4	939.2	941.0	942.8	944.6	946.4	948.2
510	950.0	951.8	953.6	955.4	957.2	959.0	960.8	962.6	964.4	966.2
520	968.0	969.8	971.6	973.4	975.2	977.0	978.8	980.6	982.4	984.2
530	986.0	987.8	989.6	991.4	993.2	995.0	996.8	998.6	1000.4	1002.2
540	1004.0	1005.8	1007.6	1009.4	1011.2	1013.0	1014.8	1016.6	1018.4	1020.2
550	1022.0	1023.8	1025.6	1027.4	1029.2	1031.0	1032.8	1034.6	1036.4	1038.2
560	1040.0	1041.8	1043.6	1045.4	1047.2	1049.0	1050.8	1052.6	1054.4	1056.2
570	1058.0	1059.8	1061.6	1063.4	1065.2	1067.0	1068.8	1070.6	1072.4	1074.2
580	1076.0	1077.8	1079.6	1081.4	1083.2	1085.0	1086.8	1088.6	1090.4	1092.2
590	1094.0	1095.8	1097.6	1099.4	1101.2	1103.0	1104.8	1106.6	1108.4	1110.2
600	1112.0	1113.8	1115.6	1117.4	1119.2	1121.0	1122.8	1124.6	1126.4	1128.2
610	1130.0	1131.8	1133.6	1135.4	1137.2	1139.0	1140.8	1142.6	1144.4	1146.2
620	1148.0	1149.8	1151.6	1153.4	1155.2	1157.0	1158.8	1160.6	1162.4	1164.2
630	1166.0	1167.8	1169.6	1171.4	1173.2	1175.0	1176.8	1178.6	1180.4	1182.2
640	1184.0	1185.8	1187.6	1189.4	1191.2	1193.0	1194.8	1196.6	1198.4	1200.2
650	1202.0	1203.8	1205.6	1207.4	1209.2	1211.0	1212.8	1214.6	1216.4	1218.2
660	1220.0	1221.8	1223.6	1225.4	1227.2	1229.0	1230.8	1232.6	1234.4	1236.2
670	1238.0	1239.8	1241.6	1243.4	1245.2	1247.0	1248.8	1250.6	1252.4	1254.2
680	1256.0	1257.8	1259.6	1261.4	1263.2	1265.0	1266.8	1268.6	1270.4	1272.2
690	1274.0	1275.8	1277.6	1279.4	1281.2	1283.0	1284.8	1286.6	1288.4	1290.2
700	1292.0	1293.8	1295.6	1297.4	1299.2	1301.0	1302.8	1304.6	1306.4	1308.2
710	1310.0	1311.8	1313.6	1315.4	1317.2	1319.0	1320.8	1322.6	1324.4	1326.2
720	1328.0	1329.8	1331.6	1333.4	1335.2	1337.0	1338.8	1340.6	1342.4	1344.2
730	1346.0	1347.8	1349.6	1351.4	1353.2	1355.0	1356.8	1358.6	1360.4	1362.2
740	1364.0	1365.8	1367.6	1369.4	1371.2	1373.0	1374.8	1376.6	1378.4	1380.2
750	1382.0	1383.8	1385.6	1387.4	1389.2	1391.0	1392.8	1394.6	1396.4	1398.2
760	1400.0	1401.8	1403.6	1405.4	1407.2	1409.0	1410.8	1412.6	1414.4	1416.2
770	1418.0	1419.8	1421.6	1423.4	1425.2	1427.0	1428.8	1430.6	1432.4	1434.2
780	1436.0	1437.8	1439.6	1441.4	1443.2	1445.0	1446.8	1448.6	1450.4	1452.2
790	1454.0	1455.8	1457.6	1459.4	1461.2	1463.0	1464.8	1466.6	1468.4	1470.2

For interpolation										
°C	0.1	0.2	0.3	0.4	0.5	0.6	0.7	0.8	0.9	0.10
°F	0.18	0.36	0.54	0.72	0.90	1.08	1.26	1.44	1.62	1.80

TEMPERATURES, CELSIUS TO FAHRENHEIT (contd)
For temperatures above 0°C

Temp. °C	0	1	2	3	4	5	6	7	8	9
800	1472.0	1473.8	1475.6	1477.4	1479.2	1481.0	1482.8	1484.6	1486.4	1488.2
810	1490.0	1491.8	1493.6	1495.4	1497.2	1499.0	1500.8	1502.6	1504.4	1506.2
820	1508.0	1509.8	1511.6	1513.4	1515.2	1517.0	1518.8	1520.6	1522.4	1524.2
830	1526.0	1527.8	1529.6	1531.4	1533.2	1535.0	1536.8	1538.6	1540.4	1542.2
840	1544.0	1545.8	1547.6	1549.4	1551.2	1553.0	1554.8	1556.6	1558.4	1560.2
850	1562.0	1563.8	1565.6	1567.4	1569.2	1571.0	1572.8	1574.6	1576.4	1578.2
860	1580.0	1581.8	1583.6	1585.4	1587.2	1589.0	1590.8	1592.6	1594.4	1596.2
870	1598.0	1599.8	1601.6	1603.4	1605.2	1607.0	1608.8	1610.6	1612.4	1614.2
880	1616.0	1617.8	1619.6	1621.4	1623.2	1625.0	1626.8	1628.6	1630.4	1632.2
890	1634.0	1635.8	1637.6	1639.4	1641.2	1643.0	1644.8	1646.6	1648.4	1650.2
900	1652.0	1653.8	1655.6	1657.4	1659.2	1661.0	1662.8	1664.6	1666.4	1668.2
910	1670.0	1671.8	1673.6	1675.4	1677.2	1679.0	1680.8	1682.6	1684.4	1686.2
920	1688.0	1689.8	1691.6	1693.4	1695.2	1697.0	1698.8	1700.6	1702.4	1704.2
930	1706.0	1707.8	1709.6	1711.4	1713.2	1715.0	1716.8	1718.6	1720.4	1722.2
940	1724.0	1725.8	1727.6	1729.4	1731.2	1733.0	1734.8	1736.6	1738.4	1740.2
950	1742.0	1743.8	1745.6	1747.4	1749.2	1751.0	1752.8	1754.6	1756.4	1758.2
960	1760.0	1761.8	1763.6	1765.4	1767.2	1769.0	1770.8	1772.6	1774.4	1776.2
970	1778.0	1779.8	1781.6	1783.4	1785.2	1787.0	1788.8	1790.6	1792.4	1794.2
980	1796.0	1797.8	1799.6	1801.4	1803.2	1805.0	1806.8	1808.6	1810.4	1812.2
990	1814.0	1815.8	1817.6	1819.4	1821.2	1823.0	1824.8	1826.6	1828.4	1830.2
1000	1832.0	1833.8	1835.6	1837.4	1839.2	1841.0	1842.8	1844.6	1846.4	1848.2
1010	1850.2	1851.8	1853.6	1855.4	1857.2	1859.0	1860.8	1862.6	1864.4	1866.2
1020	1868.0	1869.8	1871.6	1873.4	1875.2	1877.0	1878.8	1880.6	1882.4	1884.2
1030	1886.0	1887.8	1889.6	1891.4	1893.2	1895.0	1896.8	1898.6	1900.4	1902.2
1040	1904.0	1905.8	1907.6	1909.4	1911.2	1913.0	1914.8	1916.6	1918.4	1920.2
1050	1922.0	1923.8	1925.6	1927.4	1929.2	1931.0	1932.8	1934.6	1936.4	1938.2
1060	1940.0	1941.8	1943.6	1945.4	1947.2	1949.0	1950.8	1952.6	1954.4	1956.2
1070	1958.0	1959.8	1961.6	1963.4	1965.2	1967.0	1968.8	1970.6	1972.4	1974.2
1080	1976.0	1977.8	1979.6	1981.4	1983.2	1985.0	1986.8	1988.6	1990.4	1992.2
1090	1994.0	1995.8	1997.6	1999.4	2001.2	2003.0	2004.8	2006.6	2008.4	2010.2
1100	2012.0	2013.8	2015.6	2017.4	2019.2	2021.0	2022.8	2024.6	2026.4	2028.2
1110	2030.0	2031.8	2033.6	2035.4	2037.2	2039.0	2040.8	2042.6	2044.4	2046.2
1120	2048.0	2049.8	2051.6	2053.4	2055.2	2057.0	2058.8	2060.6	2062.4	2064.2
1130	2066.0	2067.8	2069.6	2071.4	2073.2	2075.0	2076.8	2078.6	2080.4	2082.2
1140	2084.0	2085.8	2087.6	2089.4	2091.2	2093.0	2094.8	2096.6	2098.4	2100.2
1150	2102.0	2103.8	2105.6	2107.4	2109.2	2111.0	2112.8	2114.6	2116.4	2118.2
1160	2120.0	2121.8	2123.6	2125.4	2127.2	2129.0	2130.8	2132.6	2134.4	2136.2
1170	2138.0	2139.8	2141.6	2143.4	2145.2	2147.0	2148.8	2150.6	2152.4	2154.2
1180	2156.0	2157.8	2159.6	2161.4	2163.2	2165.0	2166.8	2168.6	2170.4	2172.2
1190	2174.0	2175.8	2177.6	2179.4	2181.2	2183.0	2184.8	2186.6	2188.4	2190.2

For °C	0.1	0.2	0.3	0.4	0.5	0.6	0.7	0.8	0.9	0.10
interpolation °F	0.18	0.36	0.54	0.72	0.90	1.08	1.26	1.44	1.62	1.80

TEMPERATURES, CELSIUS TO FAHRENHEIT (contd)
For temperatures above 0°C.

Temp. °C	0	1	2	3	4	5	6	7	8	9
1200	2192.0	2193.8	2195.6	2197.4	2199.2	2201.0	2202.8	2204.6	2206.4	2208.2
1210	2210.0	2211.8	2213.6	2215.4	2217.2	2219.0	2220.8	2222.6	2224.4	2226.2
1220	2228.0	2229.8	2231.6	2233.4	2235.2	2237.0	2238.8	2240.6	2242.4	2244.2
1230	2246.0	2247.8	2249.6	2251.4	2253.2	2255.0	2256.8	2258.6	2260.4	2262.2
1240	2264.0	2265.8	2267.6	2269.4	2271.2	2273.0	2274.8	2276.6	2278.4	2280.2
1250	2282.0	2283.8	2285.6	2287.4	2289.2	2291.0	2292.8	2294.6	2296.4	2298.2
1260	2300.0	2301.8	2303.6	2305.4	2307.2	2309.0	2310.8	2312.6	2314.4	2316.2
1270	2318.0	2319.8	2321.6	2323.4	2325.2	2327.0	2328.8	2330.6	2332.4	2334.2
1280	2336.0	2337.8	2339.6	2341.4	2343.2	2345.0	2346.8	2348.6	2350.4	2352.2
1290	2354.0	2355.8	2357.6	2359.4	2361.2	2363.0	2364.8	2366.6	2368.4	2370.2
1300	2372.0	2373.8	2375.6	2377.4	2379.2	2381.0	2382.8	2384.6	2386.4	2388.2
1310	2390.0	2391.8	2393.6	2395.4	2397.2	2399.0	2400.8	2402.6	2404.4	2406.2
1320	2408.0	2409.8	2411.6	2413.4	2415.2	2417.0	2418.8	2420.6	2422.4	2424.2
1330	2426.0	2427.8	2429.6	2431.4	2433.2	2435.0	2436.8	2438.6	2440.4	2442.2
1340	2444.0	2445.8	2447.6	2449.4	2451.2	2453.0	2454.8	2456.6	2458.4	2460.2
1350	2462.0	2463.8	2465.6	2467.4	2469.2	2471.0	2472.8	2474.6	2476.4	2478.2
1360	2480.0	2481.8	2483.6	2485.4	2487.2	2489.0	2490.8	2492.6	2494.4	2496.2
1370	2498.0	2499.8	2501.6	2503.4	2505.2	2507.0	2508.8	2510.6	2512.4	2514.2
1380	2516.0	2517.8	2519.6	2521.4	2523.2	2525.0	2526.8	2528.6	2530.4	2532.2
1390	2534.0	2535.8	2537.6	2539.4	2541.2	2543.0	2544.8	2546.6	2548.4	2550.2

For Interpolation										
°C	0.1	0.2	0.3	0.4	0.5	0.6	0.7	0.8	0.9	0.10
°F	0.18	0.36	0.54	0.72	0.90	1.08	1.26	1.44	1.62	1.80

DENSITIES OF THE ELEMENTS

Source: CRC Handbook of Chemistry and Physics, R. C. Weast, M. J. Astle, and W. H. Beyer, eds., CRC Press, Boca Raton, FL (1984).

Element	Density, g/cm^3	Temp., °C	Element	Density, g/cm^3	Temp., °C
Ac	10.07	20	Mg	1.738	20
Ag	10.50	20	Mn	7.20	20
Al	2.6989	20	Mo	10.22	20
Am	13.67	20	Na	0.971	20
As (yellow)	1.97	20	Nb	8.57	20
As (gray)	5.73	20	Nd (cub)	6.80	20
Au	18.88	20	Nd (hex)	7.007	20
B (amorph)	2.37	20	Ni	8.902	25
B (cryst)	2.34	20	Np	20.25	20
Ba	3.51	20	Os	22.57	20
Be	1.848	20	P (white)	1.82	20
Bi	9.747	20	P (red)	2.20	20
C (amorph)	1.8-2.1	20	P (black)	2.25-2.69	20
C (graph)	1.9-2.3	20	Pa	15.37	20
C (diam)	3.15-3.53	20	Pb	11.35	20
Ca	1.55	20	Pd	12.02	20
Cd	8.65	20	Pm	7.22	25
Ce	6.657	25	Po (α)	19.84	25
Cm	13.51	20	Pr (α)	6.773	20
Co	8.9	20	Pr (β)	6.64	20
Cr	7.18-7.20	20	Pt	21.45	20
Cs	1.873	20	Pu (α)	19.84	20
Cu	8.96	20	Ra	(5)	20
Dy	8.550	20	Rb	1.532	20
Er	9.066	25	Re	21.02	20
Eu	5.243	25	Rh	12.41	20
Fe	7.874	20	Ru	12.41	20
Ga (sol)	5.904	29.6	S (rhomb)	2.07	20
Ga (liq)	6.095	29.6	S (monocl)	1.957	20
Gd	7.9004	25	Sb	6.691	20
Ge	5.323	25	Sc	2.989	25
Hf	13.31	20	Se (gray)	4.79	20
Hg	13.546	20	Se (vitr)	4.28	20
Ho	8.795	25	Si	2.33	25
In	7.31	20	Sm (α)	7.520	20
Ir	22.42	17	Sm (β)	7.40	20
K	0.862	20	Sn (gray)	5.75	20
La	6.145	25	Sn (white)	5.75	20
Li	0.534	20	Sr	2.54	20
Lu	9.840	25	Ta	16.654	20

DENSITIES OF THE ELEMENTS (contd)

Element	Density, g/cm^3	Temp., °C	Element	Density, g/cm^3	Temp., °C
Tb	8.229	20			
Tc	11.50	20			
Te	6.24	20			
Th	11.72	20			
Ti	4.54	20			
Tl	11.85	20			
Tm	9.321	25			
U	18.95	20			
V	6.11	18.7			
W	19.3	20			
Y	4.469	20			
Yb (α)	6.965	20			
Yb (β)	6.54	20			
Zn	7.153	25			
Zr	6.506	20			

MELTING AND BOILING POINTS OF ELEMENTS

Source: <u>CRC Handbook of Chemistry and Physics</u>, R. C. Weast, M. J. Astle, and W. H. Beyer, eds., CRC Press, Boca Raton, FL (1984).

Element	Melt. Pt., °C	Boil. Pt., °C	Element	Melt. Pt., °C	Boil. Pt., °C
Ac	1050	3200	K	63.25	760
Ag	960.8	2212	Kr	-156.6	-152.30
Al	660.37	2467	La	921	3457
Am	994	2607	Li	180.54	1342
Ar	-189.2	-185.7	Lu	1663	3395
As	---	subl 613	Mg	648.8	1090
At	302	(337)	Mn	1244	1962
Au	1064.43	3080	Mo	2617	4612
B	2300	2550	N	-209.86	-195.8
Ba	725	1640	Na	97.81	882.9
Be	1278	2970	Nb	2468	4742
Bi	271.3	1560	Nd	1021	3068
Br	-7.2	58.78	Ne	-248.67	-246.048
C	~3550		Ni	1453	2732
Ca	839	1484	Np	640	3902
Cd	320.9	765	O	-218.4	-182.962
Ce	799	3426	Os	3045	5027
Cl	-100.98	-34.6	P	44.1	280
Co	1495	2870	Pb	327.502	1740
Cm	(247)	1340	Pd	1554	2970
Cr	1857	2672	Pm	1168	2460
Cs	28.40	669.3	Po	254	962
Cu	1083.4	2567	Pr	931	3512
Dy	1412	2562	Pt	1772	3827
Er	159	2863	Pu	641	3232
Eu	822	1597	Ra	700	1140
F	-219.62	-188.14	Rb	38.89	686
Fe	1535	2750	Re	3180	(5627)
Fr	27	677	Rh	1966	3727
Ga	29.78	2403	Rn	-71	-61.8
Gd	1313	3266	Ru	2310	3900
Ge	937.4	2830	S rhom	112.8	444.674
H	-259.14	-252.5	mono	119.0	444.67
He	<-272.2	-278.934	Sb	630.74	1950
Hf	2227	4602	Sc	1541	2831
Hg	-38.842	356.58	Se	217	684.9
Ho	1474	2695	Si	1410	2355
I	113.5	184.35	Sm	1077	1791
In	156.61	2080	Sn	231.9681	2270
Ir	2410	4130	Sr	769	1384

MELTING AND BOILING POINTS OF ELEMENTS (contd)

Element	Melt. Pt., °C	Boil. Pt., °C	Element	Melt. Pt., °C	Boil. Pt., °C
Ta	2996	5425			
Tb	1356	3123			
Tc	2172	4877			
Te	449.5	989.8			
Th	1750	-4790			
Ti	1660	3287			
Tl	303.5	1457			
Tm	1545	1947			
U	1132.3	3818			
V	1890	3380			
W	3410	5660			
Xe	-111.9	-107.1			
Y	1522	3338			
Yb	819	1194			
Zn	419.58	907			
Zr	1852	4377			

VAPOR PRESSURE EQUATIONS FOR ELEMENTS

Source: Smithells Metals Reference Book, 6th ed., E. A. Brandes, ed., Butterworths (1983).

The constants that are listed are for the following equation:

$$\log p\ (\text{mm Hg}) = A + B/T + C \log T + 10^{-3}\ DT$$

where T = temperature in Kelvin

Element	A	B	C	D	Temp. Range (K)
Ag	11.66	-14710	-0.755	-	298 - 1234
Ag	12.23	-14260	-1.055	-	1234 - 2400
Al	12.36	-16450	-1.023	-	1200 - 2800
Am	13.97	-13700	-1.0	-	1103 - 1453
As4	9.82	-6160	-	-	600 - 900
Au	10.81	-19820	-0.306	-0.16	298 - 1336
Au	12.38	-19280	-1.01	-	1336 - 3240
B	13.88	-29900	-1.0	-	1000 - mp
Ba	7.83	-9730	-	-	750 - 983
Ba	7.42	-9340	-	-	983 - 1200
Be	9.067	-10734	-	-0.145	900 - 1557
Bi	12.35	-10400	-1.26	-	mp - bp
Bi2	18.1	-10730	-3.02	-	mp - bp
Ca	14.97	-10300	-1.76	-	713 - mp
Ca	12.55	-9600	-1.21	-	mp - bp
Ce	8.305	-20305	-	-	1611 - 2038
Cd	9.717	-5908	-0.232	-0.284	450 - 594
Cd	12.286	-5819	-1.257	-	594 - 1050
Co	10.817	-22210	-	-0.223	1000 - 1772
Cr	14.56	-20680	-1.31	-	298 - mp
Cs	11.38	-4075	-1.45	-	280 - 1000
Cu	10.63	-17870	-0.236	-0.16	298 - 1356
Cu	13.39	-17650	-1.273	-	1356 - 2870
Eu	8.16	-8980	-	-	696 - 900
Fe	16.89	-21080	-2.14	-	900 - 1812
Fe	13.27	-19710	1.27	-	1812 - 3000
Ga	10.07	-14700	-0.5	-	mp - bp
Ge	13.28	-20150	-0.91	-	298 - mp
Ge	12.87	-18700	-1.16	-	mp - bp
Hf(α)	11.81	-32000	-0.5	-	298 - 2023

VAPOR PRESSURE EQUATIONS FOR ELEMENTS (contd)

Element	A	B	C	D	Temp. Range (K)
Hf(β)	11.63	-31630	-0.5	-	2023 - mp
Hf	9.20	-29830	-	-	mp - bp
Hg	10.373	-3308	-0.8	-	298 - 630
I2	17.72	-3578	-2.51	-	298 - mp
I2	23.65	-3205	-5.18	-	mp - bp
In	9.79	-12580	-0.45	-	mp - bp
Ir	13.18	-35070	-0.7	-	298 - mp
K	11.58	-4770	-1.370	-	350 - 1050
La	10.39	-22120	-0.33	-	298 - mp
La	9.89	-21530	-0.33	-	mp - bp
Li	11.34	-8415	-1.0	-	mp - bp
Mg	11.41	-7780	-0.855	-	298 - mp
Mg	12.79	-7550	-1.41	-	mp - bp
Mn	17.88	-14850	-2.52	-	993 - 1373
Mn	17.27	-13900	-2.52	-	mp - bp
Mo	11.66	-34700	-0.236	-0.145	298 - mp
Na	9.235	-5561	-0.5	-	400 - 1200
Nb	8.94	-37650	+0.715	-0.166	298 - mp
Ni	13.60	-22500	-0.96	-	298 - mp
Ni	16.95	-22400	-2.01	-	mp - bp
P4 (yell)	19.09	-3530	-3.5	-	298 - 317
P4	7.84	-2740	-	-	317 - 553
Pb	11.16	-10130	-0.985	-	600 - 2030
Pd	11.82	-19800	-0.755	-	298 - mp
Pd	4.81	-17500	+1.0	-	mp - bp
Pr	8.10	-17190	-	-	1425 - 1692
Pt	13.24	-29200	-0.855	-	298 - mp
Pt	14.30	-28500	-1.26	-	mp - bp
Pu	7.90	-17590	-	-	1392 - 1793
Rb	12.00	-4560	-1.45	-	312 - 952
Re	14.20	-40800	-1.16	-	298 - 3000
Rh	13.50	-29360	-0.88	-	298 - mp
Ru	10.76	-33550	-	-	2000 - 2500
S2	16.22	-6975	-1.53	-1.0	mp - bp
Sx	23.88	-4380	-5.0	-	mp - bp
Sbx	22.40	-11560	-3.52	-	298 - mp
Sb2	18.54	-11170	-3.02	-	mp - bp
Sc (β)	13.07	-19700	-1.0	-	1607 - mp
Sex	8.09	-4990	-	-	493 - 958
Si	10.84	-20900	-0.565	-	mp - bp

VAPOR PRESSURE EQUATIONS FOR ELEMENTS (contd)

Element	A	B	C	D	Temp. Range (K)
Sm	13.76	-11170	-1.56	-	298 - mp
Sn	8.23	-15500	-	-	505 - bp
Sr	13.08	-9450	-1.31	-	813 - mp
Sr	12.63	-9000	-1.31	-	mp - bp
Ta	10.29	-40800	-	-	298 - mp
Te2	19.68	-9175	-2.71	-	298 - mp
Te2	22.29	-7830	-4.27	-	mp -
Th	12.95	-30200	-1.0	-	298 - mp
Ti (β)	13.18	-24400	-0.91	-	1155 - mp
Ti	11.74	-23200	-0.66	-	mp - bp
Tl	11.10	-9300	-0.892	-	700 - 1800
Tm	9.18	-12550	-	-	807 - 1219
U	18.58	-25580	-2.62	-	298 - mp
U	13.20	-24090	-1.26	-	mp - 4200
V	10.12	-26900	+0.33	-0.265	298 - mp
W	8.76	-44000	+0.50	-	298 - mp
Y	11.835	-22230	-0.66	-	298 - mp
Y	16.13	-22280	-1.97	-	mp - bp
Zn	9.418**	-6883	-0.0503	-0.33	473 - 692.5
Zn	12.00	-6670	-1.126	-	692.5 - 1000
Zr	11.78	-31820	-0.50	-	1125 - mp
Zr	9.38	-30300	-	-	mp - bp

B. THERMODYNAMICS

B.1 Enthalpy and Heat Capacity

B.1.1 Uranium-Zirconium Alloys

Measurements of the heat capacity of uranium-zirconium alloys have been reported by Federov and Smirnov [1], who used an electrical-pulse technique for their work. Samples of pure zirconium and uranium were investigated, and also alloys with uranium contents of 11, 27, 39, 59, and 87 at.%. Federov and Smirnov give the following equations for heat capacity C_p (cal K^{-1} mol^{-1}) for the temperature ranges 203-873 K for U(α) and the alloys and 293-1073 K for Zr(α).

Zr(α) $C_p = 6.15 + (1.927 \times 10^{-3}\ T) - (3.485 \times 10^{4}\ T^{-2})$
U(α) $C_p = 2.69 + (9.698 \times 10^{-3}\ T) - (1.072 \times 10^{5}\ T^{-2})$
11 at.% U $C_p = 3.89 + (6.48 \times 10^{-3}\ T) + (7.71 \times 10^{4}\ T^{-2})$
27 at.% U $C_p = 3.08 + (8.43 \times 10^{-3}\ T) + (9.83 \times 10^{4}\ T^{-2})$
39 at.% U $C_p = 3.47 + (9.32 \times 10^{-3}\ T) + (7.01 \times 10^{4}\ T^{-2})$
59 at.% U $C_p = 0.265 + (1.32 \times 10^{-2}\ T) + (2.62 \times 10^{5}\ T^{-2})$
87 at.% U $C_p = 0.356 + (1.425 \times 10^{-2}\ T) + (2.59 \times 10^{5}\ T^{-2})$

Heat-capacity data for the alloy of interest, U-10 wt % Zr (U-22.5 at.% Zr) were obtained by linear interpolation. The following equations give heat capacity, C_p (J $K^{-1}mol^{-1}$), and enthalpy, H(T) - H(298) (J mol^{-1}), for that alloy.

$$C_p(\text{U-10 wt \% Zr}) = 1.359 + 0.05812T + (1.086 \times 10^{6}\ T^{-2})$$

$$H(T) - H(298)(\text{U-10 wt \% Zr}) = 654.0 + 1.359T + 0.02906T^{2} - (1.086 \times 10^{6}\ T^{-1})$$

The data of Federov and Smirnov for pure uranium and zirconium are high by about 3-4% when compared with the best current values [3,4]. Uncertainties of about ±5% are reasonable for these estimates for the U-10 wt % Zr alloy.

Obtaining heat-capacity and enthalpy data for the high-temperature body-centered-cubic (bcc) alloy phases is somewhat more difficult. For the heat capacities of U(γ) and Zr(β) and the high-temperature bcc alloy phases, the data of Federov and Smirnov are presented graphically. Values obtained from their plots at 1100 K, in (at. % U) and cal K^{-1} mol^{-1}, given in an IAEA publication [2] are: (0) 7.45, (11) 8.2, (27) 8.9, (39) 9.3, (59) 9.5, and (87) 9.5. These values are constant in the temperature range of the bcc solid solution. At the higher temperatures Federov and Smirnov give only heat capacity. In order to calculate enthalpy of the higher-temperature bcc solid solutions, we need an enthalpy value in the higher-temperature phase. Federov and Smirnov [5] also measured the emf of cells of the type

$$U(c)|KCl\text{-}NaCl\text{-}0.5\text{ wt \% }UC\ell_3|(U\text{-}Zr)\text{alloy}$$

The temperature range of their measurements was 1033-1183 K. Thermodynamic properties for U-Zr alloys were calculated at 1100 K from the emf data of Federov and Smirnov [5] by Chiotti et al. [2]. Included in the tabulation of Chiotti et al. is the enthalpy of mixing from which the requisite values could be estimated. However, there are significant discrepancies in the U-Zr system [2], and Pelton [6] discounts the data entirely. We have calculated the enthalpy of the U-10 wt % Zr alloy at 1200 K assuming an ideal solution, and have used the heat-capacity data of Federov and Smirnov to calculate enthalpies at other temperatures. The values calculated in this way are about 10% higher than those resulting from using the enthalpy-of-mixing data. Because of the lack of data, the details of the transition region from

890 to about 1000 K are not considered in the present analysis. The transition region is simply treated as a single phase transition. The enthalpy data resulting from these considerations are shown in Fig. B.1.1-A (along with data for U and Zr), and are combined with heat-capacity data in Table B.1.1-1. Data are given up to the solidus temperature (1487 K). Values at the liquidus (1657 K) and above were estimated using an ideal solution assumption. For values between the solidus and liquidus temperatures, linear interpolation is recommended.

TABLE B.1.1-1. Enthalpy and Heat Capacity of Uranium-10 wt % Zirconium

T (K)	C_p ($J\ K^{-1}\ mol^{-1}$)	H(T) - H(298) ($kJ\ mol^{-1}$)
298	30.9	0.0
400	31.4	3.13
500	34.8	6.43
600	39.2	10.1
700	44.3	14.3
800	49.6	18.9
890	54.5	23.7
1000(γ)	36.8	31.7
1100	36.8	35.4
1200	36.8	39.1
1400	36.8	46.4
1500	36.8	50.1
1506(γ)	36.8	50.3
1669(ℓ)	45.2	69.0
1700	45.2	70.4
1800	45.2	74.8
1900	45.2	79.4
2000	45.2	84.0

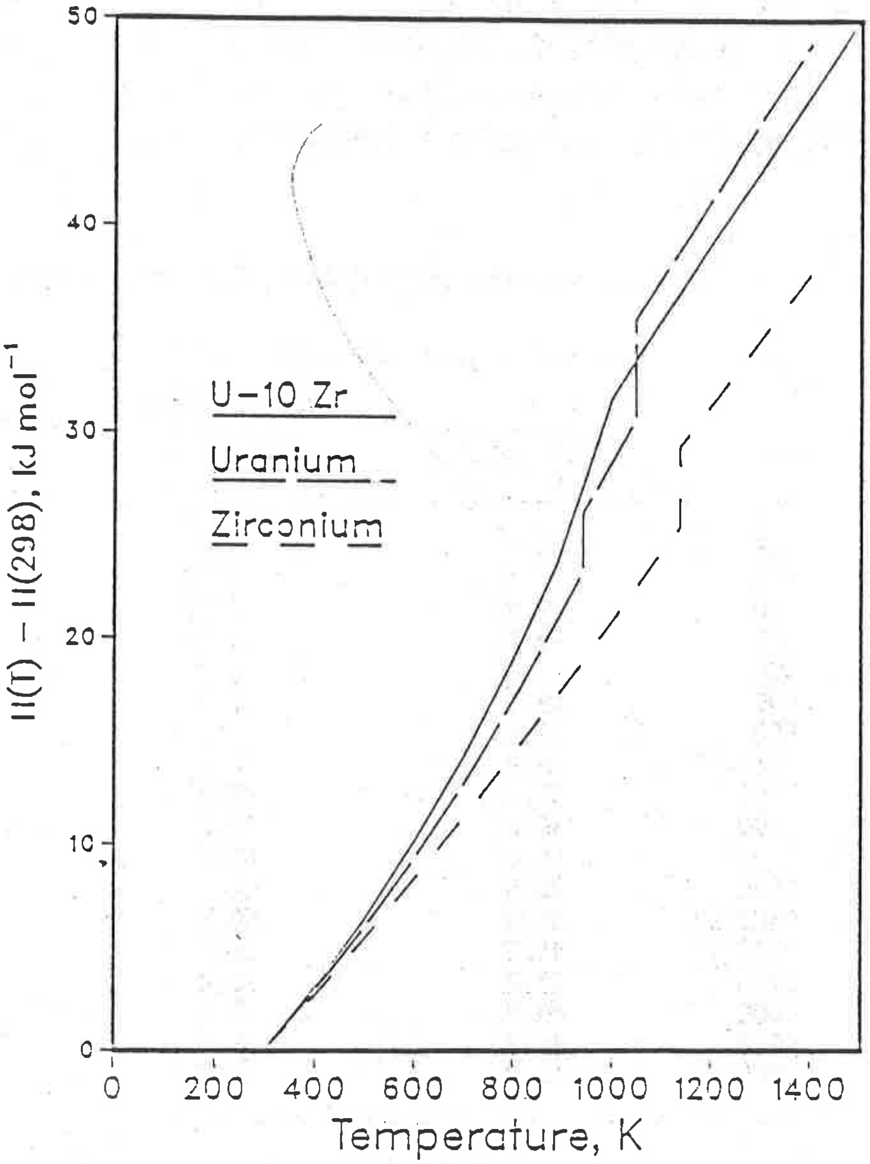

Fig. B.1.1-A. Enthalpy, H(T) - H(298), kJ mol^{-1}, of U-10 wt % Zr

B.1.2 Uranium-Plutonium-Zirconium Alloys

Measurements have been reported of the enthalpy of U-15 wt % Pu-10 wt % Zr (U-12.8 at.% Pu-22.5 at.% Zr) from about 306 to 1140°C [7]. The data appear to be reliable (probably to 1%) [8] and cover most of the solid range of this alloy. The experimental values as given in [7] are presented in Table B.1.2-1.

TABLE B.1.2-1 Enthalpy of U-15 wt % Pu-10 wt % Zr

Temperature (°C)	H(T)-H(25°C) (cal/g)
306.5	10.2
402.4	14.1
505.3	18.7
599.6	23.9
696.1	34.7
798.1	38.9
897.0	43.3
997.0	47.4
1097.0	52.4
1140.3	55.1

These data were fit to two quadratic equations in [7] covering the temperature ranges above and below the solid-state phase transitions. These equations are reproduced below (a sign error has been corrected).

$$H(T) - H(25°C) = -0.9 + 0.0310T + (1.55 \times 10^{-5}\ T^2) \quad 25\text{-}600°C$$
$$H(T) - H(25°C) = 14.2 + 0.0185T + (1.52 \times 10^{-5}\ T^2) \quad 650\text{-}1150°C$$

Enthalpies are given in cal/g and temperatures are in °C. Heat capacities may be obtained simply by differentiating the enthalpy equations. The coefficients of the "T" terms given for heat capacity in [7] are too large by a factor of ten. After correction of the coefficients, these enthalpy equations yield the following equations with temperatures in K and enthalpies in J/mol. A correction was made in the low-temperature equation so that H(T) - H(298) was zero at T = 298.15. The higher-temperature equation was modified to the current estimate of the solidus temperature (1379 K)[6].

$$H(T) - H(298) = -6948 + 19.34T + 0.0133T^2 \qquad 298\text{-}873K$$

$$H(T) - H(298) = 8772 + 8.752T + 0.01304T^2 \qquad 923\text{-}1379K$$

The enthalpies and heat capacity of the ternary alloy are given in Table B.1.2-2. Included in the table are values above the liquidus temperature (1588 K) that were calculated assuming an ideal solution. For values between the solidus and liquidus temperature, linear interpolation is recommended. The enthalpies of U-15 wt % Pu-10 wt % Zr, pure uranium, and U-10 wt % Zr are compared in Fig. B.1.2-A. To assess the possibilities of estimation and extrapolation of enthalpy data, we calculated the mole-average enthalpy for the ternary alloy, using data for U [3], Pu [3], and Zr [4] from standard sources. Because the melting point of Pu of 913 K is well below the solidus temperature of the alloy, we simply extrapolated the data for Pu(ε) above its melting point, assuming a constant heat capacity. This appeared to be a more reasonable approach than introducing data for liquid Pu. The results of this calculation are compared with the experimental values in Fig. B.1.2-B. Except for the phase-transition temperatures the agreement is reasonable, and estimates for other compositions and temperatures may be possible.

TABLE B.1.2-2 Enthalpy and Heat Capacity of Uranium-15 wt % Plutonium-10 wt % Zirconium

T (K)	C_p ($J\ K^{-1}\ mol^{-1}$)	H(T) - H(298) ($kJ\ mol^{-1}$)
298	27.3	0.0
400	30.0	2.92
500	32.6	6.05
600	35.3	9.44
700	38.0	13.1
800	40.6	17.0
873	42.6	20.1
923	32.8	28.0
1000	34.8	30.6
1100	37.4	34.2
1200	40.0	38.1
1300	42.7	42.2
1379(s)	44.7	45.6
1588(ℓ)	44.4	64.4
1600	44.4	64.9
1700	44.4	69.4
1800	44.4	73.8
1900	44.4	78.3
2000	44.4	82.7

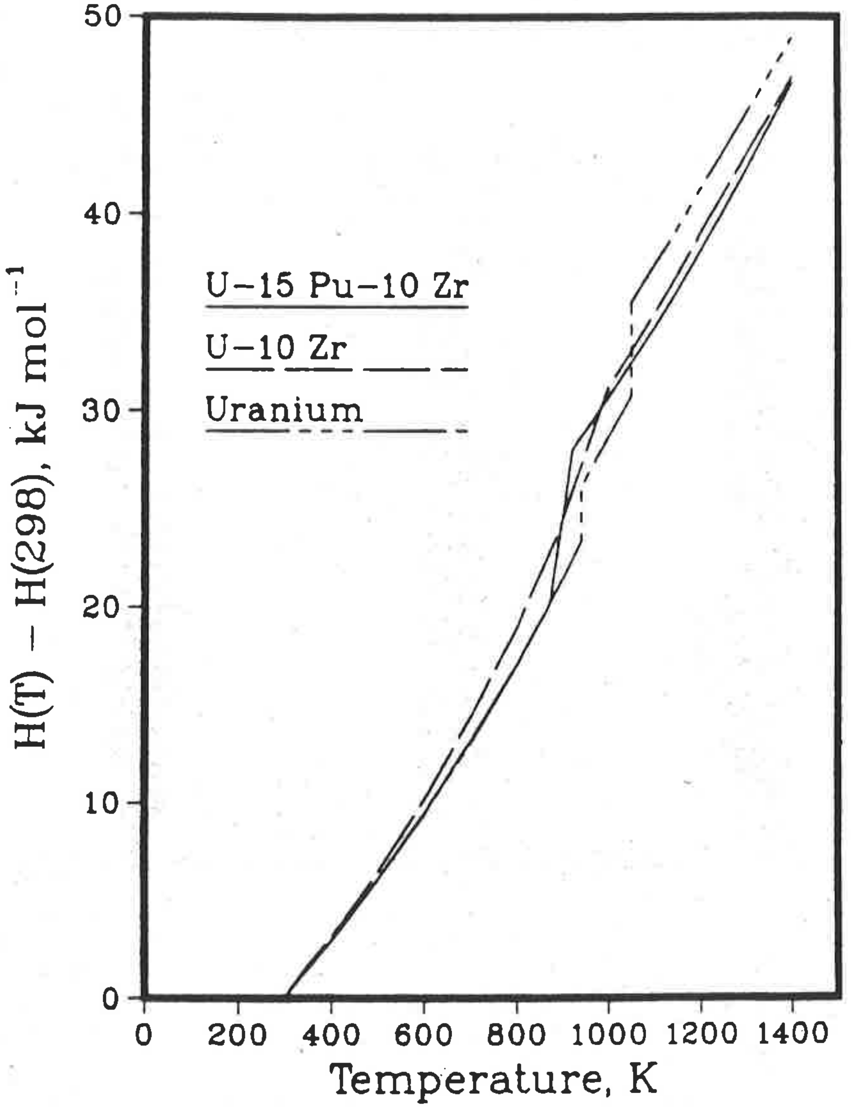

Fig. B.1.2-A Enthalpy, H(T) - H(298) kJ mol^{-1}, for Uranium, U-10 wt % Zr, and U-15 wt % Pu-10 wt % Zr

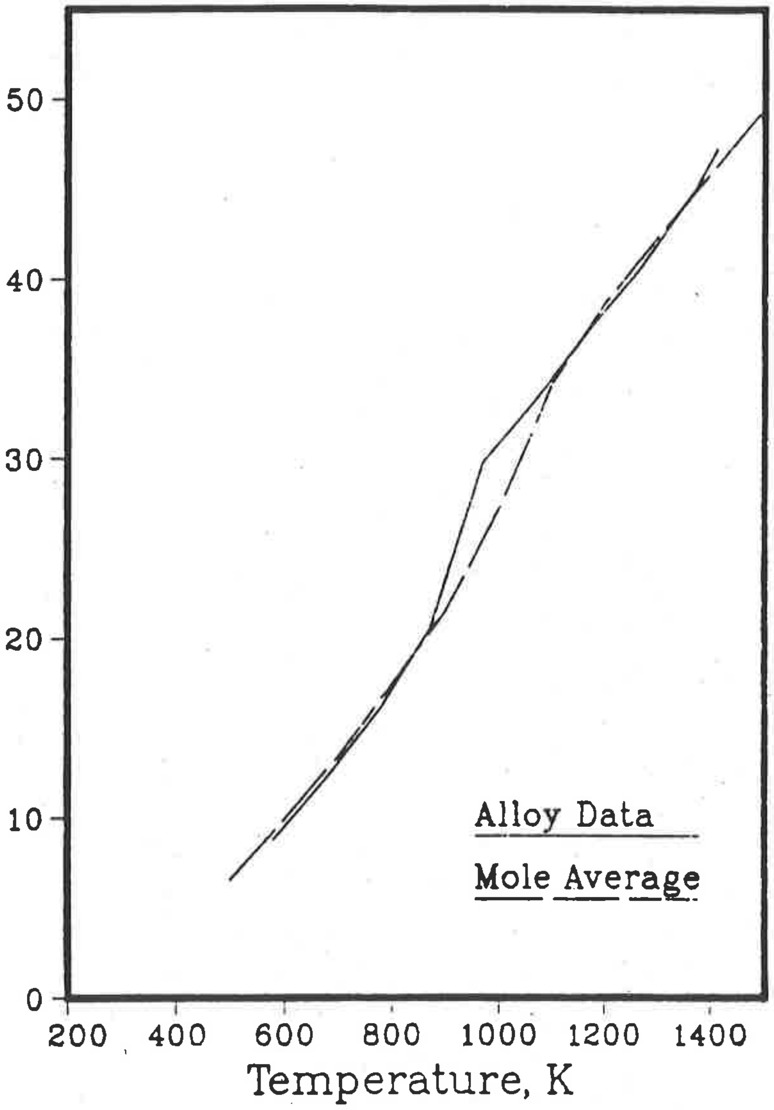

Fig. B.1.2-B Enthalpy, (H(T) - H(298) kJ mol^{-1}, for U-15 wt % Pu-10 wt % Zr Compared with Mole-average Values

B.1.3 Others

High-temperature Heat Capacity and Enthalpy of Uranium*

The high-temperature enthalpy and heat capacity of uranium have been determined by several investigators. The more precise heat-capacity results are shown in Fig. B.1.3-A. The early enthalpy measurements of Moore and Kelley [9] and of Ginnings and Corruccini [10] cover the lower temperature range, 298 to 1300 K and 298 to 1173 K, respectively. The two investigations are in good agreement on the enthalpy of the α-phase of uranium, although Ginnings and Corruccini [10] report a steeper rise in the enthalpy function, indicating a more pronounced pretransition effect. North [11], using an adiabatic method, reported heat-capacity measurements from 373 to 1073 K consistently below the values reported above. Savage and Seibel [12], using a drop calorimeter, determined the enthalpy increment of uranium in the temperature range of 413 to 1454 K. Their results are in agreement with those of Moore and Kelley [9] and Ginnings and Corruccini [10] below 1100 K, but become significantly higher above this temperature. Mit'kina [13] reported the specific heat capacity of uranium from 323 to 873 K. Her results are much lower below 573 K, but above that temperature they are in good agreement with the results of Moore and Kelley [9], and of Ginnings and Corruccini [10]. For this assessment we have adopted the heat-capacity values for α-phase uranium reported by Ginnings and Corruccini [10], since these data are believed to be the most reliable.

The heat capacities of the β- and γ-phase of uranium metal are constant at 43.43 and 38.07 J K^{-1} (as reported by Moore and Kelley [9]), and at 42.47 and 38.28 J K^{-1} mol^{-1} (as reported by Ginnings and Corruccini [10]). The adopted heat-capacity values for the β- and γ-phase of uranium

---

* This section adapted from B.1, Ref. 3.

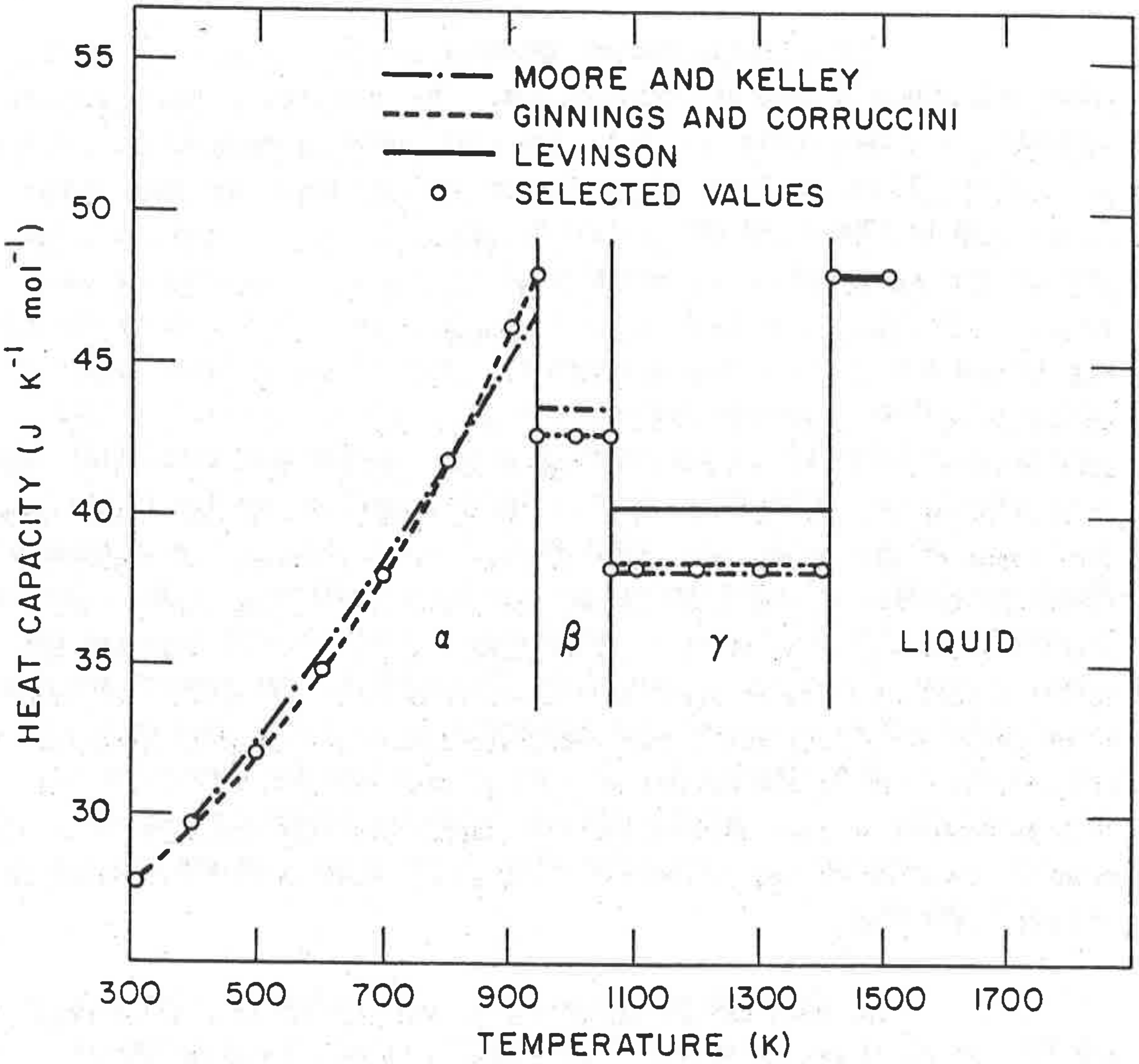

Fig. B.1.3-A Heat-capacity Data for Uranium from Various Investigators metal are based on the results of these two investigations: 42.93 J K^{-1} mol^{-1} for the β-phase and 38.28 J K^{-1} mol^{-1} for the γ-phase, respectively. Levinson [14] has determined the enthalpy increment of the γ-phase and the liquid. His resulting heat-capacity value for the γ-phase, 40.08 J K^{-1} mol^{-1} is considerably higher than the values reported earlier by Moore and Kelley [9] and by Ginnings and Corruccini [10].

The enthalpies of transition, as reported by various investigators (Table B.1.3-1), are in fairly good agreement. However, the values for the enthalpies of transition used in this compilation are chosen so as to reproduce the measured enthalpy increments for the β- and γ-phases.

TABLE B.1.3-1 Enthalpies of Transition for Uranium

Source	$\Delta H_t(\alpha\leftrightarrow\beta)$ (kJ mol^{-1}) (T_t=942K)	$\Delta H_t(\beta\leftrightarrow\gamma)$ (kJ mol^{-1}) (T_t=1049K)
Moore and Kelley [9]	2.845	4.874
Ginnings and Corruccini [10]	2.820	4.732
North [11]	2.979	4.782
Savage and Seibel [12]	3.284	4.581
Adopted value	2.791	4.757

The selected values for heat capacity and enthalpy of the solid phases are identical with those tabulated by Hultgren et al. [4], except for minute differences resulting from the use of an equation for the heat capacity for the α-phase and correction to the International Practical Temperature Scale (IPTS-1968).

Melting Point and Enthalpy of Fusion

The melting point of uranium metal has been reported by several investigators: by Blumenthal [15] as (1405 ± 0.8) K, by Buzzard et al. [16] as 2406 K, by Udy and Boulger [17] as (1405 ± 10) K, and by Dahl and Cleaves [18] as (1406 ± 2) K. The agreement is remarkable, and (1406 ± 2) K is selected as the melting point of uranium on IPTS-1948, which becomes (1408 ± 2) K on IPTS-1968. Ackermann and Rauh [19] measured (1408 ± 1) K on the latter scale.

There have been two determinations of the enthalpy of liquid uranium. Levinson [14] measured H(T)-H(310) for U(ℓ) contained in tantalum from 1205 to 1579 K, obtaining a value for the enthalpy of fusion of (8.326 ± 0.130) kJ mol^{-1} and a constant value for the heat capacity of U(ℓ) of 47.91 J K^{-1} mol^{-1}. When corrected for tantalum solubility (Ackermann and Rauh [20]), this latter value becomes 44.35 J K^{-1} mol^{-1}.

However, we have preferred the much more extensive enthalpy results of Stephens [21] from 1428 to 2348 K. These results were obtained by levitation calorimetry, which avoids the problems of reactions with containers. His data, which are represented by the equation

$$H(T) - H(298) = 48.66T - 10138 \text{ J mol}^{-1}$$

when combined with the selected data for the solid thus give a value for the enthalpy of fusion of 9.14 kJ mol^{-1} at 1408 K and a constant value of C_p^o U(ℓ) of 48.66 J K^{-1} mol^{-1}.

Recently, Thayer and Robbins [22] have determined the heat capacity of U(ℓ) by using a prompt-burst reactor to heat thin wafers of the metal very rapidly. Their value of (37.66 ± 2.1) J K^{-1} mol^{-1} for the heat capacity of U(ℓ) is appreciably lower than the other two measurements. The uncertainties in this interesting technique at this time lead us to prefer the very extensive measurements of Stephens [21].

The heat capacity of U(α), $298 \leq T \leq 942$ K, in J K^{-1} mol^{-1} is given by the following equation:

$$C_p(U\alpha) = 26.92 - (2.502 \times 10^{-3}\ T) + (26.556 \times 10^{-6}\ T^2) - (7.7 \times 10^{4}\ T^{-2}).$$

For U(β), U(γ), and U(ℓ), the heat capacity is constant. The recommended enthalpies are shown in Table B.1.3-2 and Fig. B.1.3-B

High-temperature Heat Capacity and Enthalpy of Plutonium*

The high-temperature heat capacity of plutonium has been reported by two investigators (Engel [23] and Loasby [24]). Their results are plotted in Fig. B.1.3-C, along with the low-temperature heat-capacity measurements of Sandenaw and Gibney [25], who took measurements up to 370 K, within 25 K of the α→β transition. Kay and Loasby [24] report high-temperature heat-capacity data (error span ±5%) for plutonium metal up to the melting point. However, to allow for unsuspected errors in their chemical and isotopic analyses used in the calculation of the self-heating coefficients (Taylor [26]), they increased the error span to ±10%. They used an adiabatic calorimeter and utilized the self-heating of the isotopic mixture of plutonium as the heat source in determining the heat-capacity value. Such a method has the advantage of ensuring uniform heating of the specimen; however, it has the disadvantage of errors arising from nonequilibrium conditions, in particular in the transformation regions.

---

* This section adapted from B.1, Ref. 3.

TABLE B.1.3-2 High-temperature Heat Capacity and Enthalpy of Uranium

T (K)	C_p ($J\ K^{-1}\ mol^{-1}$)	H(T) - H(298) ($J\ mol^{-1}$)
298	27.665	0
300	27.700	51
400	29.684	2919
500	31.997	5999
600	34.762	9333
700	38.021	12968
800	41.791	16955
900	46.081	21344
942(α)	48.038	23320
942(β)	42.928	26111
1000	42.928	28600
1049(β)	42.928	30704
1049(γ)	38.284	35461
1100	38.284	37414
1200	38.284	41242
1300	38.284	45070
1400	38.284	48899
1408(γ)	38.284	49205
1408(ℓ)	48.660	58347
1500	48.660	62842
1600	48.660	67690
1700	48.660	72556
1800	48.660	77422
1900	48.660	82288
2000	48.660	87154
2100	48.660	92020
2200	48.660	96886
2300	48.660	101752
2400	48.660	106618
2500	48.660	111484

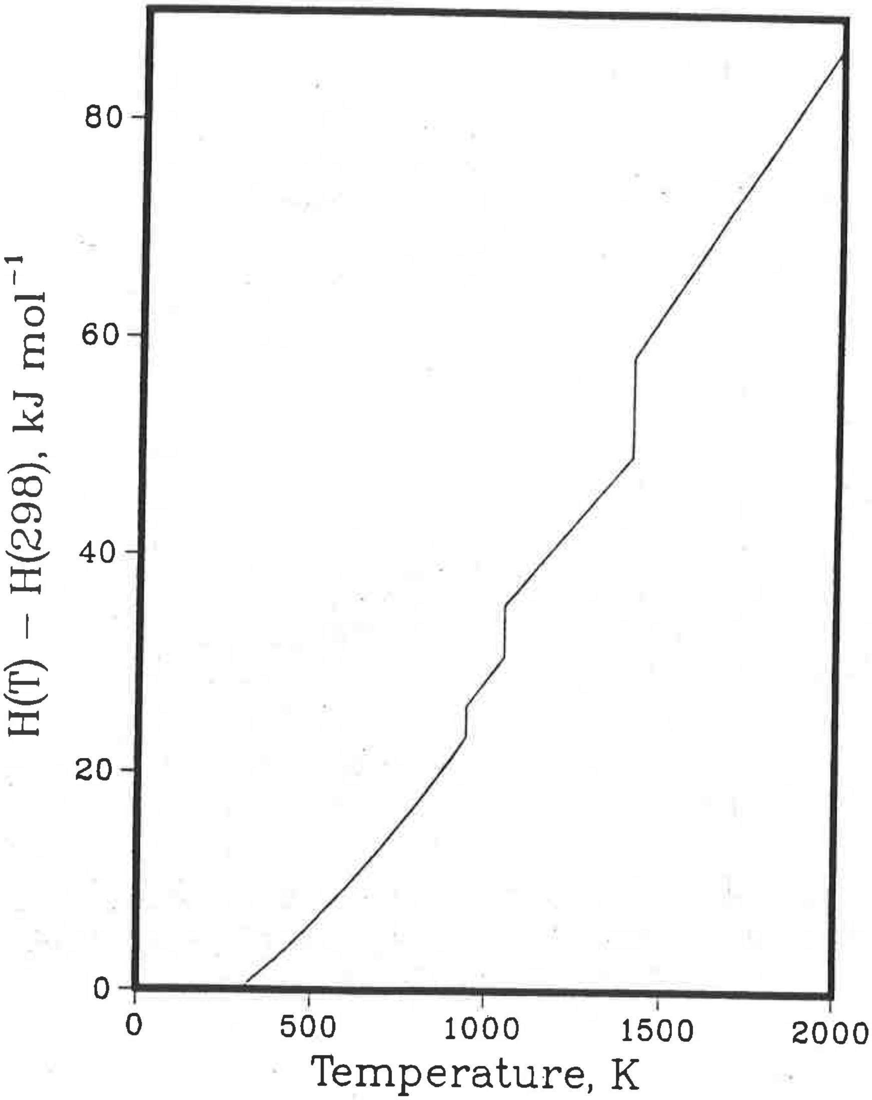

Fig. B.1.3-B Enthalpy, H(T) - H(298) kJ mol^{-1} for Uranium

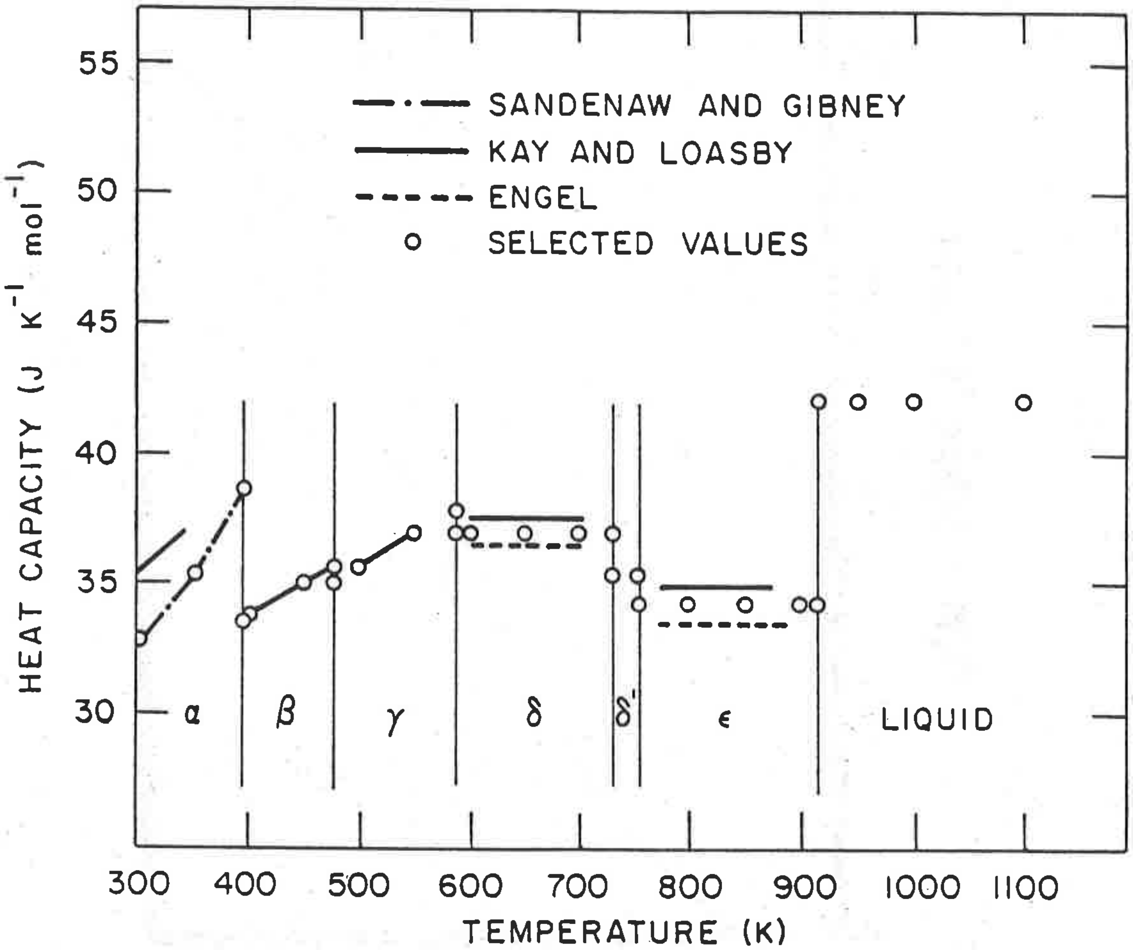

Fig. B.1.3-C Heat-capacity Data for Plutonium
from Various Investigators

Other sources of error in these heat-capacity measurements lie in assuming an accurate value of each isotopic power output, as well as in making an accurate isotopic analysis of the metal specimen. Recent power-output values for the individual plutonium isotopes (Oetting [27]) differ somewhat from the values cited by Kay and Loasby [24]; however, an error band of ±10% covers the error involved in the power values.

A comparison of the heat-capacity values of Kay and Loasby [24] and of Sandenaw and Gibney [25], from room temperature to the $\alpha \to \beta$ transformation (395 K), shows the values of Kay and Loasby to be higher by about 7%. As it is believed that the low-temperature data of Sandenaw and Gibney are more accurate, their values were adopted for the heat capacity of the α-phase of plutonium above room temperature.

Kay and Loasby [24] indicate a slight temperature dependence for the heat capacity of the β- and γ-phases but no temperature dependence for the δ- and ϵ-phases. Engel [23] also found no temperature dependence for the heat capacity of the δ-, δ'- and ϵ-phases of plutonium. The agreement between the heat capacity values for the δ- and ϵ-phases of Engel and Kay and of Loasby is quite good, i.e., 2.6% and 4.0% respectively. The averages of the two values are taken for this compilation. The value of 35.56 J K^{-1} mol^{-1} given by Engel for the heat capacity of the δ'-phase is also used.

The consistency of the thermodynamic data for the plutonium allotropes can be checked by a consideration of the thermal properties of a Pu-Ga alloy with ~3.3 at.% Ga, which stablizes the δ-phase at low temperatures. Taylor et al. [28] have measured the low-temperature heat capacities. The specific power for the sample used was consistent with the latest specific powers for the plutonium isotopes given by Oetting [27]. Integration of the C_p values gives

$$Pu_{0.968}Ga_{0.032}(\delta - \text{phase})S^0(298) = 67.82 \text{ J K}^{-1} \text{ mol}^{-1}$$

Rose et al., [29] have measured the enthalpy increments of an alloy of very similar composition. Their data give a smooth continuation of the heat-capacity values of Taylor et al., [28] as follows:

$$Pu_{0.967}Ga_{0.033}(\delta\text{ - phase})S(588) - S(298) = 22.59\ J\ K^{-1}\ mol^{-1}$$

and hence S(588) = 90.41 cal K^{-1} mol^{-1}.

Since $S^0(588) - S^0(298)$ for Ga(c) can be estimated from the values for the neighbouring elements (Hultgren et al.[4]) to be ~17.32 J K^1 mol^{-1}, we have:

Phase	S(588)(J K^{-1} mol^{-1})
Ga(c)	58.16
$Pu_{0.967}Ga_{0.033}(\delta)$	90.42
Pu(δ)	91.50

This is in excellent agreement with the value obtained by integration through the α-, β- and γ-phases, namely 91.17 J K^{-1} mol^{-1}.

Melting Point and Enthalpy of Fusion

Table B.1.3-3 includes a survey of the reported values for the melting point and enthalpy of fusion of plutonium metal. Again, more weight is given to the more recent data, and the suggested values are (913 ± 2) K for the melting point, and (2824 ± 105) J mol^{-1} for the enthalpy of fusion. The heat capacity of the liquid plutonium, measured just above the melting point, has been reported informally by two investigators (Loasby [30] and Engel [23]), with good agreement (41.84 and 42.68 J K^{-1} mol^{-1}, respectively). The average value of (42.4 ± 0.8) J K^{-1} mol^{-1} used in this assessment is in good agreement with the recent value of 42.7 J K^{-1} mol^{-1} (Thayer and Robbins, [22]).

TABLE B.1.3-3 Temperature and Enthalpy of Plutonium Transitions

Ref.	Method[a]	α→β		β→γ		γ→δ		δ→δ'		δ→ε		ε→liq	
		T (K)	ΔH_t (J mol^{-1})	T (K)	ΔH_t (J mol^{-1})	T (K)	ΔH_t (J mol^{-1})	T (K)	ΔH_t (J mol^{-1})	T (K)	ΔH_t (J mol^{-1})	T (K)	ΔH_t (J mol^{-1})
31	Dil	388		458		583		725		753			
32	TA	392 ± 2	3531 ± 42	477 ± 6	515 ± 25	588 ± 2	653 ± 63	730 ± 2	79 ± 25	752 ± 4	1724 ± 105		
23	Cal							741 ± 2	29 ± 13	754	1925 ± 33		
33		390 ± 0.5											
24	Cal	392	3360 ± 42	477	636 ± 63	584	523 ± 21	731	84 ± 42	753	1858 ± 42	911	2900 ± 42
34	Cal	400	3389 ± 21	480	519 ± 50	593	569 ± 29	733	105 ± 33	754	1845 ± 33	913	2741 ± 25
35	Dil	385 ± 1		457 ± 2									
36		395 ± 2		479 ± 3		592 ± 6		724 ± 4		749 ± 4		913	
37	Dil	383 ± 4		476 ± 6		586 ± 7		733 ± 5		749 ± 4			
38	TA	399 ± 2		482 ± 3		589 ± 2		729		757 ± 2		914 ± 2	
38	Dil	406		481		579		733		749		907	
39		396 ± 6	5021	488 ± 3	586	588 ± 2	544		<167	752 ± 7	1590	914 ± 2	2218
40	Res	396.7 ± 0.3	3925 ± 42	475 ± 2		591 ± 2		729 ± 2		757 ± 3			
41	Dil, TA	395	3201 ± 502	484	699 ± 105	588	799 ± 105	713	-0	733	1598 ± 293	908	3301 ± 502
42	Cal	394	4008 ± 42	481	586 ± 63	589	653 ± 63	728	71 ± 42	752	1966 ± 42		
43	Dil, TA	395 ± 2		478 ± 3		593 ± 5		725 ± 4		749 ± 5		913 ± 2	
*		395 ± 4	3431 ± 84	480 ± 5	565 ± 63	588 ± 3	586 ± 63	730 ± 2	84 ± 42	752 ± 4	1841 ± 84	913 ± 2	2824 ± 105

[a] Cal - calorimetric, Dil - dilatometric, Res - resistivity, TA - thermal analysis

* Suggested values

The heat capacity of Pu(α), $298 \le T \le 395$ K, in J K^{-1} mol^{-1} is given in the following equation:

$$C_p, Pu(\alpha) = 37.610 - (7.380 \times 10^{-2}\ T) + (1.939 \times 10^{-4}\ T^2).$$

The heat capacity of Pu(β), $395 \le T \le 480$ K, in J K^{-1} mol^{-1} is given by the following equation:

$$C_p, Pu(\beta) = 25.288 + (2.176 \times 10^{-2}\ T)$$

The heat capacity of Pu(γ), $480 \le T \le 588$ K, in J K^{-1} mol^{-1} is given by the following equation:

$$C_p, Pu(\gamma) = 21.615 + (2.824 \times 10^{-2}\ T)$$

For Pu(δ), Pu(δ'), Pu(ε), and Pu(ℓ), the heat capacity is constant. Recommended enthalpy data for plutonium are given in Table B.1.3-4 and Fig. B.1.3-D

High-temperature Heat Capacity and Enthalpy of Zirconium*

The selected values agree with the heat-content measurements of Douglas and Victor for 373-1173 K [44]; and with Jaeger and Veenstra for 505-1074 K [45]; except that the latter's data show more scatter and are about 3% lower below 600 K. The heat-content data of Fieldhouse and Lange for 472-1807 K [46] are 2% lower below 900 K, trending to 5% higher at 1100 K and averaging about 2.5% higher in the β range. Those of Redmond and Lones for 404-1309 K [47] are highly scattered, averaging about 7% higher in α and varying from

---

* This section adapted from B.1, Ref. 4.

TABLE B.1.3-4 High-temperature Heat Capacity and Enthalpy of Plutonium

T (K)	C_p ($J\ K^{-1}\ mol^{-1}$)	H(T) - H(298) ($J\ mol^{-1}$)
298	32.844	0
300	32.922	61
395(α)	38.715	3436
395(β)	33.882	6867
400	33.991	7036
480(β)	35.731	9825
480(γ)	35.171	10390
500	35.736	11099
588(γ)	38.221	14353
588(δ)	37.154	14939
600	37.154	15385
700	37.154	19100
730(δ)	37.154	20215
730(δ')	35.564	20299
752(δ')	35.564	21081
752(ε)	34.434	22922
800	34.434	24575
900	34.434	28018
913(ε)	34.434	28466
913(ℓ)	42.258	31290
1000	42.258	34967
1100	42.258	39192
1200	42.258	43418
1300	42.258	47644
1400	42.258	51870
1500	42.258	56096
1600	42.258	60322
1700	42.258	64547
1800	42.258	68733
1900	42.258	72999
2000	42.258	77225
2100	42.258	81451
2200	42.258	85657
2300	42.258	89903
2400	42.258	94128
2500	42.258	98354

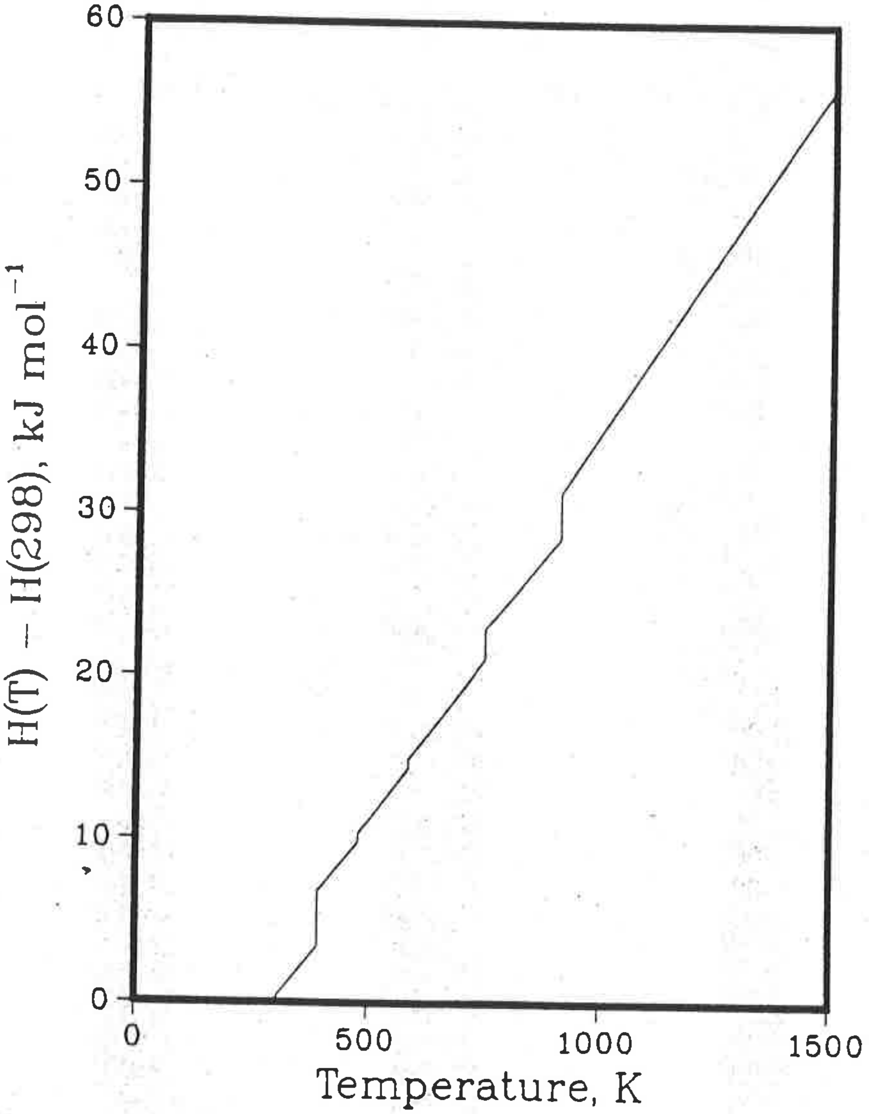

Fig. B.1.3-D Enthalpy, H(T) - H(298) kJ mol^{-1}, for Plutonium

8% to 0.4% lower in β. The heat-content data of Skinner for 1102-1798 K [48] are about 2% lower. Those of Coughlin and King for 390-1371 K [49] are about 3% higher in α and only about 1% higher in β. The C_p values of Klein and Danielson for 298-2118 K [50], obtained by a pulse heating method, are 10% lower in α and trend from 15% lower to 7% higher in β. Those of Scott for 333-1233 K [51] are 7% lower than the selected values.

Hertzricken and Slyuser [52], using a differential calorimeter, found $\Delta H(\alpha \rightarrow \beta) = 2979 \pm 250$ J mol^{-1}, considerably lower than the selected value; while Scott [8], from adiabatic calorimetry, found $\Delta H(\alpha \rightarrow \beta) = 4155 \pm 105$ J mol^{-1}, only slightly higher than the value chosen. $C_p(\beta) = 31.4$ J K^{-1} mol^{-1} was assumed to remain constant to the melting point. $\Delta S_m = 7.9$ J K^{-1} mol^{-1} was estimated.

The heat capacity of Zr(α), $298 \leq T \leq 1136$ K, in J K^{-1} mol^{-1} is given by the following equation:

$$\begin{aligned} C_p,Zr(\alpha) = 27.186 &+ (3.092 \times 10^{-3}\ T) \\ &+ (3.002 \times 10^{-6}\ T^2) \\ &- (2.651 \times 10^5\ T^{-2}). \end{aligned}$$

The heat capacities of Zr(β) and Zr(ℓ) are constant. Recommended enthalpy values are shown in Fig. B.1.3-E and Table B.1.3-5.

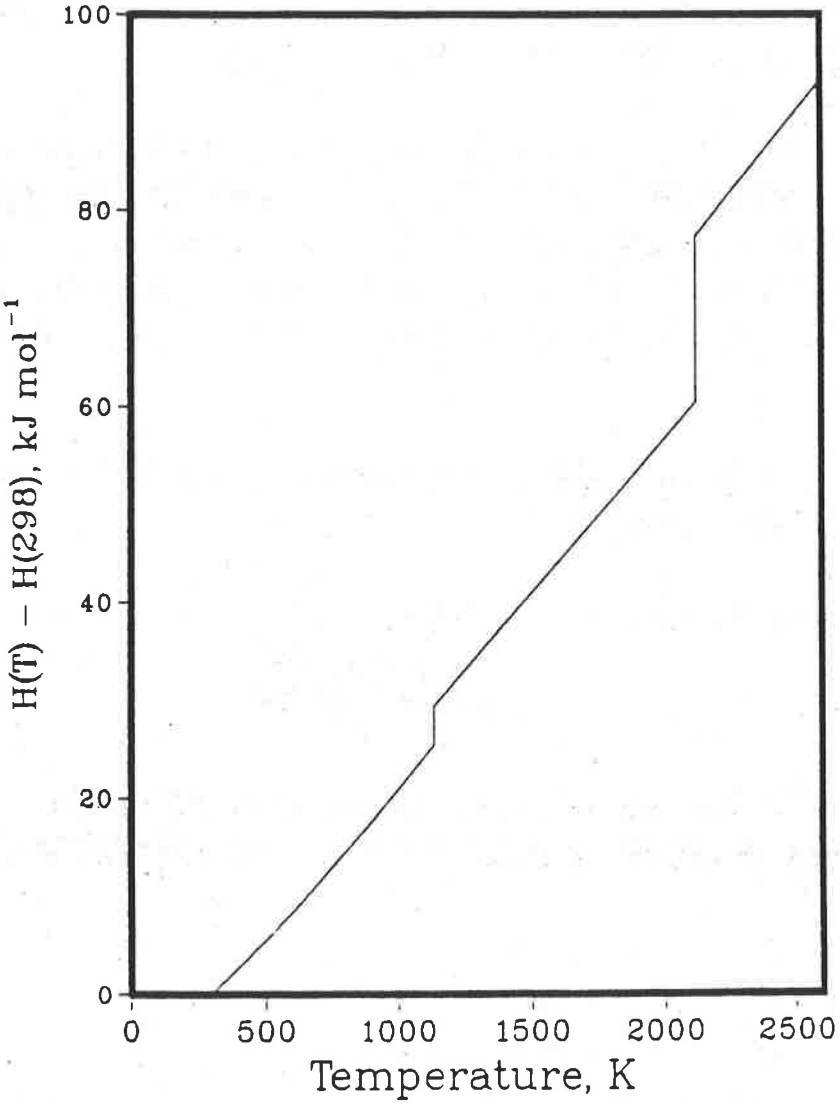

Fig. B.1.3-E Enthalpy, H(T) - H(298) kJ mol^{-1}, for Zirconium

TABLE B.1.3-5 High-temperature Heat Capacity and Enthalpy of Zirconium

T (K)	C_p ($J\ K^{-1}\ mol^{-1}$)	H(T) - H(298) ($J\ mol^{-1}$)
298	25.36	0
400	27.36	2703
500	28.37	5494
600	29.33	8381
700	30.25	11355
800	31.17	14431
900	32.13	17594
1000	33.05	20853
1100	34.02	24204
1136(α)	34.31	25434
1136(β)	31.4	29372
1200	31.4	31380
1300	31.4	34518
1400	31.4	37656
1500	31.4	40794
1600	31.4	43932
1700	31.4	47070
1800	31.4	50208
1900	31.4	53346
2000	31.4	56484
2100	31.4	59622
2125(β)	31.4	60409
2125(ℓ)	33.5	77304
2200	33.5	79814
2400	33.5	86508
2600	33.5	93203

B. THERMODYNAMICS

B.2 Phase Equilibria

B.2.1 Uranium-Zirconium Alloys (and Other Binary Systems)

U-Zr: The uranium-zirconium phase diagram, as shown in Fig. B.2.1-A, was taken from Ref. 18. Only one intermediate phase, δ, exists in this system. It is unstable above 890 K. The body-centered cubic forms of uranium (γ) and zirconium (β) are completely miscible. The δ-phase has a composition range of 67-73 at.% Zr. Its crystal structure appears to be uncertain and has been described as simple hexagonal, body-centered cubic, or hexagonal--isotypic with $InNi_2$ [10].

U-Pu: Figure B.2.1-B shows the U-Pu phase diagram, taken from Ref. 18. The diagram indicates that although there is agreement on its general form, precise values for the phase limits as a function of temperature are still not well established. There are two phases in addition to the nine allotropes of the end members: a ζ-phase, entending from about 25 to 70 at.% U, and a tetragonal η-phase which is stable only between 551 and 978 K, from about 5 to 70 at.% U. The ζ-phase is described as "cubic (at 300 K)" in Ref. 18 and as tetragonal in Ref. 10. Note that Pu(ε) and U(γ) form a continuous solid-solution region although this solid solution is stable over a range of only about 20 K between 25 and 45 at.% U.

Pu-Zr: The Pu-Zr phase diagram, shown in Fig. B.2.1-C, was also taken from Ref. 9. Elliot [11] describes the Pu-Zr system as having the following features: continuous solid solubility between Pu (ε) and Zr (β), with a constantly rising solidus from Pu to Zr; two intermediate phases; an extended Pu (δ) solid-solution field (to about 70 at.% Zr) which gives rise to two eutectoids; and a rather large Zr (α) solid-solution field (13-15 at.% Pu). The two intermediate phases are Pu_6Zr and $PuZr_2$. These are believed to be, respectively, orthorhombic and hexagonal.

Assessed U-Zr Phase Diagram

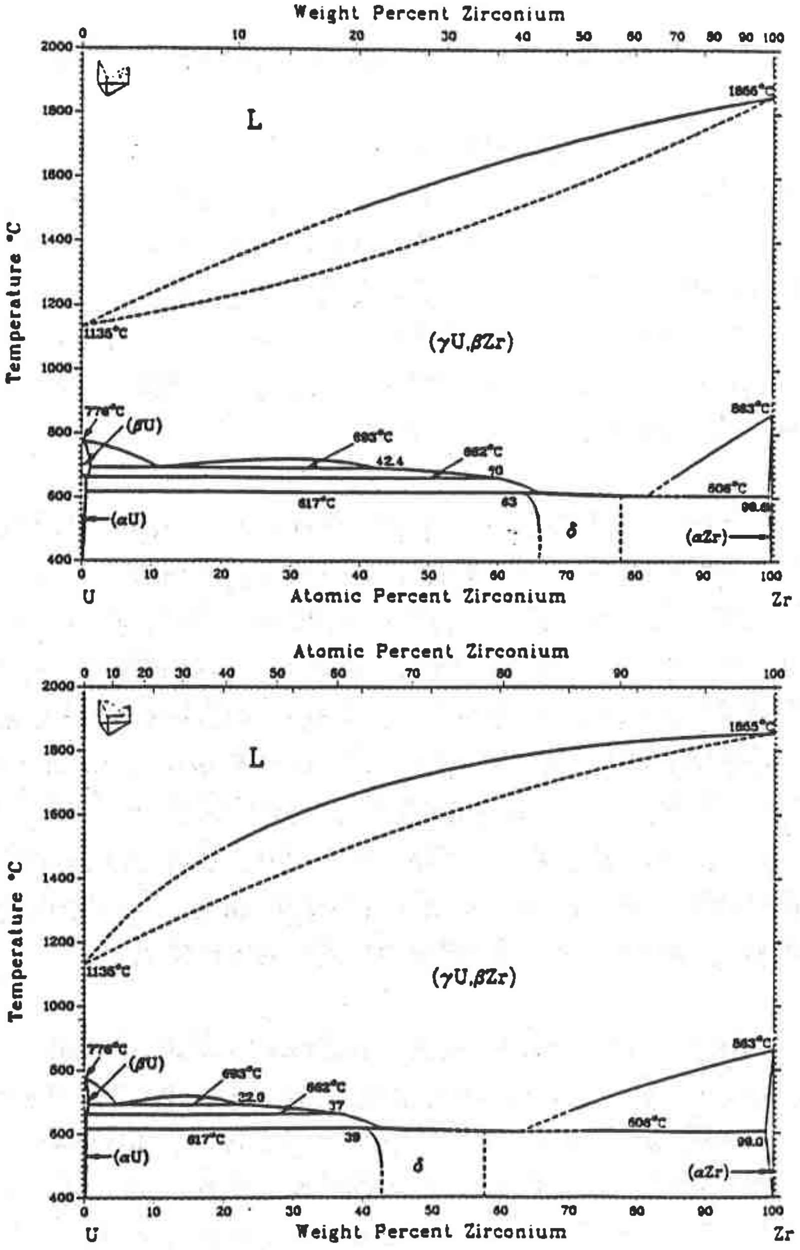

Fig. B.2.1-A. Phase Diagram of the System Uranium-Zirconium

Assessed Pu-U Phase Diagram

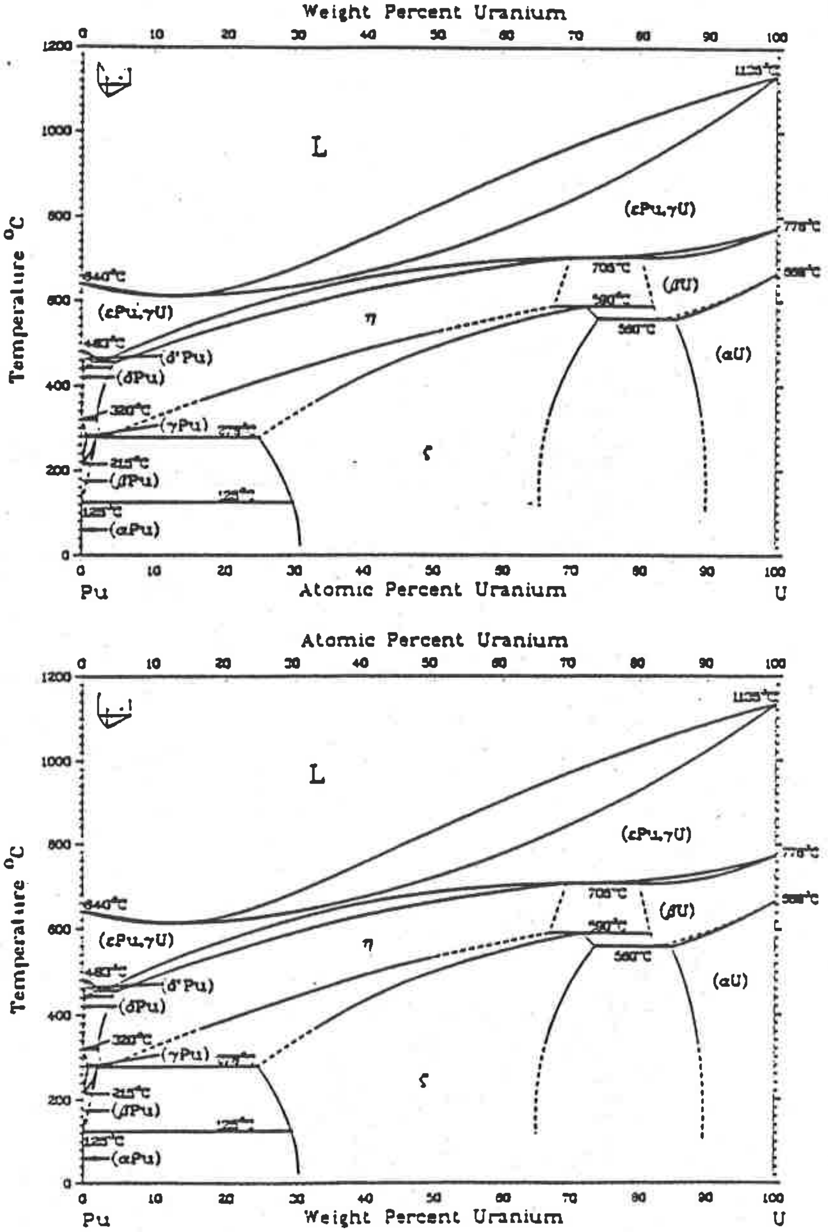

Fig. B.2.1-B. Phase Diagram of the System Plutonium-Uranium

Pu-Zr Phase Diagram

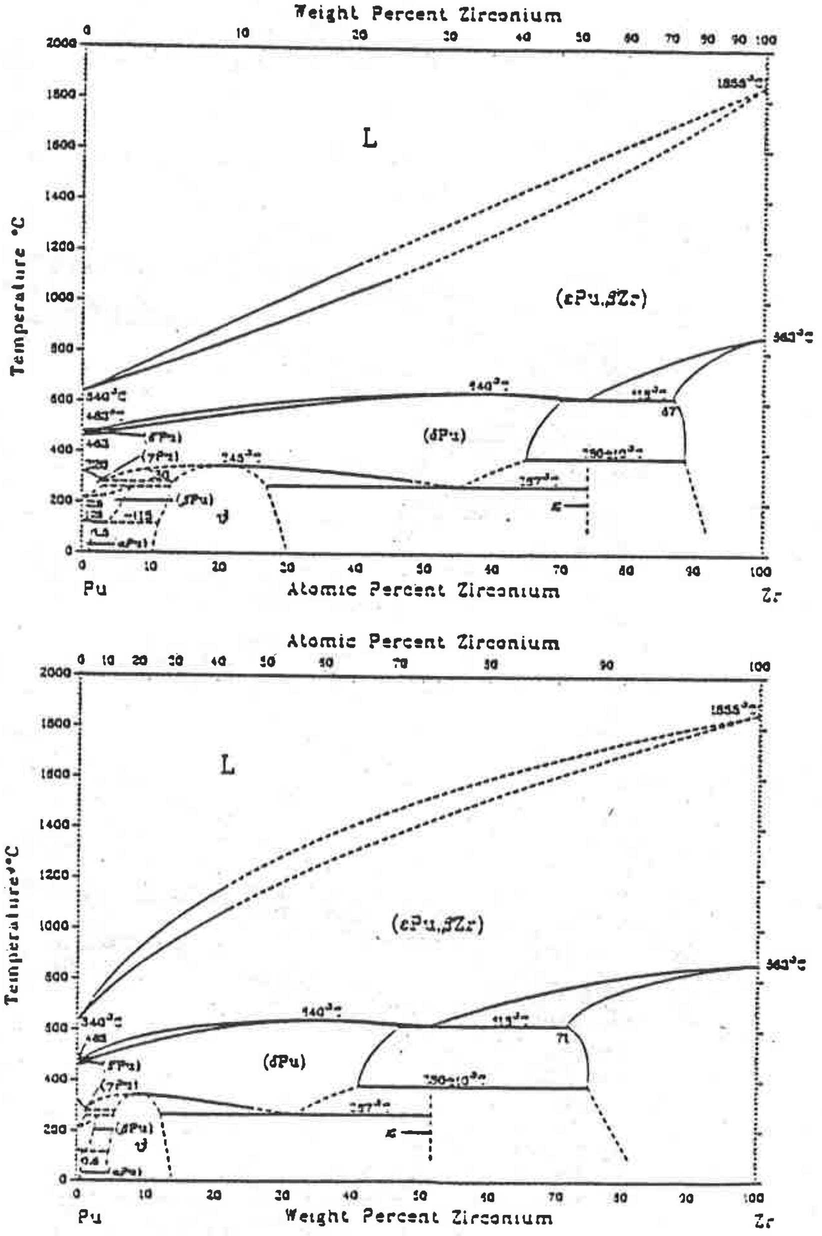

Fig. B.2.1-C. Phase Diagram of the Plutonium-Zirconium System

B.2.2 Uranium-Plutonium-Zirconium Alloys

Solid-state Transitions: A detailed study of solid-state transitions in the ternary system performed at Argonne National Laboratory was reported by O'Boyle and Dwight [1]. A study of the system was performed by the Mound Laboratory [3] with emphasis on melting in the plutonium corner of the phase diagram. Some early measurements on phase transitions in the solid state were reported by CEA [12] and by Argonne [13].

The following description of the phases in the ternary system is taken from Ref. 1. The same nomenclature is used to identify both the binary and the ternary phases. The following are the phases existing in the ternary alloy.

γ:	Body-centered cubic phase showing complete miscibility for U(γ), Pu(ϵ), and Zr(β). The designations γ_1 and γ_2 are used in [1] to denote the uranium-rich and zirconium-rich sides of the miscibility gap in the γ phase.
α,β:	Orthorhombic and tetragonal uranium allotropes dissolving up to 15 and 20 at.% Pu respectively, but little Zr.
η:	Tetragonal intermediate phase in the U-Pu binary with limited solubility for Zr.
ζ:	Tetragonal intermediate phase in the U-Pu system with up to 5 at.% solubility for Zr. This is referred to in Ref. 1 as a cubic phase but is likely tetragonal [7].

δ:	Hexagonal phase in the U-Zr system with extensive solid solubility for Pu.
Pu (δ):	Face-centered cubic Pu phase with extensive solid solubility for Zr but very limited solubility for U.

Reference 1 displays these phase relationships in a series of isothermal ternary diagrams at temperatures from 500°C to 700°C. These diagrams contain some errors and inconsistencies, especially in agreement with the U-Pu binary. For example, the 500°C diagram is missing a boundary between the ζ and α + ζ phase fields. Therefore, the diagrams must be used cautiously.

The general features of the solid-phase equilibria are as follows: Below the solidus temperature the three elements show complete miscibility of the body-centered-cubic high-temperature allotropes U (γ), Pu (ε), Zr (β). The body-centered cubic γ-phase is stabilized by additions of zirconium and plutonium. With decreasing temperatures from 700 to 600°C, the gamma single-phase boundary sweeps rapidly from the U-Zr and U-Pu binary sides of the system toward the Zr-Pu side of the system. The major four-phase reactions in the uranium corner of the system are $\gamma + \beta \rightarrow \alpha + \zeta$ at 650°C and $\gamma + \alpha \rightarrow \delta + \zeta$ at 595°C. These reactions may be involved in the zone formation observed on heating the ternary alloy in thermal gradients [14,15].

Solidus-Liquidus: Calculations of the solidus and liquidus surfaces for the ternary U-Pu-Zr system have been performed by Dr. Arthur D. Pelton, McGill University, Ecole Polytechnique, using the system "Facility for the Analysis of Chemical Thermodynamics" (F*A*C*T) [8]. These calculations were performed using data and methods described in [19]. Data for the three binary systems were critically evaluated and used to calculate thermodynamic properties for the ternary system. From these data ternary phase diagrams were calculated. Error limits on the binary and ternary solidus and liquidus curves were estimated. Activity coefficients for all three components of the ternary system were calculated for solutions near the melting region. In the figure that follows (B.2.2-A) isothermal sections are presented showing solidus and liquidus curves from 700-1700°C. The equations used to calculate solidus and liquidus temperatures are given in [19]. Near the median of the composition triangle, error limits are estimated as ±75° for the liquidus and ±125° for the solidus. For example, the proposed PRISM fuel (U-26Pu-10Zr) has a measured solidus of 1059±6°C and a calculated one of 1024°C, while the measured liquidus is 1314±13°C as opposed to a calculated 1262°C [20].

Curves giving solidus temperatures for this system have been published previously [16] but no detail has been given on the source of the data. These calculations are in good agreement with measured solidus and liquidus temperatures reported in Ref. 17. Ternary isotherms in the Pu corner of the diagram reported by Mound [3] give liquidus temperatures in the Pu-Zr binary much higher than any other reported values and have been discounted by Pelton.

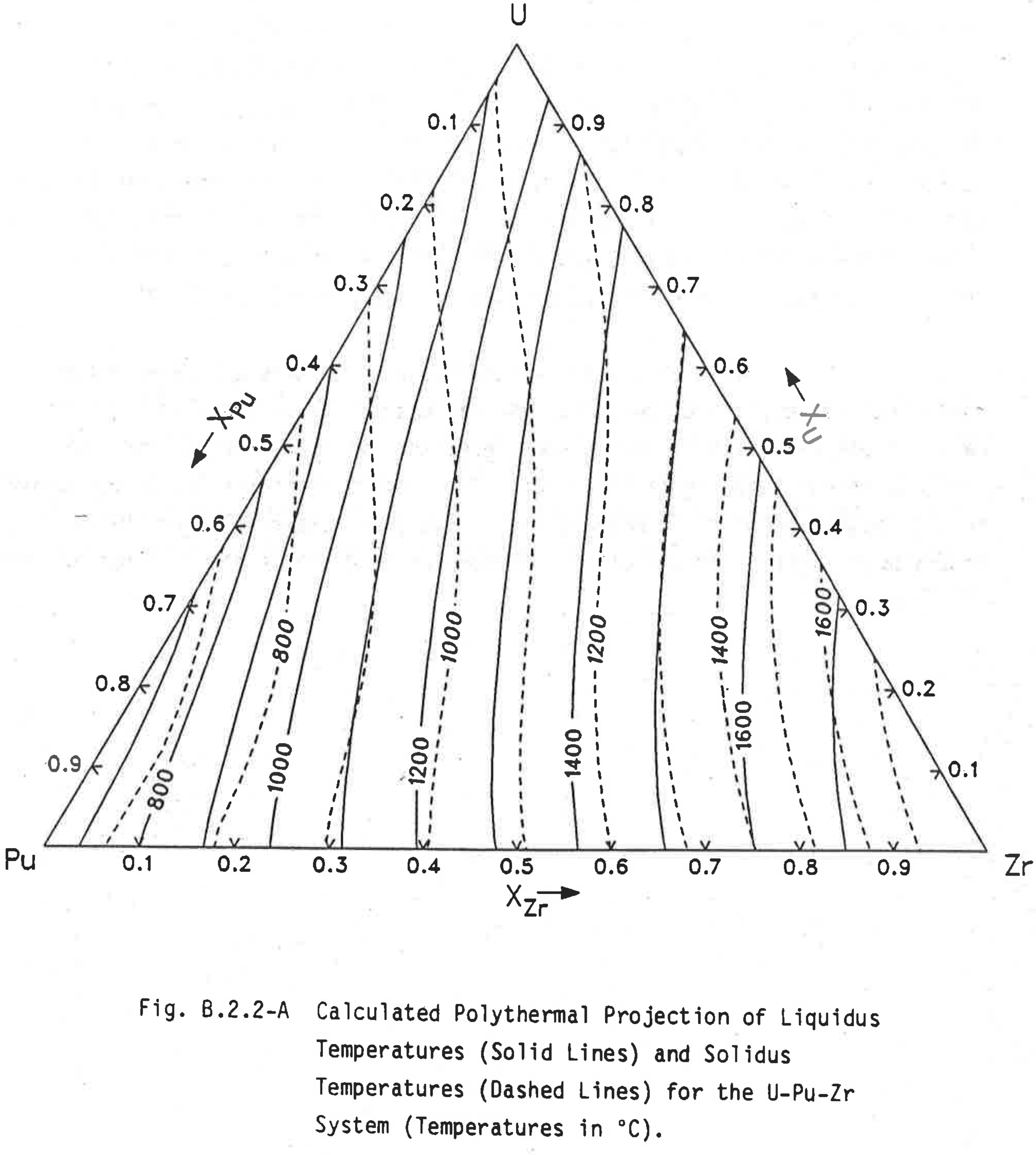

Fig. B.2.2-A Calculated Polythermal Projection of Liquidus Temperatures (Solid Lines) and Solidus Temperatures (Dashed Lines) for the U-Pu-Zr System (Temperatures in °C).

B.2.3 Others

The phase-transition temperatures, heats of transition, and crystal structures for the allotropic forms of uranium, plutonium, and zirconium are summarized in Table B.2.3-1. Data for uranium and plutonium have been taken from an IAEA assessment [4], while data for zirconium have been taken from the compilation of Hultgren and coworkers [5]. For the convenience of the readers, Fig. B.2.3-A and Table B.2.3-2, adapted from Ref. 6, have been included. These show the differences among the crystal systems discussed, in terms of the axes a, b, and c and the angles α, β, and γ.

The IAEA [4] in its assessment relied heavily on the data of Blumenthal [7] for transition temperatures of uranium because of the high purity of his uranium and his avoidance of effects of hysteresis, superheating, and undercooling. The IAEA [4] converted Blumenthal's temperatures from the 1948 International Practical Temperature Scale (IPTS-1948) to IPTS-1968, which raised his values by about 2 K at the melting point. For this reason there are slight differences between Ref. 4 which uses IPTS-1968, and Ref. 5, which uses IPTS-1948, even though the same data are recommended. Pelton [8] questions the value chosen by the IAEA [4] for the enthalpy of fusion of uranium (9.142 kJ/mol) on the basis that it gives poor agreement with the Pu-U binary phase diagram, and recommends 12.134 kJ/mol. It seems unlikely that the IAEA value, obtained calorimetrically, is in error by such a large amount, and we have retained the IAEA value. There is clearly an inconsistency, however, which at present remains unresolved.

Plutonium is unique in having six allotropes stable at atmospheric pressure. Extensive studies have been made on the crystalline forms of plutonium but there is comparatively wide scatter in the results. This is probably due to the presence of impurities, hysteresis, sluggish transformations, and self-heating of the sample material. In its assessment the IAEA [4] heavily weighted the more recent data.

TABLE B.2.3-1 Phase Transitions and Structures in U, Pu, and Zr

Phase	Structure[a]	Transition[b]	T (K)	ΔH_t (kJ mol^{-1})
U(α)	orthorhombic	α → β	942	2.791
U(β)	tetragonal	β → γ	1049	4.757
U(γ)	b.c. cubic	γ → liq	1408	9.142
Pu(α)	monoclinic	α → β	395	3.431
Pu(β)	b.c. monoclinic	β → γ	480	0.565
Pu(γ)	f.c. orthorhombic	γ → δ	588	0.586
Pu(δ)	f.c. cubic	δ → δ'	730	0.084
Pu(δ')	b.c. tetragonal	δ' → ε	752	1.841
Pu(ε)	b.c. cubic	ε → liq	913	2.824
Zr(α)	h.c.p.	α → β	1136	3.937
Zr(β)	b.c. cubic	β → liq	2125	16.895

[a] b.c = body-centered; f.c = face centered; h.c.p = hexagonal close packed

[b] liq = liquid

TABLE B.2.3-2. The Crystal System [6]

System	Axes and Interaxial Angles
Triclinic	$a \neq b \neq c$; $\alpha \neq \beta \neq \gamma \neq 90°$
Monoclinic	$a \neq b \neq c$; $\alpha = \gamma = 90° \neq \beta$
Orthorhombic	$a \neq b \neq c$; $\alpha = \beta = \gamma = 90°$
Tetragonal	$a = b \neq c$; $\alpha = \beta = \gamma = 90°$
Cubic	$a = b = c$; $\alpha = \beta = \gamma = 90°$
Hexagonal	$a = b \neq c$; $\alpha = \beta = 90°$; $\gamma = 120°$
Trigonal	$a = b = c$; $\alpha = \beta = \gamma \neq 90°$

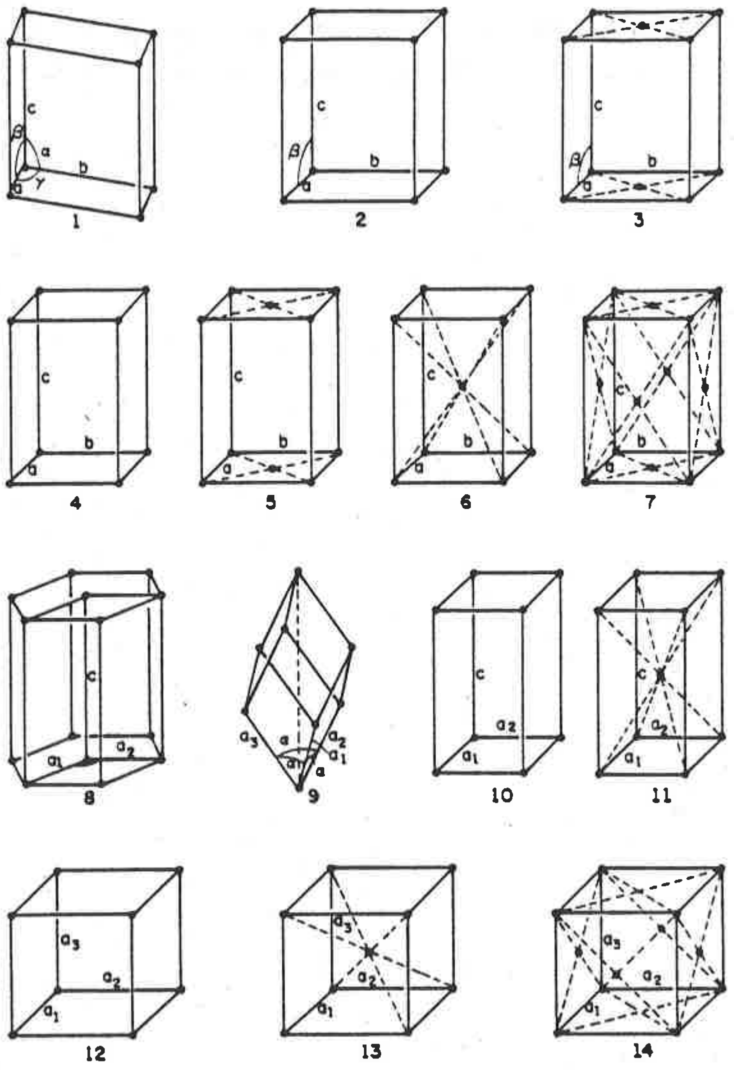

Fig. B.2.3-A The 14 Space Lattices Illustrated by a Unit Cell of Each: (1) triclinic, simple (2) monoclinic, simple, (3) monoclinic, base-centered, (4) orthorhombic, simple, (5) orthorhombic, base-centered, (6) orthorhombic, body-centered, (7) orthorhombic, face-centred, (8) hexagonal, (9) rhombohedral, (10), tetragonal, simple, (11) tetragonal, body-centered, (12) cubic, simple, (13) cubic-body-centered, (14) cubic, face-centred. [6]

Of particular importance is the fact that the high-temperature phases for all three metals, U(γ), Pu(ε), and Zr(β) have the same structure, namely body-centered cubic. As was seen earlier in the binary and ternary systems, continuous solid solution exists for the high-temperature solids.

B. THERMODYNAMICS

B.3 Density and Thermal Expansion

General Relations

The thermal-expansion coefficient (α_P), is a thermodynamic quantity defined as

$$\alpha_P = \frac{1}{V}\left(\frac{\partial V}{\partial T}\right)_P$$

where P, V, and T are respectively pressure, volume, and temperature. We will refer to (α_P) as the instantaneous volumetric thermal-expansion coefficient. For simplicity we will eliminate the subscript P from the coefficients in the following discussion and understand that constant pressure is implied in all the equations following. The mean volumetric thermal-expansion coefficient is defined as

$$\bar{\alpha} = \frac{1}{V_o}\left(\frac{V - V_o}{T - T_o}\right)$$

where V and V_o are the volumes at temperatures T and T_o respectively. Because many measurements of thermal expansion involve measurement of a length change, it is common to find tabulations of the fractional (or percent) change in length,

$$\frac{\Delta L}{L_o} = \left(\frac{L - L_o}{L_o}\right)$$

where L and L_o are respectively the sample lengths at temperatures T and T_o. The instantaneous and mean linear thermal-expansion coefficients are thus respectively

$$\alpha_\ell = \frac{1}{L}\left(\frac{\partial L}{\partial T}\right)$$

and

$$\bar{\alpha}_\ell = \frac{1}{L_o}\left(\frac{L - L_o}{T - T_o}\right)$$

The instantaneous volumetric thermal-expansion coefficient is just three times the instantaneous linear thermal-expansion coefficient; i.e, $\alpha = 3\alpha_\ell$. The same relation does not hold exactly for the mean coefficient, as the following considerations show. We write the mean volumetric coefficent as:

$$\bar{\alpha} = \frac{1}{\Delta T}\left(\frac{V}{V_o} - 1\right)$$

Since $V = L^3$ we find from the definition of the mean linear coefficient

$$\frac{V}{V_o} = (1 + \bar{\alpha}_\ell \Delta T)^3$$

whence

$$\bar{\alpha} = 3\bar{\alpha}_\ell + 3\Delta T\bar{\alpha}_\ell^2 + \Delta T^2\bar{\alpha}_\ell^3$$

The error introduced by taking only the first term in this equation will generally be small in many applications. For example if we take $\Delta T = 1000$ and $\bar{\alpha}_\ell = 1 \times 10^{-5}$, only a 1% error will be introduced by ignoring the last two terms. The relation between linear thermal expansion and density (ρ) is given by

$$\frac{\Delta\rho}{\rho_o} = \frac{1 - (1 + \Delta L/L_o)^3}{(1 + \Delta L/L_o)^3}$$

where $\Delta\rho = \rho - \rho_o$ is the difference between densities at temperatures T and T_o.

B.3.1 Uranium-Zirconium Alloys

Data for the thermal expansion of U-10 wt % Zr and U-20 wt % Zr are given in [1], which cites Saller et al. [9] as the source. The tabulated values for density were calculated by us, using ρ_0 values obtained assuming an ideal solution [10]. These data are plotted in Fig. B.3.1-A along with data for uranium [1]. The tabulated values of $\Delta L/L_0$ for well-annealed alloys are considered accurate to within ±7% over the entire temperature range [1]. The tabulated values for the 10% and 20% alloys are represented by the following equations given in Ref. 1:

$$\frac{\Delta L}{L_0}(\%)(\text{U-10 Zr}) = -0.424 + (1.658 \times 10^{-3}\ T) - (1.052 \times 10^{-6}\ T^2) + (1.115 \times 10^{-9}\ T^3) \qquad (293 \le T \le 900\text{K})$$

$$\frac{\Delta L}{L_0}(\%)(\text{U-20 Zr}) = -0.301 + (1.160 \times 10^{-3}\ T) - (7.790 \times 10^{-7}\ T^2) + (1.080 \times 10^{-9}\ T^3) \qquad (293 \le T \le 900\text{K})$$

From the linear thermal-expansion data and the above equation, the following equations were derived for ρ/ρ_0 for U-10 wt % Zr.

$$\rho/\rho_0 = 1.0122 - (4.629 \times 10^{-5}\ T) + (2.438 \times 10^{-8}\ T^2) - (2.805 \times 10^{-11} T^3) \qquad (293 \le T \le 900\text{K})$$

$$\rho/\rho_0 = 1.0125 - (6.25 \times 10^{-5}\ T) \qquad (1000 \le T \le 1200\text{K})$$

For compositions for which data are not available, an ideal-solution approximation should provide reasonable estimates. Values for density as well as mean and instantaneous linear thermal-expansion coefficients are given in Tables B.3.1-1 and B.3.1-2.

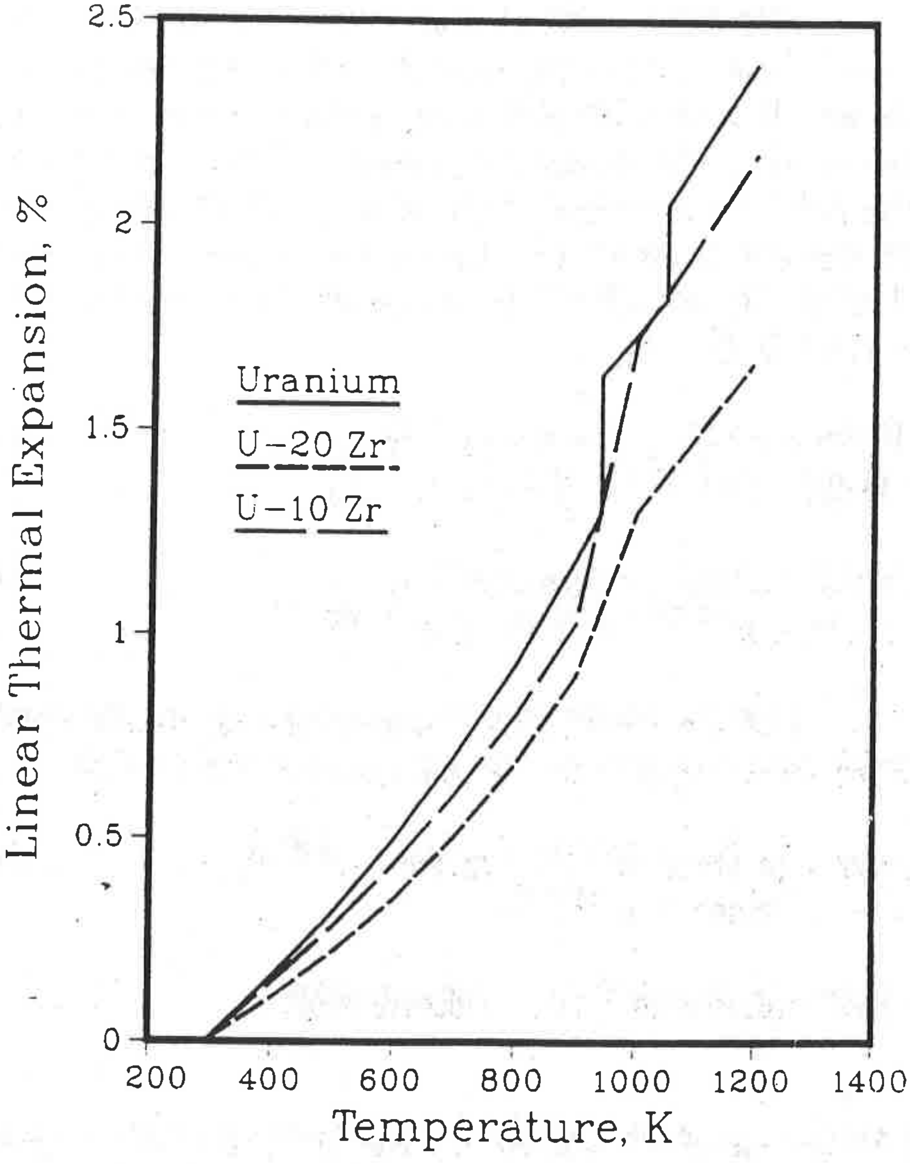

Fig. B.3.1-A. Mean Linear Thermal Expansion ($\Delta L/L_0$,%) for Uranium, U-10 wt % Zr, and U-20 wt % Zr

TABLE B.3.1-1. Density and Linear Thermal Expansion of U-10 wt % Zr

T (K)	ρ (g cm^{-3})	$\Delta L/L_o$ (%)	$\alpha_\ell \times 10^6$ (K^{-1})
293	16.02	0.000	13.2
400	15.95	0.142	13.5
500	15.89	0.281	14.2
600	15.81	0.433	16.0
700	15.73	0.603	18.2
800	15.64	0.799	21.1
900	15.54	1.027	24.7
1000	15.22	1.725	22.5
1100	15.12	1.950	22.5
1200	15.02	2.175	22.5

TABLE B.3.1-2. Density and Linear Thermal Expansion of U-20 wt % Zr

T (K)	ρ (g cm^{-3})	$\Delta L/L_o$ (%)	$\alpha_\ell \times 10^6$ (K^{-1})
293	13.81	0.000	9.8
400	13.77	0.107	10.5
500	13.72	0.219	11.9
600	13.67	0.348	13.9
700	13.60	0.500	16.6
800	13.53	0.681	19.9
900	13.44	0.899	24.1
1000	13.29	1.300	18.7
1100	13.21	1.487	18.7
1200	13.14	1.674	18.7

B.3.2 Uranium-Plutonium-Zirconium Alloys

Data on density and thermal expansion coefficients for some ternary alloys have been reported by CEA [11], ANL [12], and LASL [13]. The available density (for "as-cast" alloys) and thermal-expansion data are summarized in Table B.3.2-1.

In this table $\bar{\alpha}_1$ and $\bar{\alpha}_2$ are the mean thermal-expansion coefficients below and above the solid-state phase-transition region, between about 600 and 700°C, and $\Delta L/L_0$ is the expansion within the transition region. The densities given in Ref. 11 are at 20°C; those in [12] are at 25°C; no temperature is given in [13] but "room temperature" may be assumed. The transition ranges tabulated are those reported in each reference. For Ref. 13, for which heating and cooling ranges are reported, the temperatures tabulated were those for the start of the transition on heating. In calculating expansion of these alloys, $\bar{\alpha}_1$ should be applied up to the start of the transition, $\Delta L/L_0$ through the transition, and $\bar{\alpha}_2$ above the transition region to the solidus temperatures. For the alloy U-15 wt % Pu-10 wt % Zr, we have chosen the data of [12b]. For calculations of densities for compositions or temperatures where there are no data, an ideal-solution approximation is recommended for the present. Thermal-expansion data for the U-15 wt % Pu-10 wt % Zr alloy are shown in Fig. B.3.2-A and Table B.3.2-2.

New experimental data for U-19 wt % Pu-10 wt % Zr and U-26 wt % Pu-10 wt % Zr have been obtained. These are respectively provided in Tables B.3.2-3 and B.3.2-4 and Figs. B.3.2-B and B.3.2-C.

TABLE B.3.2-1. Density and Thermal-expansion Coefficients of U-Pu-Zr Alloys

Composition (Pu-Zr wt %)	Ref.	Density (g/cm^3)	$\bar{\alpha}_1 \times 10^6$ (K^{-1})	$\Delta L/L_o \times 10^3$	$\bar{\alpha}_2 \times 10^6$ (K^{-1})	Transition Range (°C)
15-10	11	15.67	16.3	-	-	600-645
20-10	11	15.73	17.3	-	-	586-650
11.1-6.3	12b	16.8	18.3	5.1	18.1	595-680
15-10	12b	15.8	17.6	5.2	20.1	595-665
18.5-14.1	12b	14.8	17.5	5.0	20.0	595-660
15-6.8	13	16.6	-	-	-	588-643
15-13.5	13	15.0	-	-	-	588-638

TABLE B.3.2-2. Density and Linear Thermal Expansion of U-15 wt % Pu-10 wt % Zr

T (K)	ρ (g cm^{-3})	$\Delta L/L_o$ (%)	$\alpha_\ell \times 10^6$ (K^{-1})
298	15.80	0.000	17.6
400	15.72	0.180	17.6
500	15.63	0.356	17.6
600	15.55	0.532	17.6
700	15.47	0.708	17.6
800	15.39	0.884	17.6
868	15.33	1.004	17.6
938	15.17	1.524	20.1
1000	15.11	1.649	20.1
1100	15.02	1.850	20.1
1200	14.93	2.051	20.1
1300	14.85	2.252	20.1
1378	14.78	2.409	20.1

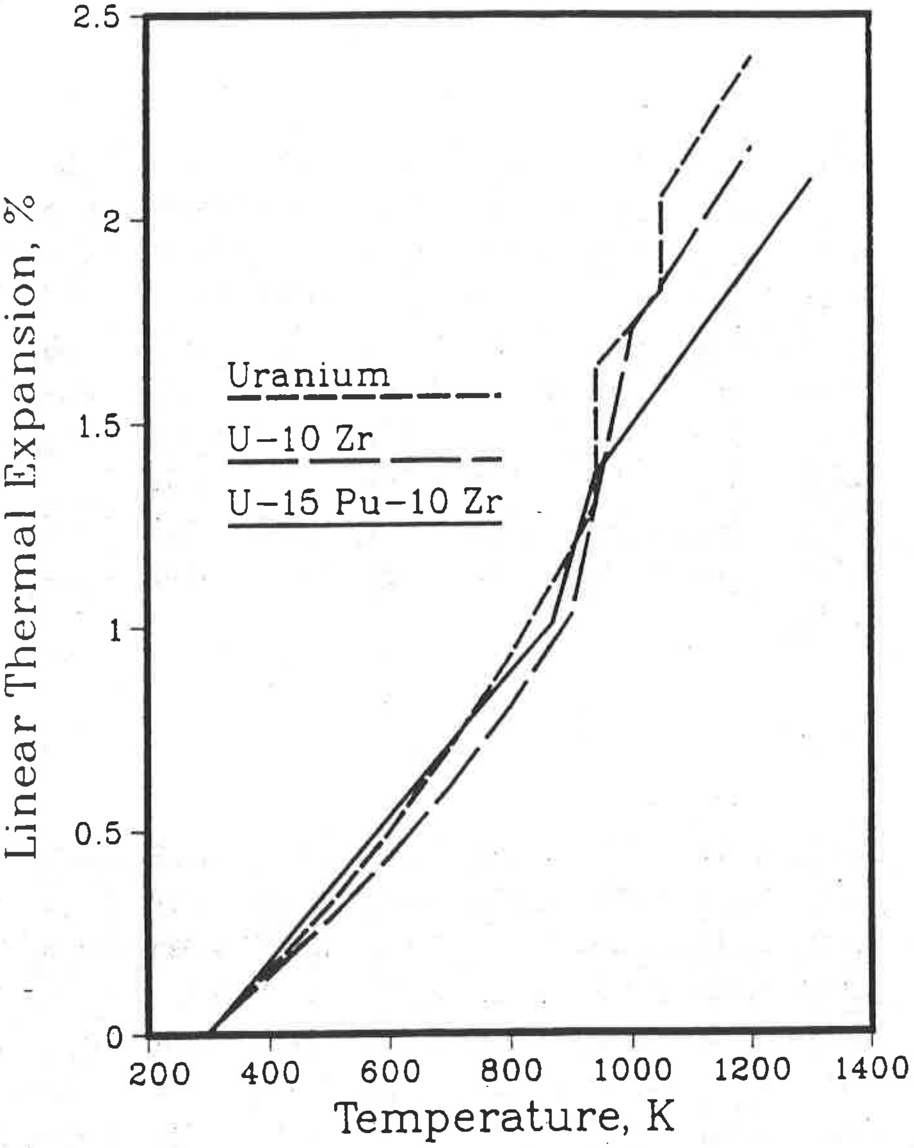

Fig. B.3.2-A. Mean Linear Thermal-expansion Coefficients ($\Delta L/L_0$,%) for Uranium, U-10 wt % Zr, and U-15 wt % Pu-10 wt % Zr

TABLE B.3.2-3. Thermal Expansion U-19 wt % Pu-10 wt % Zr

Heating T,°C	0	10	20	30	40	50	60	70	80	90
100	0.103	0.115	0.128	0.141	0.154	0.168	0.181	0.195	0.210	0.225
200	0.242	0.259	0.278	0.296	0.314	0.332	0.351	0.370	0.390	0.411
300	0.431	0.452	0.473	0.493	0.514	0.535	0.556	0.576	0.597	0.618
400	0.638	0.659	0.681	0.703	0.724	0.746	0.768	0.791	0.814	0.837
500	0.860	0.884	0.907	0.931	0.955	0.980	1.004	1.029	1.058	1.105
600	1.146	1.178	1.210	1.244	1.283	1.333	1.457	1.548	1.620	1.643
700	1.662	1.683	1.705	1.726	1.748	1.770	1.792	1.814	1.837	1.859
800	1.881	1.903	1.926	1.948	1.970	1.992	2.015	2.037	2.059	2.082
900	2.104	2.127	2.150	2.172	2.195	2.218	2.241	2.264	2.288	2.310
1000	2.334									

Cooling T,°C										
100	0.112	0.126	0.139	0.155	0.169	0.184	0.199	0.215	0.232	0.249
200	0.267	0.285	0.303	0.322	0.342	0.362	0.382	0.403	0.423	0.444
300	0.465	0.486	0.508	0.530	0.552	0.574	0.595	0.618	0.640	0.662
400	0.685	0.708	0.730	0.753	0.776	0.799	0.822	0.846	0.870	0.894
500	0.918	0.943	0.967	0.991	1.017	1.042	1.067	1.093	1.134	1.179
600	1.215	1.247	1.288	1.410	1.509	1.573	1.605	1.626	1.646	1.666
700	1.687	1.707	1.728	1.748	1.769	1.790	1.811	1.832	1.853	1.874
800	1.896	1.917	1.939	1.961	1.982	2.004	2.025	2.047	2.068	2.090
900	2.112	2.133	2.156	2.177	2.200	2.222	2.244	2.267	2.290	2.312
1000	2.335									

TABLE B.3.2-4. Thermal Expansion U-26 wt % Pu-10 wt % Zr

Heating T,°C	0	10	20	30	40	50	60	70	80	90
100	0.108	0.121	0.134	0.148	0.162	0.176	0.190	0.205	0.220	0.236
200	0.253	0.271	0.289	0.310	0.329	0.348	0.368	0.389	0.410	0.432
300	0.455	0.478	0.499	0.522	0.545	0.568	0.590	0.614	0.637	0.660
400	0.683	0.706	0.729	0.753	0.776	0.801	0.824	0.849	0.874	0.899
500	0.924	0.950	0.975	1.001	1.028	1.055	1.081	1.114	1.182	1.239
600	1.276	1.315	1.357	1.405	1.465	1.568	1.705	1.791	1.823	1.846
700	1.868	1.890	1.913	1.936	1.959	1.981	2.004	2.026	2.049	2.072
800	2.095	2.118	2.141	2.163	2.186	2.209	2.232	2.255	2.278	2.301
900	2.327	2.347	2.371	2.394	2.418	2.440	2.464			

Cooling T,°C										
100	0.118	0.133	0.147	0.162	0.177	0.192	0.208	0.224	0.241	0.258
200	0.276	0.295	0.315	0.334	0.355	0.375	0.396	0.417	0.440	0.463
300	0.485	0.508	0.532	0.555	0.579	0.602	0.627	0.650	0.674	0.698
400	0.723	0.747	0.771	0.796	0.821	0.846	0.871	0.897	0.922	0.948
500	0.974	1.001	1.027	1.054	1.080	1.108	1.135	1.194	1.254	1.296
600	1.333	1.373	1.435	1.600	1.721	1.771	1.795	1.818	1.840	1.862
700	1.885	1.907	1.929	1.951	1.973	1.995	2.018	2.040	2.063	2.085
800	2.107	2.129	2.151	2.174	2.196	2.219	2.241	2.264	2.285	2.308
900	2.331	2.353	2.375	2.398	2.420	2.443	2.466			

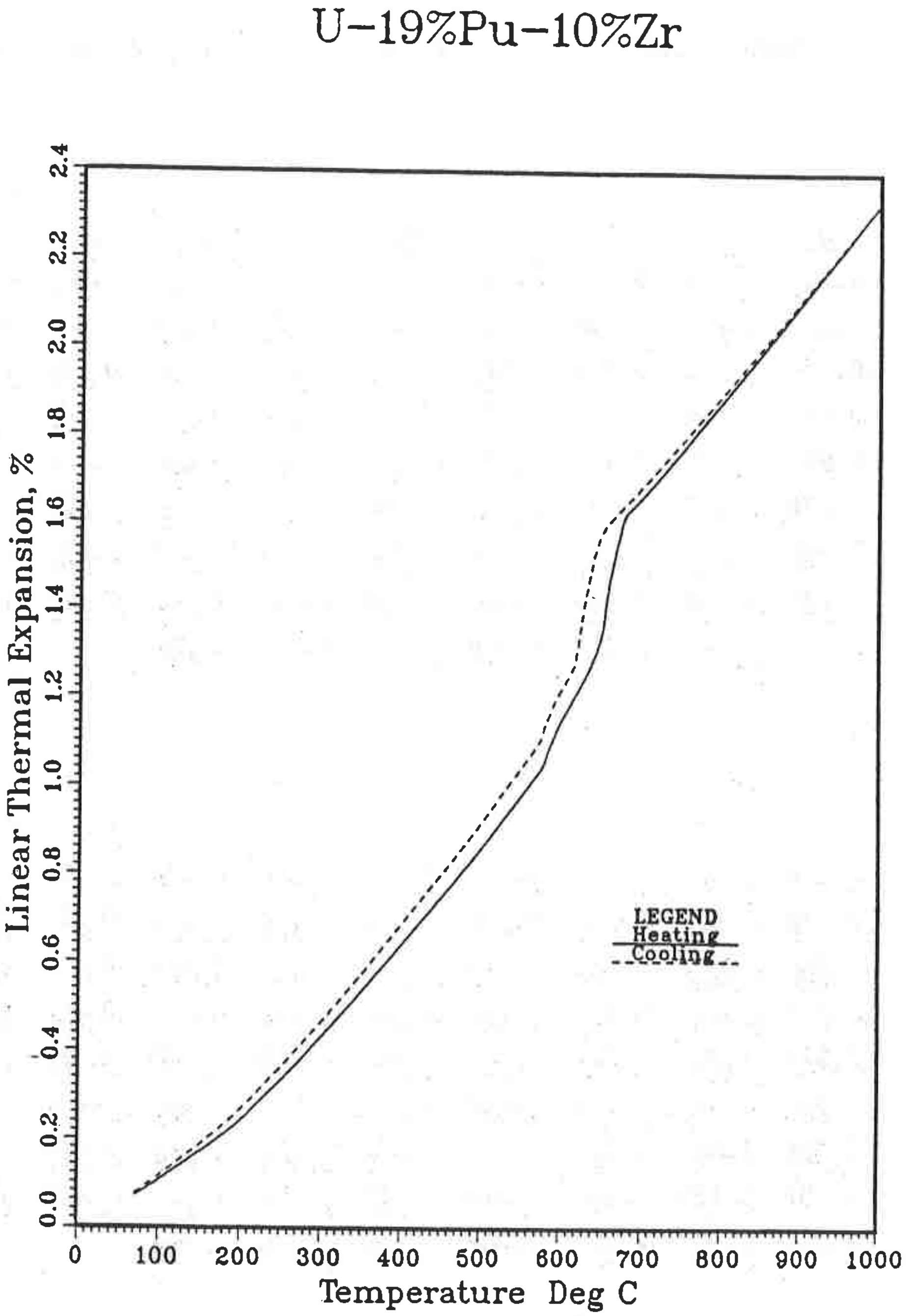

Fig. B.3.2-B Thermal Expansion of U-19 wt % Pu-10 wt % Zr

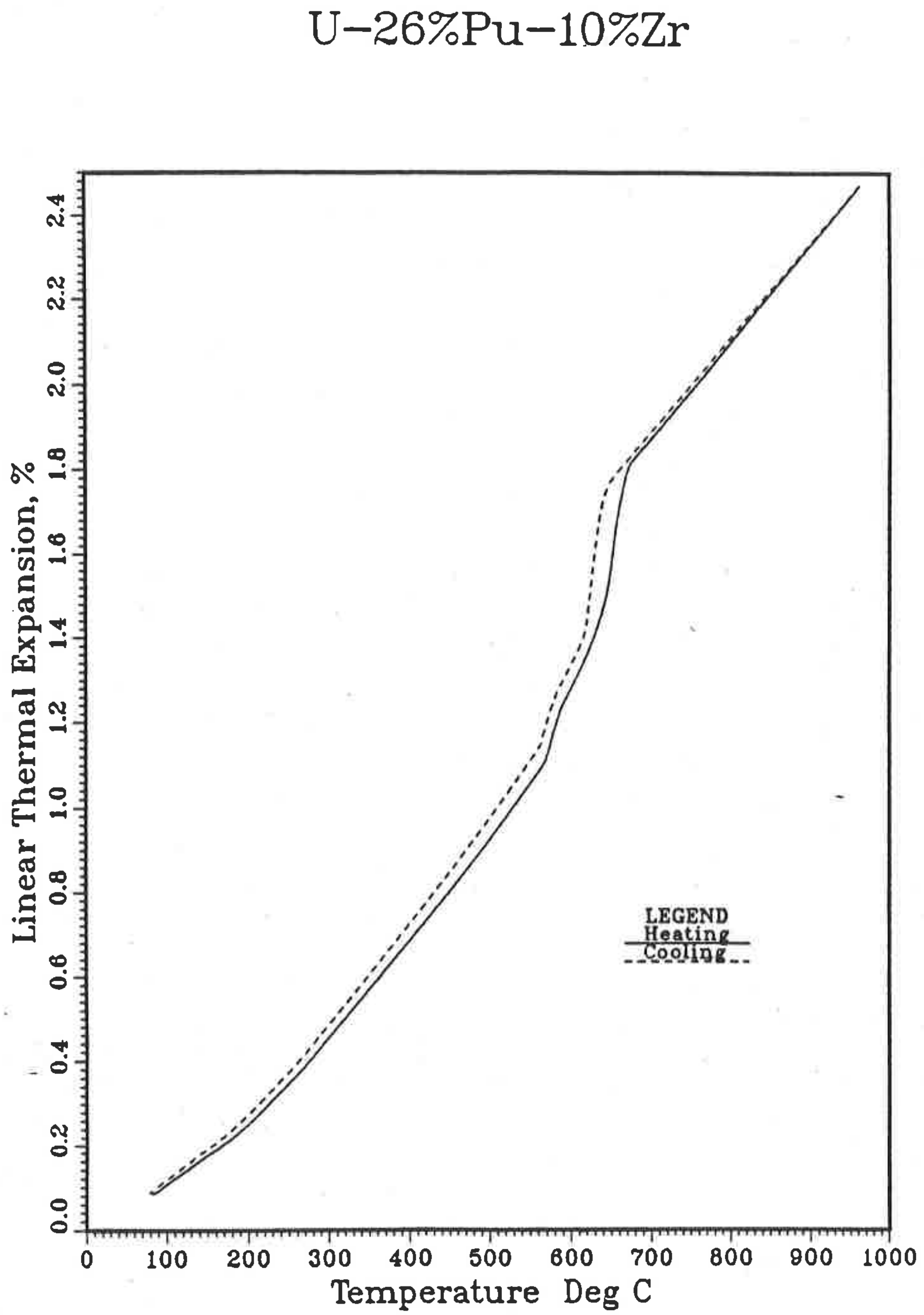

Fig. B.3.2-C Thermal Expansion of U-26 wt % Pu-10 wt % Zr

B.3.3 Others

Uranium, Zirconium, Plutonium

The data for the elements were taken from the compilation of the Thermophysical Properties Research Center (Purdue) [1]. The thermal-expansion data are shown in Fig. B.3.3-A, and Tables B.3.3-1 through -3. Density values given in the tables were calculated by us, using ρ_o values from Ref. 1. For uranium the tabulated values for $\Delta L/L_o$ are considered accurate to within ±5% below 941 K and ±7% above. They are represented approximately by the following equations given in Ref. 1.

$$\frac{\Delta L}{L_o}(\%) = -0.379 + (1.264 \times 10^{-3}\ T) - (8.982 \times 10^{-8}\ T^2) + (6.844 \times 10^{-10}\ T^3) \quad (293 \le T \le 941\text{K})$$

$$\frac{\Delta L}{L_o}(\%) = -0.149 + (1.775 \times 10^{-3}\ T) + (4.382 \times 10^{-7}\ T^2) - (1.239 \times 10^{-10}\ T^3) \quad (1048 \le T \le 1400\text{K})$$

For zirconium the tabulated values for $\Delta L/L_o$ are considered accurate to within ±3% below 1137 K and ±10% above. They are represented approximately by the following equations:

$$\frac{\Delta L}{L_o}(\%) = -0.111 + (2.325 \times 10^{-4}\ T) + (5.595 \times 10^{-7}\ T^2) - (1.768 \times 10^{-10}\ T^3) \quad (293 \le T \le 1137\text{K})$$

$$\frac{\Delta L}{L_o}(\%) = -0.759 + (1.474 \times 10^{-3}\ T) - (5.140 \times 10^{-7}\ T^2) + (1.559 \times 10^{-10}\ T^3) \quad (1137 \le T \le 1800\text{K})$$

Note that there are very large differences in thermal expansion behavior among these three metals, with plutonium being particularly irregular. This will

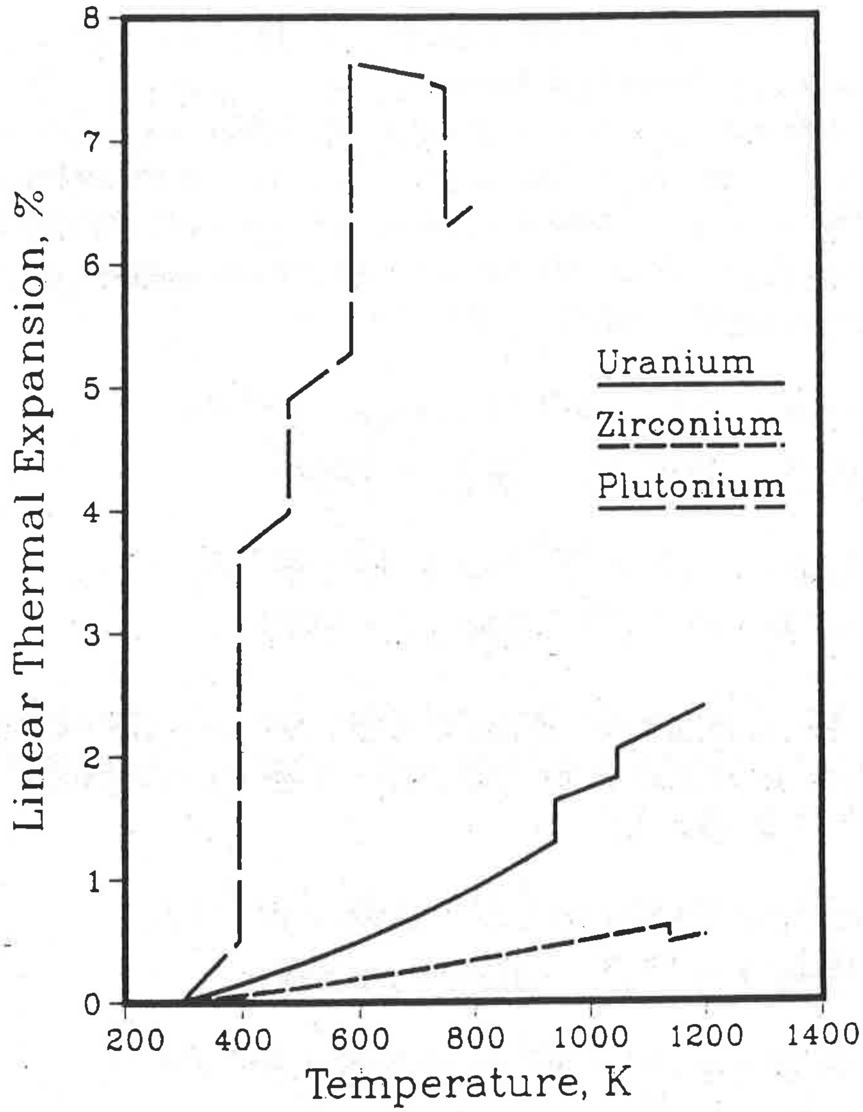

Fig. B.3.3-A. Mean Linear Thermal Expansion ($\Delta L/L_0$,%) of Uranium, Plutonium, and Zirconium

TABLE B.3.3-1. Density and Linear Expansion of Uranium

T (K)	ρ (g cm^{-3})	$\Delta L/L_0$ (%)	$\alpha_\ell \times 10^6$ (K^{-1})
293	19.07	0.000	13.9
400	18.98	0.157	15.2
500	18.89	0.315	16.9
600	18.79	0.494	19.0
700	18.68	0.697	21.4
800	18.55	0.924	24.3
900	18.41	1.186	27.7
941(α)	18.39	1.300	29.1
941(β)	18.16	1.635	17.3
1000	18.11	1.737	17.3
1048(β)	18.07	1.820	17.3
1048(γ)	17.94	2.050	22.9
1100	17.88	2.168	22.9
1200	17.76	2.398	22.9
1400	17.53	2.855	22.9
1408(γ)	17.52	2.866	22.9
1408(ℓ)	16.95	4.006	25.5
1500	16.84	4.232	25.5
1600	16.71	4.502	25.5

TABLE B.3.3-2. Density and Linear Thermal Expansion of Zirconium

T (K)	ρ (g cm^{-3})	$\Delta L/L_0$ (%)	$\alpha_\ell \times 10^6$ (K^{-1})
293	6.57	0.000	5.7
400	6.56	0.060	5.9
500	6.55	0.123	6.6
600	6.53	0.192	7.1
700	6.52	0.265	7.6
800	6.50	0.343	7.9
900	6.49	0.442	8.0
1000	6.47	0.505	8.2
1100	6.46	0.586	8.2
1137(α)	6.45	0.617	8.2
1137(β)	6.48	0.482	9.0
1200	6.46	0.539	9.1
1400	6.43	0.725	9.5

TABLE B.3.3-3. Density and Linear Thermal Expansion of Plutonium

T (K)	ρ (g cm^{-3})	$\Delta L/L_0$ (%)	$\alpha_\ell \times 10^6$ (K^{-1})
293	19.75	0.000	46.7
350	19.59	0.279	49.4
395(α)	19.46	0.502	51.0
395(β)	17.73	3.663	37.3
450	17.62	3.868	37.3
480(β)	17.57	3.980	37.3
480(γ)	17.11	4.901	34.6
550	16.99	5.144	34.6
588(γ)	16.93	5.275	34.6
588(δ)	15.84	7.628	-8.6
600	15.85	7.618	-8.6
700	15.88	7.532	-8.6
730(δ)	15.90	7.506	-8.6
730(δ')	15.92	7.458	-16.1
753(δ')	15.93	7.421	-16.1
753(ε)	16.45	6.287	36.6
800	16.37	6.459	36.6

pose some problems, as we shall see later in understanding the alloys. Data for liquid uranium are not given in Ref. 1 and require some additional discussion.

For liquid uranium four sets of density measurements have been reported. The earliest of these was published by Grosse and coworkers [2] in 1961. An Archimedean method was used to determine densities from the melting point to about 1900 K. Several years later workers at Mound Laboratory [3] reported data on the density of liquid uranium which disagreed with the Grosse data. A pycnometric technique was used by the Mound group and data were obtained from 1410 to 1518 K. Measurements of the density of liquid uranium were subsequently reported by Shaner [4] (to about 5000 K) using a unique isobaric-expansion method (IEX) and by Drotning [5] (1419-1567 K), who used gamma densitometry. The four sets of measurements, which do not agree very well, are compared with solid density data in Fig. B.3.3-B, and some of the essential aspects of the experiments are summarized in Table B.3.3-4.

TABLE B.3.3-4. Measurements of Density of Liquid Uranium, $\rho(g/cm^3) = \alpha - \beta T(K)$

Reference	Method	α	$\beta \times 10^4$
TPRC [1]	(Solid)	19.22	11.4
Grosse et al. [2]	Archimedean	19.36	10.33
Rohr & Wittenberg [3]	Pycnometry	19.52	16.01
Shaner [4]	Isobaric Expansion	20.00	17.
Drotning [5]	Gamma Densitometry	18.77	12.9

As is clear from Fig. B.3.3-B, two of the measurements indicate a density increase on melting while two show the more usual density decrease on melting. There is, fortunately, some additional information that can help to

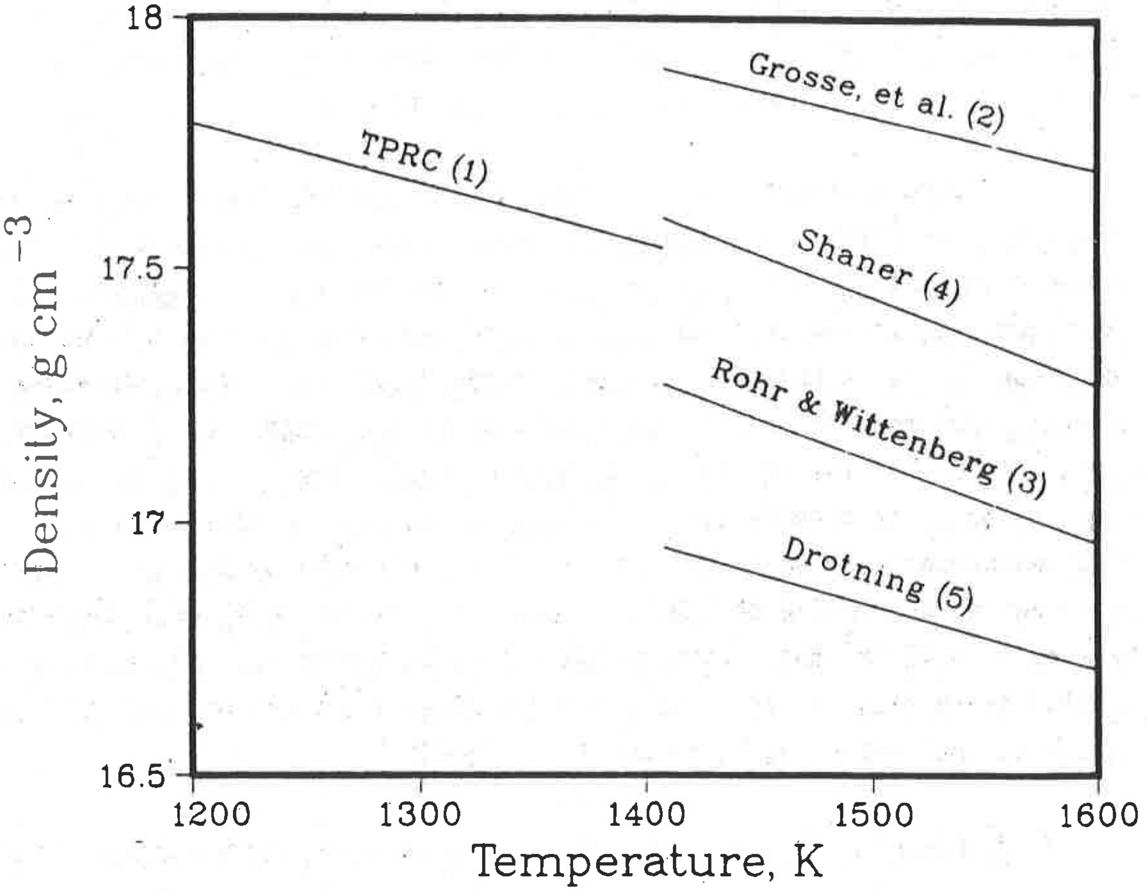

Fig. B.3.3-B. Density of Solid and Liquid Uranium make a reasonable decision among these conflicting values. First, in conjunction with sessile-drop measurements of interfacial tension of uranium [6], observations were made of the volume change on melting. It was estimated that about a 3% expansion occurred on melting. Second, measurements were made of the pressure-temperature phase diagram of uranium [7]. From the slope of the γ-liquid phase boundary the volume change on melting was calculated to be 0.49 cm^3/mol. Finally, observations made during casting operations [8] clearly indicate that the liquid shrinks on freezing.

Based on these facts it seems clear that the density data of Grosse et al. are incorrect. The values of Shaner, which show a very small density increase on melting, are also suspect. In fact Shaner, in commenting on his technique, points out that because of basic experimental difficulties the IEX technique is less accurate than other standard methods. Its chief value is in allowing measurements over a very wide temperature range, not of principal concern here. Of the remaining two sets of measurements we recommend the Drotning data for general use. His work is recent, and most importantly he made measurements on solid uranium, which was not done by the Mound workers, which agree very well with the TPRC data. The resulting volume change on melting is 0.46 cm^3/mol, which agrees well with the value reported from the uranium phase diagram [7]. Table B.3.3-5 gives a summary of some pertinent values at the melting point of uranium (1408 K).

TABLE B.3.3-5. Density and Volume of Solid and Liquid Uranium ($T=T_m$)

Phase	Density (g/cm^3)	Volume (cm^3/mol)
liquid	16.95	14.04
gamma	17.52	13.58
Δ	-0.57	0.46

(This section is incomplete at this time)

C. TRANSPORT

C.1 Thermal Conductivity

C.1.1 Uranium-Zirconium Alloys (Unirradiated)

Touloukian et al.[1] have summarized the data for U-Zr alloys. Based on the data they present, the following correlation has been developed:

$$k_o = A + BT + CT^2, \text{ W/m·K} \qquad (1)$$

where $A = 17.5\ (1 - 2.23\ W_z)/(1 + 1.61\ W_z)$
$B = 1.54 \times 10^{-2}\ (1 + 0.061\ W_z)/(1 + 1.61\ W_z)$
$C = 9.38 \times 10^{-6}$
W_z = weight fraction of Zr
T = temperature in K.

In the temperature range of interest (300-900°C) for fuel performance under normal operating conditions, the correlation shows excellent agreement with the U-Zr data for $0.015 \le W_z \le 0.20$ with an average deviation from the data of less than 1%. However, the correlation yields values lower than the U-40Zr data by ~20%. If it is assumed that the data are accurate to within ±20%, then the accuracy of Eq. 1 is taken to be the same as that for the data for $W_z \le 0.20$. Table C.1.1-1 gives the data and the values predicted by Eq. 1 for several temperatures and Zr weight fractions. The same information is given in Fig. C.1.1-A in graphical form. The thermal-conductivity values for pure uranium [1] are included in Fig. C.1.1-A and Table C.1.1-1 for reference.

TABLE C.1.1-1 Summary of U-Zr Alloy Thermal-conductivity Data and Values (in Parentheses) Calculated from Eq. 1.

	k_o (W/cm·°C)					
T (°C)	U	U-1.5Zr	U-5Zr	U-11.4Zr[a]	U-20Zr	U-40Zr
20	0.270 (0.228)	0.226 (0.217)	0.19 (0.194)	--- (0.157)	0.11 (0.116)	0.07 (0.048)
100	0.291 (0.245)	0.240 (0.234)	0.21 (0.210)	--- (0.172)	0.13 (0.130)	0.08 (0.060)
200	0.311 (0.269)	0.260 (0.257)	0.23 (0.232)	--- (0.193)	0.15 (0.150)	0.10 (0.078)
300	0.334 (0.294)	0.285 (0.282)	0.25 (0.256)	--- (0.216)	0.17 (0.171)	0.12 (0.097)
400	0.358 (0.321)	0.310 (0.309)	0.28 (0.282)	0.265 (0.241)	0.20 (0.195)	0.14 (0.118)
500	0.382 (0.350)	0.340 (0.337)	0.31 (0.310)	0.273 (0.268)	0.22 (0.220)	0.17 (0.142)
600	0.406 (0.380)	0.370 (0.368)	0.34 (0.340)	0.306 (0.296)	0.25 (0.247)	0.20 (0.167)
700	0.432 (0.413)	0.405 (0.400)	0.37 (0.371)	0.337 (0.327)	0.28 (0.277)	0.24 (0.193)
800	0.457 (0.448)	0.445 (0.434)	0.41 (0.405)	0.355 (0.359)	0.31 (0.307)	0.28 (0.222)
900	0.483 (0.484)	--- ---	0.44 (0.440)	0.365 (0.393)	0.34 (0.340)	0.33 (0.253)

---

[a] Interpolated from fifty data points in the temperature range of 363-927°C.

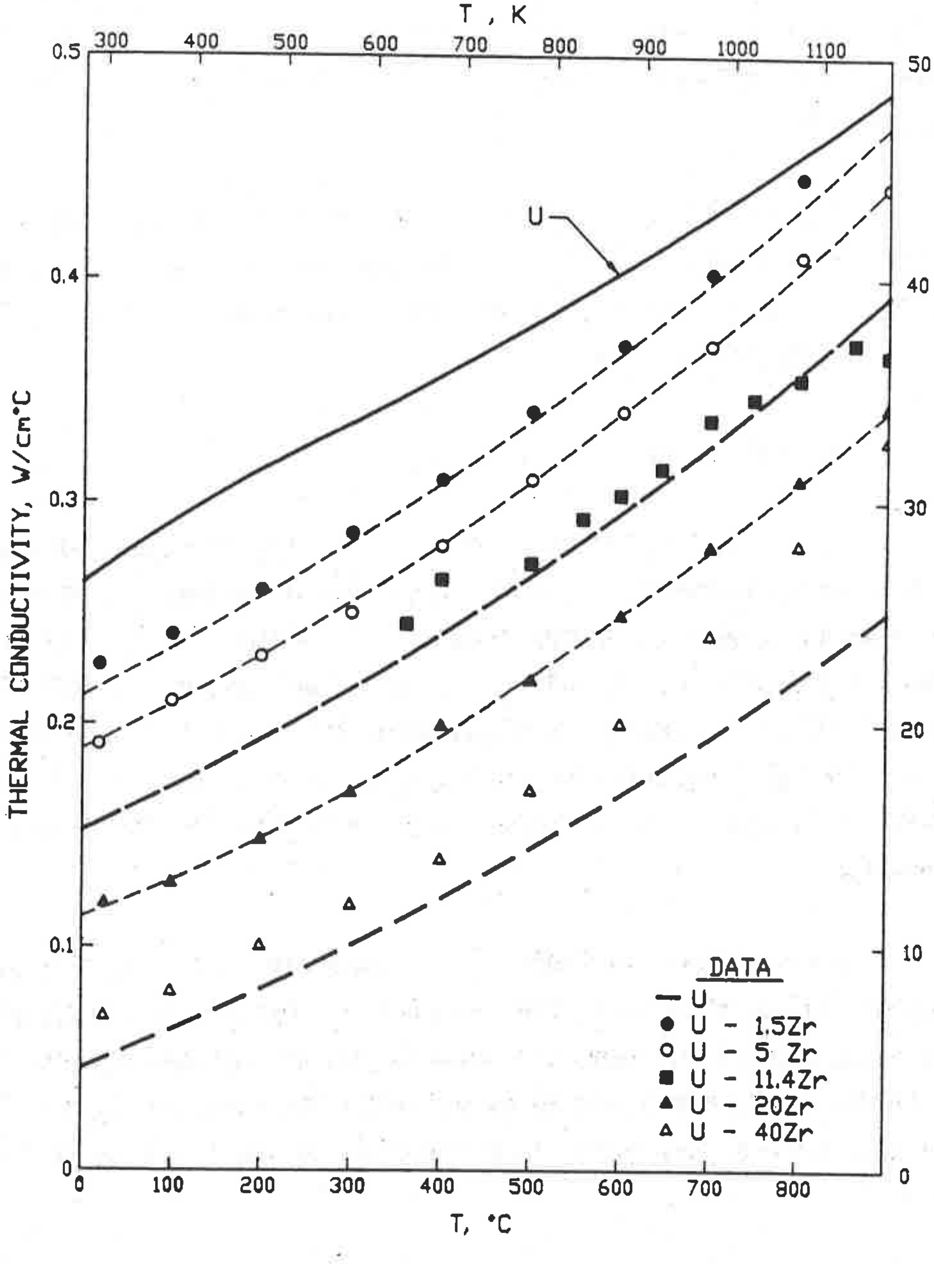

Fig. C.1.1-A Comparison Between U-Zr Thermal-conductivity Data and the Recommended Correlation (Eq. 1). The thermal conductivity of pure uranium is also included for reference purposes. The dashed lines are calculated from the correlation.

Also included in Table C.1.1-1 and Fig. C.1.1-A are the more recent data of Leibowitz and Veleckis [10] for U-11.4Zr. They generated 50 data points in the temperature range of 363-927°C. The uncertainty in these data is about ±8%.

The correlation (Eq. 1) agrees with these new data to within 9% in the temperature range of interest. Because most of the experimental U-Zr fuels have a Zr weight fraction of 10%, the recommended uncertainty for unirradiated U-10Zr fuel is ±10%.

Justification

In reviewing the data for U-Zr alloys, it appeared that the decrease in thermal conductivity with increasing Zr content correlated better with atom fraction than with weight fraction, particularly for low Zr content. The coefficients (A, B, and C) in Eq. 1 were chosen to vary linearly with Zr atom fraction at several temperatures for the U-1.5Zr, U-5Zr, and U-20Zr cases. The coefficients were then converted to weight-fraction dependencies because of the more common use of weight fraction in specification of fuel parameters.

As indicated in Table C.1.1-1 and Fig. C.1.1-A, the correlation is a very good representation of the data for $0.015 \le W_z \le 0.20$. This gives considerable confidence in using the correlation to interpolate the data for $W_z = 0.1$, particularly given the agreement with the data for $W_z = 0.114$. However, there is less confidence in extrapolating the correlation to $W_z = 0.0$ or $W_z = 0.4$.

Irradiated U-Zr

No data are available on the effects of irradiation on the thermal conductivity of U-Zr. The unirradiated thermal conductivity of U-Zr with 5 to 10 wt.% Zr is comparable to that of U-5Fs (see C.1.3). If it is assumed that U-10Zr behaves in a similar manner (under irradiation conditions) to U-5Fs with regard to fission-gas swelling and sodium logging, then the same porosity correction factor may be used from startup to major interlinkage of porosity (see C.1.3):

$$f_p = k/k_o = (1 - P)/(1 + \beta P), \qquad (2)$$

where P is the porosity fraction referenced to initial (i.e. 100% dense) fuel volume and $\beta = 1.7$. The minimum value for f_p is taken as 0.5 ± 0.1. The long-time value of f_p is taken as 0.7 ± 0.1 to account for the combined effects of gas-filled and sodium-filled porosity. For design studies, an uncertainty of ±30% is assumed after porosity interlinkage. This uncertainty will be reduced in the future as more information is obtained on the amount and the effect of sodium logging for irradiated U-Zr fuel. Preliminary results from the postirradiation examinations of 10 at.% burnup U-10Zr fuel indicate that 10-20% of the bond sodium is located in the fuel after cool down.

Several other effects must also be considered in calculating the in-reactor thermal conductivity of U-Zr fuels in the context of the IFR application. While negligible weight fractions of Pu are produced in EBR-II, the opposite may be true for U-Zr in an IFR. Transmutation of U to Pu results in lowering of the thermal conductivity of the fuel (see C.1.2). Physics calculations can be used to provide input on the amount of Pu produced as a function of burnup. The coefficients in Eq. 1 can then be modified (as has been done in C.1.2) to reflect the change in conductivity due to Pu generation:

$$A = 17.5\ [(1 - 2.23\ W_z)/(1 + 1.61\ W_z) - 2.62\ W_p]$$
$$B = 1.54 \times 10^{-2}\ [(1 + 0.061\ W_z)/(1 + 1.61\ W_z) + 0.90\ W_p]$$
$$C = 9.38 \times 10^{-6}\ (1 - 2.70\ W_p)$$

where W_p = the weight fraction of Pu.

Another phenomenon that will affect the local thermal conductivity of U-Zr is the redistribution of U and Zr (and Pu and fission products) under the thermal gradient. Work is in progress to model this phenomenon to provide input to the thermal-conductivity equation as a function of burnup and operating conditions.

C.1.2 Uranium-Zirconium-Plutonium Alloys (Unirradiated)

Thermal-conductivity data for U-Pu-Zr fuels have been summarized in ANL-AFP-38 [2]. The correlation recommended to describe the thermal conductivity of unirradiated, 100%-dense U-Pu-Zr fuels is

$$k_0 = A + BT + CT^2, \text{ W/m·K}, \qquad (1)$$

where $A = 17.5 \left[(1 - 2.23\, W_z)/(1 + 1.61\, W_z) - 2.62\, W_p\right]$

$B = 1.54 \times 10^{-2} \left[(1 + 0.061\, W_z)/(1 + 1.61\, W_z) + 0.90\, W_p\right]$

$C = 9.38 \times 10^{-6} (1 - 2.70\, W_p)$

W_z = Zr weight fraction

W_p = Pu weight fraction

T = temperature in K.

Table C.1.2-1 and Fig. C.1.2-A summarize the data [2] used in developing the correlation. The data are assumed to be accurate within ±20%. In the temperature range of interest (300-900°C), the maximum deviation between the correlation and the data is 10%. Thus, the accuracy of the correlation is taken as the accuracy of the data. For design calculations, an uncertainty of 20% is recommended.

Justification

The form of the correlation represented by Eq. 1 was chosen on the basis of the data set for U-Zr alloys (see C.1.1), which is more extensive than the data base for U-Pu-Zr alloys. The coefficients (A, B, and C) were modified slightly to give reasonably good agreement at 300°C and 800°C. It is interesting to note that the curvature suggested by the U-Pu-Zr data is different in sign from that suggested by the U-Zr data. No fundamental reason for this can be found. While better fits to the U-Pu-Zr data can be deter-

TABLE C.1.2-1 Summary of Thermal-conductivity Data for Unirradiated, 100%-dense U-Pu-Zr Alloys. The values calculated from the recommended correlation (Eq. 1) are included in parentheses.

	k_0 (W/cm °C)			
T (°C)	U-16.2Pu-6.2Zr	U-14.7Pu-9.7Zr	U-18.4Pu-11.5Zr	U-19Pu-10Zr
20	--- (0.115)	--- (0.101)	--- (0.075)	--- (0.081)
100	0.109 (0.131)	0.100 (0.117)	0.092 (0.090)	--- (0.096)
200	0.142 (0.152)	0.132 (0.137)	0.117 (0.110)	--- (0.116)
300	0.177 (0.173)	0.164 (0.158)	0.144 (0.130)	--- (0.137)
400	0.210 (0.196)	0.196 (0.181)	0.171 (0.152)	--- (0.158)
500	0.241 (0.220)	0.225 (0.204)	0.197 (0.174)	--- (0.181)
600	0.264 (0.245)	0.253 (0.229)	0.219 (0.198)	--- (0.204)
700	0.280 (0.271)	0.278 (0.255)	0.234 (0.222)	--- (0.229)
800	0.293 (0.298)	0.301 (0.282)	0.248 (0.247)	--- (0.254)
900	--- (0.327)	--- (0.310)	--- (0.274)	--- (0.280)

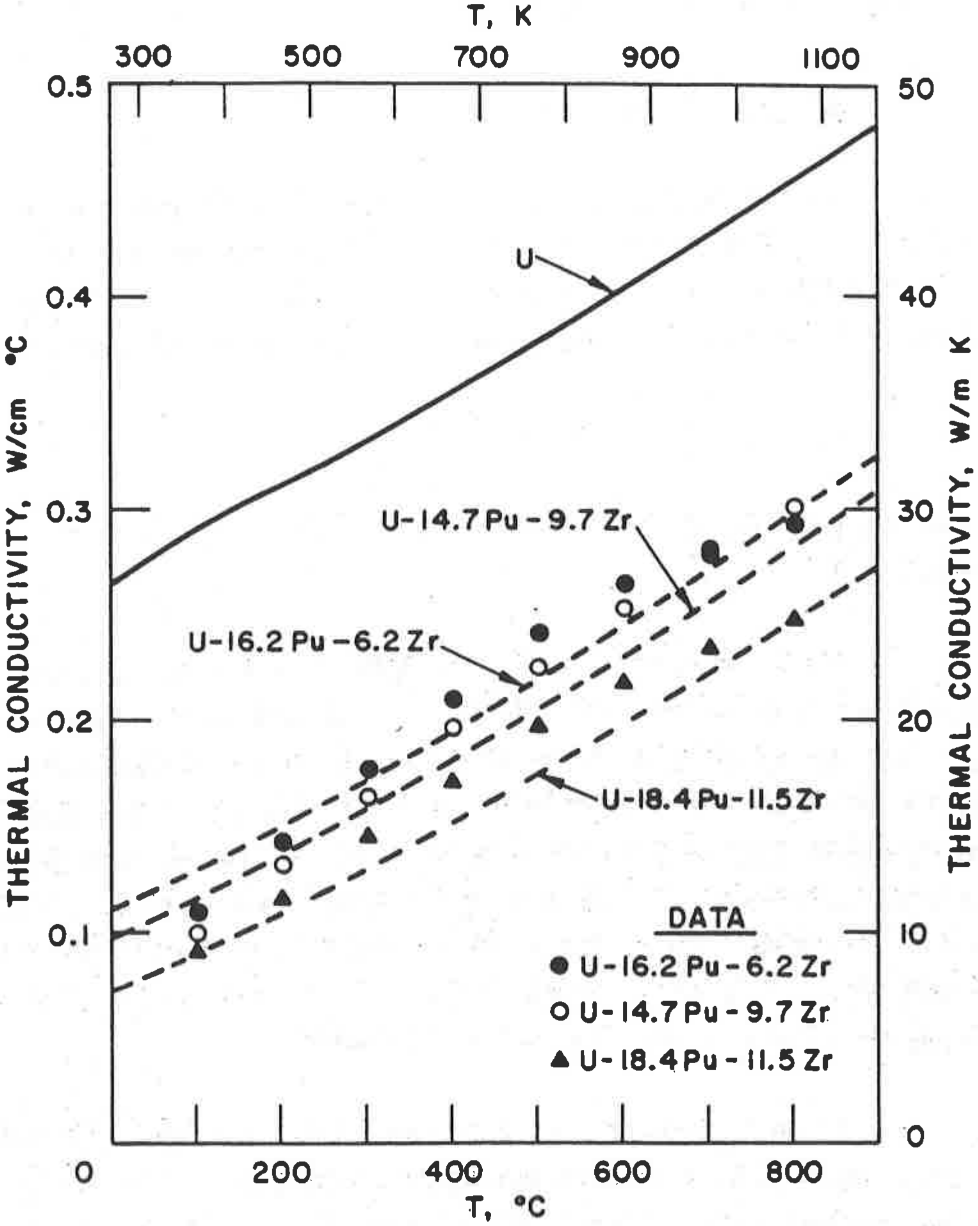

Fig. C.1.2-A Comparison Between Correlation Predictions (Dashed Lines) and Data for the Thermal Conductivity of Unirradiated, 100%-dense U-Pu-Zr Alloys. A curve based on the data for pure U is also included [1].

mined to match the temperature, no additional confidence would be realized, because of the uncertainty in the data.

Irradiated U-Pu-Zr

As in the case for U-Zr, no data are available for the thermal conductivity of irradiated U-Pu-Zr. Based on the behavior of U-5Fs (see C.1.3), it is assumed that until porosity interlinkage, the decrease in conductivity with increasing fission-gas porosity can be represented by

$$f_p = k/k_0 = (1 - P)/(1 + \beta P) \qquad (2)$$

where P is the porosity fraction referenced to initial (100% dense) fuel volume and $\beta = 1.7$.

The minimum value of f_p is taken as 0.5 ± 0.1 and the long-time value is 0.7 ± 0.1 to reflect the influence of sodium logging and fuel hot pressing. For design purposes an uncertainty of ±32% is recommended after porosity interlinkage. This uncertainty will be reduced in the future as better data become available on the thermal conductivity of 100% dense U-Pu-Zr fuel and more information is obtained on the amount and effect of sodium logging for irradiated U-Pu-Zr fuel. Preliminary results from postirradiation examinations of 10 at.% burnup U-19Pu-10Zr fuel indicate that 10-20% of the bond sodium is located in the fuel after cool down.

A sample calculation is presented for a U-19Pu-10Zr fuel element to give the user some idea of the temperature uncertainty associated with fuel thermal conductivity. LIFE-METAL was used to predict the maximum fuel temperature for the U-19Pu-10Zr fuel element T179 (from the EBR-II lead experimental subassembly X419) at a position of X/L = 0.94 from the bottom of the fuel column at a burnup of 1.9 at.%. This is a useful example because postirradiation data are available on the radial redistribution of U, Pu, and Zr and on the radial distribution of fission gas porosity.

Table C.1.2-2 shows the nominal operating conditions and calculations, as well as the one-sigma uncertainty estimates for this case. Clearly the uncertainty of the irradiated fuel thermal conductivity dominates all other uncertainties. The calculated maximum fuel temperature at this location is 720 ± 65°C.

Additional effects that should be considered are increased Pu (or Zr) weight fractions with burnup, redistribution of U, Pu, and Zr, and local concentrations of solid (and liquid) fission products. For IFR design studies in which it is primarily the Pu that fissions, no further degradation of thermal conductivity with fission-product generation is recommended. However, in test runs employing highly enriched U, the replacement of the highly conducting U with fission products may cause additional degradation of thermal conductivity with burnup. More work needs to be done in this area. The interim recommendation is that Eqs. 1 and 2 be used for prediction of U-Pu-Zr thermal conductivity and that physics calculations be used to determine the weight fractions of U, Pu, Zr as a function of burnup. No recommendation is made at this time with regard to fuel-constituent redistribution and solid-fission-product concentration. An uncertainty of ±32% is arbitrarily assumed for the in-reactor thermal conductivity of U-Pu-Zr alloys.

TABLE C.1.2-2 Sample Calculations for Experimental Fuel Element T179 (U-19Pu-10Zr) to Show the Effects of Uncertainties on the Predicted Maximum Fuel Temperature at 1.9 at.% Burnup and an Axial Position (X/L = 0.94) Near the Top of the Fuel Column

Parameter	Nominal Value	One-Sigma ± %	Uncertainty Value (±)
Power, kW/m (kW/ft)	30 (9.1)	3	0.9 (0.3)
Fuel Surface Temperature, °C	538	-	30
Average Porosity Fraction, %	26[a]	-	-
Average Fuel Conductivity, W/m·K	13.1[b]	32	4.2
Fuel ΔT, °C	182	32	58
Fuel T_{max}, °C	720	-	65

---

[a] Local values vary from 3 to 67% across the fuel radius.

[b] Assumes porosity correction factor is limited by $f_p \geq 0.5$ for each of the 12 fuel rings used in the analysis.

C.1.3 Others

Unirradiated 100%-dense U-5Fs

The recommended equation for unirradiated, 100%-dense U-5Fs is

$$k_o = 6.26 + 2.77 \times 10^{-2}\, T + 3.91 \times 10^{-6}\, T^2,\ \mathrm{W/m{\cdot}K} \qquad (1)$$

where T is temperature in K. Numerical values and uncertainty estimates are listed in Table C.1.3-1. Figure C.1.3-A is a graph of the correlation with a comparison to the results for pure uranium [1] and the U-5Fs data of Saller et al. [3], Zegler and Nevitt [4], and di Novi [5].

TABLE C.1.3-1 Correlation Values and Uncertainty Estimates for the Thermal Conductivity of Unirradiated, 100%-dense U-5Fs

T K	T °C	Correlation (Eq. 1) (W/m·K)	Uncertainty[a] Estimate (±%)
293	20	14.7	30
373	100	17.1	25
473	200	20.2	10
573	300	23.4	6
623	350	25.0	6
673	400	26.7	6
723	450	28.3	6
773	500	30.0	5
823	550	31.7	5
873	600	33.4	5
923	650	35.2	5
973	700	36.9	5
1023	750	38.7	5
1073	800	40.5	5
1123	850	42.3	5
1173	900	44.1	5
1223	950	46.0	5
1273	1000	47.9	5

---

[a] Based on precision of the data.

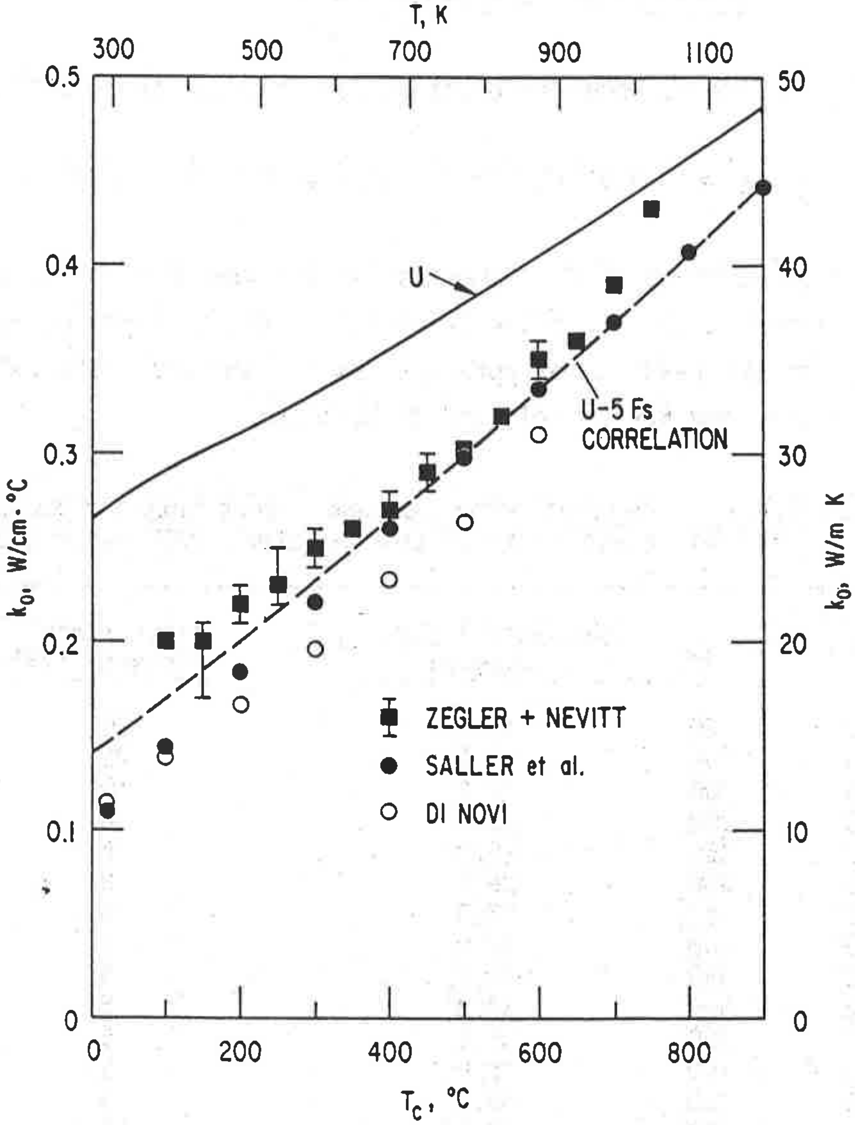

Fig. C.1.3-A Comparison Between Measured Thermal Conductivities of Unirradiated, 100%-dense U-5Fs and Values Calculated From the Correlation (Eq. 1). The thermal conductivity of pure U is included for reference purposes.

Justification

Table C.1.3-2 summarizes the experimental thermal-conductivity values for unirradiated U-5Fs. Saller et al. [3] used a steady-heat-flow method. Each thermal-conductivity value in the table represents an average of 20 readings (five thermal couples and four equilibrium runs). The authors estimate the absolute accuracy to be within ±5%.

TABLE C.1.3-2 Measured Thermal Conductivities of U-5 wt % Fs

	k_o (W/cm °C)		
T (°C)	Saller et al.[a]	Zegler & Nevitt[b]	di Novi[c]
20	0.110	---	0.116
100	0.143	0.20	0.138
150	---	0.20 (0.17-0.21)	---
200	0.183	0.22 (0.21-0.23)	0.167
250	---	0.23 (0.22-0.25)	---
300	0.221	0.25 (0.24-0.26)	0.196
350	---	0.26	---
400	0.260	0.27 (0.26-0.28)	0.233
450	---	0.29 (0.28-0.30)	---
500	0.298	0.30	0.264
550	---	0.32	---
600	0.334	0.35 (0.34-0.36)	0.311
650	---	0.36	---
700	0.370	0.39	---
750	---	0.43	---
800	0.407	---	---
900	0.44	---	---

[a] Composition: 2.5 wt % Mo, 0.1 wt % Zr, 1.5 wt % Ru, 0.3 wt % Rh and 0.5 wt % Pd.

[b] Composition: 2.45 wt % Mo, 0.069 wt % Zr, 2.08 wt % Ru, 0.3 wt % Rh, and 0.209 wt % Pd.

[c] EBR-II Mark IA fuel. Values obtained from graph of $\alpha (k_o = \rho C_p \alpha)$.

Zegler and Nevitt [4] employed a comparative method based on steady-state thermal gradients in U-5Fs and Armco iron. The authors quote a precision of ±4%. The absolute accuracy is probably of the order of ±10% for temperatures below 700°C. The data above 700°C are suspect because of the possible formation of a U-Fe eutectic in the region of contact between the U-5Fs and the Armco iron. The agreement between the two sets of data is quite good in the temperature range of 300-700°C.

The di Novi data in Table C.1.3-2 are based on a transient-pulse method to determine the thermal diffusivity (α). However, there is an inconsistency between di Novi's measured thermal diffusivity and calculated thermal conductivity ($k_0 = \alpha\rho C_p$, where ρ is density and C_p is specific heat capacity). The thermal-conductivity values in Table C.1.3-2 were obtained by using di Novi's α values and the ρ and C_p values presented in this handbook. The absolute accuracy of the thermal diffusivities is estimated to be ±10%. While the resulting thermal conductivities are consistently lower than those of the other authors for temperatures above 200°C, the agreement is reasonable if one considers the uncertainties involved.

The correlation represented by Eq. 1 was obtained by matching the mean of the Saller et al. and Zegler and Nevitt data at low temperature and the Saller et al. data at higher temperature. The choice of a parabolic equation is somewhat arbitrary. Zegler and Nevitt's data suggest it, while the data of Saller et al. suggest a linear fit. The agreement between the correlation and the data is very good for temperatures of interest ($T > 300°C$). The uncertainty of ≤6% indicated in Table C.1.3-1 for $T > 300°C$ is based on precision. The absolute uncertainty is more on the order of 10%. These values are low compared to uncertainties anticipated under irradiation conditions.

Irradiated U-5Fs

A number of in-reactor phenomena tend to lower the conductivity of the U-5Fs. Fission-gas bubbles and thermal-stress-induced microcracking will lower the density and the conductivity; solid (and liquid) fission-product buildup will tend to lower the thermal conductivity much the same as increasing amounts of fissium lower the conductivity; and irradiation damage will degrade the conductivity. From start-up to 1-2 at.% burnup, the dominant factor accounting for the degradation of thermal conductivity is assumed to be the decrease in fuel density due to fission-gas-induced swelling and microcracking. Based on the data of di Novi [5] and Beck and Fousek [6], the recommended porosity-correction factor is

$$f_p = (1 - P)/(1 + \beta P) \tag{2}$$

where P is porosity fraction relative to initial (e.g. 100% dense) fuel volume, $\beta = 1.7$ is an empirically determined factor, and f_p is the ratio of the irradiated (k) to the unirradiated (k_o) thermal conductivity.

Equation 2 is a reasonable representation of the data for burnups at which the porosity is essentially isolated. After interlinkage has occurred, the ingress of sodium into the voids may tend to improve the conductivity somewhat as suggested by the data of Beck and Fousek [6] and Betten [7]. If, for example, it is assumed that interlinkage occurs at $P \sim 0.33$, then $f_p = 0.43$ based on Eq. 2. Beyond this point in burnup, the effective conductivity will tend to increase due to sodium logging and fuel hot pressing and tend to decrease due to solid-fission-product accumulation. While modeling of these phenomena is required to predict the effective fuel thermal conductivity as a function of burnup, some preliminary guidance is offered to assist in design studies. The minimum thermal conductivity for design studies can be taken as 0.48 ± 0.11 of the unirradiated value. The long-time (i.e., intermediate to high burnup) behavior is better estimated by $f_p = 0.72 \pm 0.06$. These values are based on experimental studies which are reviewed in the following section.

Justification

R. A. di Novi [5] also used her thermal-pulse method to perform post-irradiation thermal-conductivity measurements on Mark-IA fuel that had been irradiated to ~0.6 to 1.1 at.% burnup. She reported the fractional decrease in thermal conductivity as a function of temperature for a number of samples. Based on these data, she described the ratio (f_p) of irradiated-to-unirradiated thermal conductivity of U-5Fs.

There are several difficulties associated with di Novi's assumptions and calculational methods:

(1) The porosity fraction was assumed to be directly related to the measured diametral strain $P = 3(\Delta D/D_0)$;
(2) The swelling due to solid and liquid fission products (at fuel operating temperatures) was assumed to have the same effect on thermal conductivity as gaseous fission products.
(3) No attempt was made to estimate the effects of changing fuel chemistry on thermal conductivity.

These issues are discussed below.

The calculation of P from the relationship $P = 3(\Delta D/D_0)$ is fundamentally incorrect. It is an approximation which is good for small, isotropic swelling due to fission-gas bubbles and microcracks. Let P be the change in fuel volume (relative to the initial fuel volume) due to porosity formation. Hofman [8] has estimated the swelling contribution of fission products other than Xe and Kr to be in the range of $(\Delta V/V_0)_{sl} = 0.6$ to 1.8%/at.% burnup. Because the degree of anisotropy in the samples is difficult to determine without more information, the assumption of isotropy is used to calculate porosity. In terms of measured quantities,

$$P = (1 + \Delta D/D_0)^3 - 1 - CB \tag{3}$$

where B is burnup in at.% and $6 \times 10^{-3} \leq C \leq 1.8 \times 10^{-2}$.

An estimate is now made of the effects of changing fuel chemistry with burnup. Based on information supplied by Hofman [8] and Porter [9], the increased amount of Fs at 10 at.% burnup is ~2.4 wt.%, while the total of other solid (and liquid) fission products is ~4.2 wt.% and the weight fraction of plutonium is ~0.4 wt.%. If it is assumed (to the first order) that this additional 7 wt.% of fission and transmutation products has the same effect on the thermal conductivity as does Fs, then the estimate can be made based on the thermal conductivity of U-12Fs as compared to U-5Fs. Zegler and Nevitt's [4] data on uranium with 3 to 10 wt % Fs was used to estimate the burnup correction factor as

$$f_B = 1 - 0.024B, \tag{4}$$

where B is in at.%. Thus, for di Novi's low-burnup samples, the decrease in conductivity due to changing fuel chemistry is ~2%, which is negligible compared to the uncertainty in the data. However, Eq. 4 is useful for estimating the effect of changing fuel chemistry with burnup at higher burnup levels.

Table C.1.3-3 shows the $\Delta D/D_0$ values of di Novi and the range of porosity values one would calculate using Hofman's solid-fission-product swelling rates. The data imply that the conductivity correlates better with porosity than with burnup. Figure C.1.3-B shows that the di Novi value of β = 1.7 gives a reasonable fit to the data. This value is higher than one would

Table C.1.3-3 Summary of di Novi [5] Data (28≤T≤595°C)

Burnup (at.%)	$\Delta D/D_o$ (%)	P (%)	k/k_o (%)
0.58	0.89	1.97 (1.62-2.31)	95.2 (87.2-96.8)
0.67	1.83	4.69 (4.28-5.09)	86.1 (82.3-87.8)
0.80	1.31	2.97 (2.49-3.45)	94.8 (89.7-97.3)
0.90	4.69	13.1 (12.5-13.6)	68.6 (64.2-76.8)
0.94	2.26	5.66 (5.09-6.22)	83.8 (80.4-89.4)
1.00	1.45	3.15 (2.55-3.75)	93.9 (90.5-99.0)
1.04	1.97	4.68 (4.05-5.30)	85.8 (82.7-89.2)
1.08	4.10	11.1 (10.4-11.7)	73.3 (70.3-76.7)
1.10	1.54	3.31 (2.65-3.97)	90.0 (88.3-91.8)

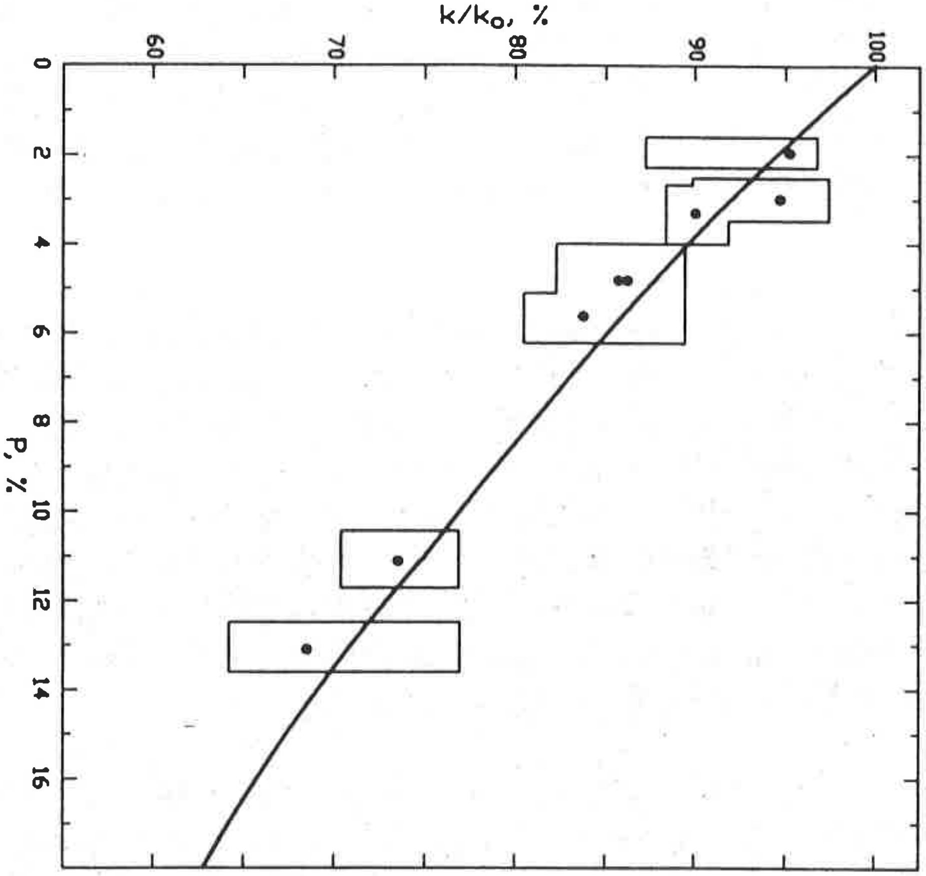

Fig. C.1.3-B Comparison Between Analytical Porosity-correction Factor, $f_p = k/k_0 = (1 - P)/(1 + \beta P)$, and the Data of di Novi [5] for $\beta = 1.7$. The dots represent nominal values while the rectangles encompass the uncertainties based on the scatter in the k/k_0 data and on the uncertainty in the solid (and liquid) fission-product swelling.

expect, for example, for sintered products with isolated spherical porosity ($\beta = 0.7$ to 1.0) or for irradiated metal fuel with isolated fission-gas bubbles. It appears likely that most of the porosity for these samples is due to partially interconnected bubbles and/or to microtearing induced by anisotropic growth. Such tearing could cause a larger reduction in thermal conductivity than spherical pores of the same porosity fraction. The question of whether such behavior is particular to the Mark-IA fuel is addressed in the following.

Two sets of in-reactor thermal-conductivity measurements were performed on EBR-II Mark-II fuel. Beck and Fousek [6] analyzed the results of the instrumented CP-59 capsule irradiated in CP-5. Thermocouples were located along the fuel centerlines and in the NaK bath adjacent to the cladding. The data are given in graphical form as a percentage decrease in thermal conductivity with fuel volumetric swelling. The volume increase of the fuel ($\Delta V/V_0$) was determined from the change in plenum pressure prior to significant gas release. Because of the low burnups involved (<0.5 at.%), the porosity was simply set equal to $\Delta V/V_0$ in analyzing these data.

The porosity factor, $(1 - P)/(1 + \beta P)$, with $\beta = 1.7$ is tested in Fig. C.1.3-C. The correlation agrees with the range of data for $0 \leq P < 10\%$ and $29 \leq P \leq 33\%$. For $10 < P < 29\%$, the correlation predicts a greater decrease in conductivity than indicated by the data. A more sophisticated mathematical treatment would be to let $f_p = (1 - P)/(1 + \beta P + \gamma P^n)$ in order to better fit the data over the full range of porosities tested. There is some physical basis for this, as the reduction factor should increase as the pores change shape and start to interconnect. However, it is not clear whether the data are accurate enough to justify such a treatment. In particular, the calculation of $\Delta V/V_0$ from the rise in plenum pressure assumes that no gas is released from the fuel until the bubbles interconnect at $\Delta V/V_0 \sim 33\%$.

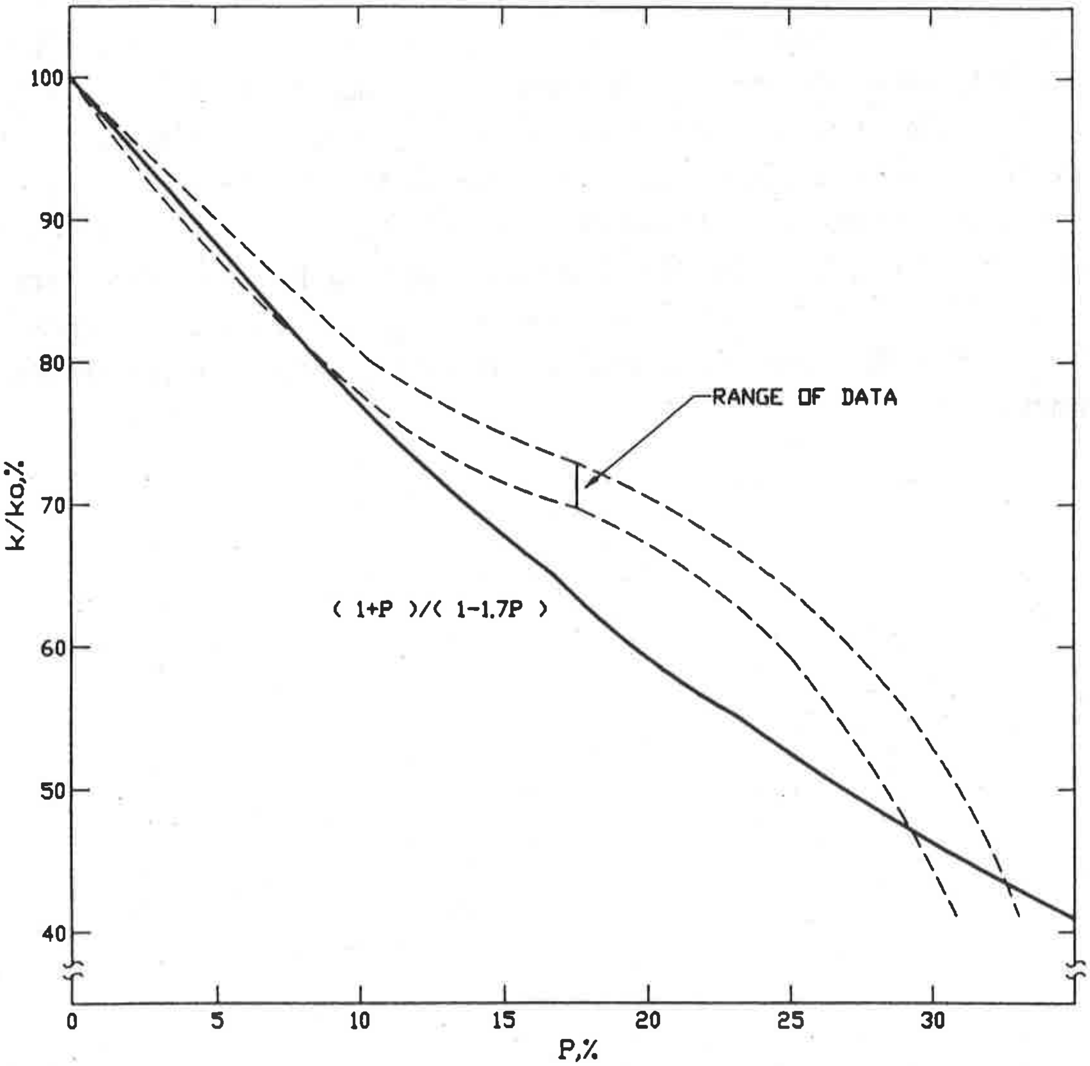

Fig. C.1.3-C Comparison of the Analytical Porosity-correction Factor, $f_p = k/k_0 = (1 - P)/(1 + \beta P)$, With the In-reactor Data of Beck and Fousek [6] for $\beta = 1.7$

Betten [7] has reported the results of instrumented subassembly XX08 in which fuel and coolant thermocouple measurements were made as a function of time to a peak subassembly burnup of 8.8 at.%. He identifies three general regions of behavior. In region 1 (0 to 1 at.% burnup), the thermal conductivity shows the expected decrease with burnup due to porosity formation. In region 2 (1 to 2 at.% burnup) two temperature peaks are observed, indicating minimum values of fuel thermal conductivity. In region 3 (burnup >2 at.%), the effective conductivity levels off to a steady-state value. The minimum value of k/k_0 during the temperature peaking is 0.475 with a standard deviation of 0.111. The long-time value of k/k_0 is 0.720 with a standard deviation of 0.059. Work is in progress to develop models to rationalize this behavior.

(This section is incomplete at this time)

C. TRANSPORT

C.3 Diffusion Coefficients

C.3.1 Uranium-zirconium Alloys

Diffusion in the high-temperature phase of the U-Zr system has been measured by Adda [1] and Muller [2]. The chemical diffusion coefficient

$$\tilde{D} = \tilde{D}_o \exp \frac{-Q}{RT}$$

was measured as a function of composition and temperature in both studies, which were in good agreement. The coefficients obtained by Adda are given in Table C.3.1-1.

TABLE C.3.1-1. Diffusion Coefficients in Gamma U-Zr

Zr Concentration (at.%)	Q (kcal mole^{-1})	D_o (cm^{2}s^{-1})
10	32	9.5×10^{-4}
20	28.6	1.3×10^{-4}
30	26.3	3.5×10^{-5}
40	27.4	4×10^{-5}
50	29.7	8×10^{-5}
60	29.7	6.3×10^{-5}
70	29.7	5.5×10^{-5}
80	34.3	3.2×10^{-4}
90	41	7.8×10^{-3}
95	47	7×10^{-3}

Measurement of the diffusion couple's interface velocity, v, as a function of time allowed the calculation of intrinsic diffusion coefficients for uranium and zirconium by means of the following relations:

$$v = (D_U - D_{Zr})\ dN_U/dx$$

and

$$\tilde{D} = N_U D_{Zr} + N_{Zr} D_U$$

where N is the atomic fraction of each component.

As shown in Fig. C.3.1-A, the diffusivity of uranium is much larger than that of zirconium in the γ-phase.

Diffusion in the lower-temperature phases has not been studied in much detail. A few experiments at the zirconium-rich side of the system have been reported by Schope [3] and Mash [4]. For temperatures below 600°C Schope reports

$$D_o = 3.8 \times 10^{-8}\ cm^2 s^{-1},\ Q = 15\ kcal\ mole^{-1}$$

This activation energy appears to be rather low, probably because more than one phase was present in the diffusion zone, and the concentration profiles were not detailed enough to determine diffusion coefficients in the separate phases.

The activation energy reported by Mash for temperatures below 600°C is even lower and suffers from the same uncertainty, since this experimenter only determined the total width of the interdiffusion zone as a function of time and temperature.

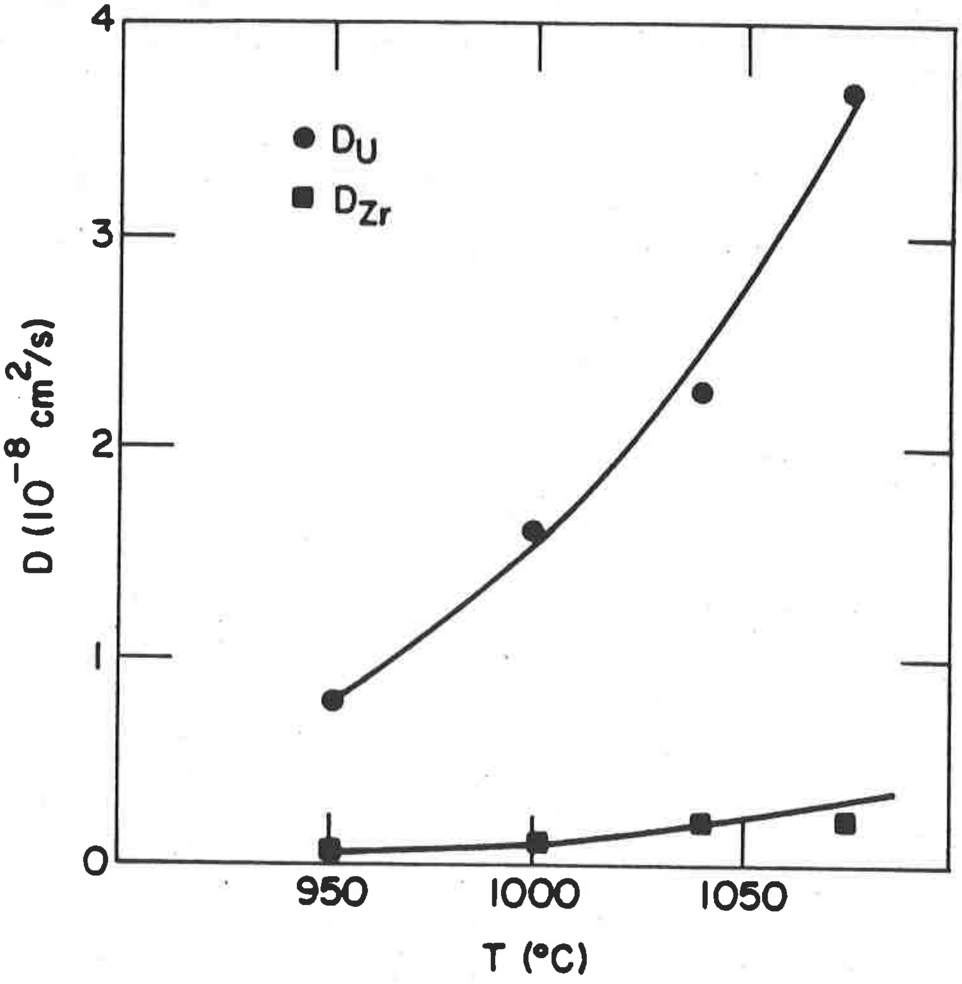

Fig. C.3.1-A. Intrinsic Diffusion Coefficients of Uranium and Zirconium in gamma U-Zr.

Both experimenters also reported values above 600°C of 47 kcal mole^{-1} and 44 kcal $\text{mole},^{-1}$ respectively, which agree rather well with the data shown at the beginning of this section (see Table C.3.1-1).

Pavlinov [29] recently reported values for U tracer diffusion in α Zr that can be fitted to an Arrhenius equation with the following parameters:

$$D_o = 1.6\,^{+1.0}_{-0.6} \times 10^{-2}\ \text{cm}^2\ \text{s}^{-1} \qquad \text{and}$$

$$Q = 44.9 \pm 1.0\ \text{Kcal mole}^{-1}$$

C.3.2 Uranium-Plutonium-Zirconium Alloys

There are presently no known diffusion data on this ternary alloy.

C.3.3 Others

Available diffusion data on U, Pu, and Zr, as well as the few available data on their binary alloys, are presented in this section to assist the experimenter in estimating diffusivities in the ternary alloy system.

Also offered are limited data on fission-gas diffusion in uranium and thermomigration in uranium and zirconium.

Uranium

Self-diffusion of uranium has been measured in the α, β, and γ phases by several experimenters [5,6,7,8], the combined results of which are shown in Fig. C.3.3-A.

The following coefficients are recommended.

	Phase		
Parameter	α	β	γ
Q (kcal $mole^{-1}$)	40	42	26.5
D_o (cm^2s^{-1})	2×10^{-3}	1×10^{-5}	1.12×10^{-3}

Plutonium

Self-diffusion of plutonium has been measured in the ε-phase by Dupuy [9] and in the δ- and γ-phases by Tate [10,26]. The data are shown in Fig. C.3.3-B. The following coefficients are recommended:

	Phase		
Parameter	ε	δ	γ
Q (kcal $mole^{-1}$)	18.5	23.8	16.7
D_o (cm^2s^{-1})	2×10^{-2}	4.5×10^{-2}	2.1×10^{-5}

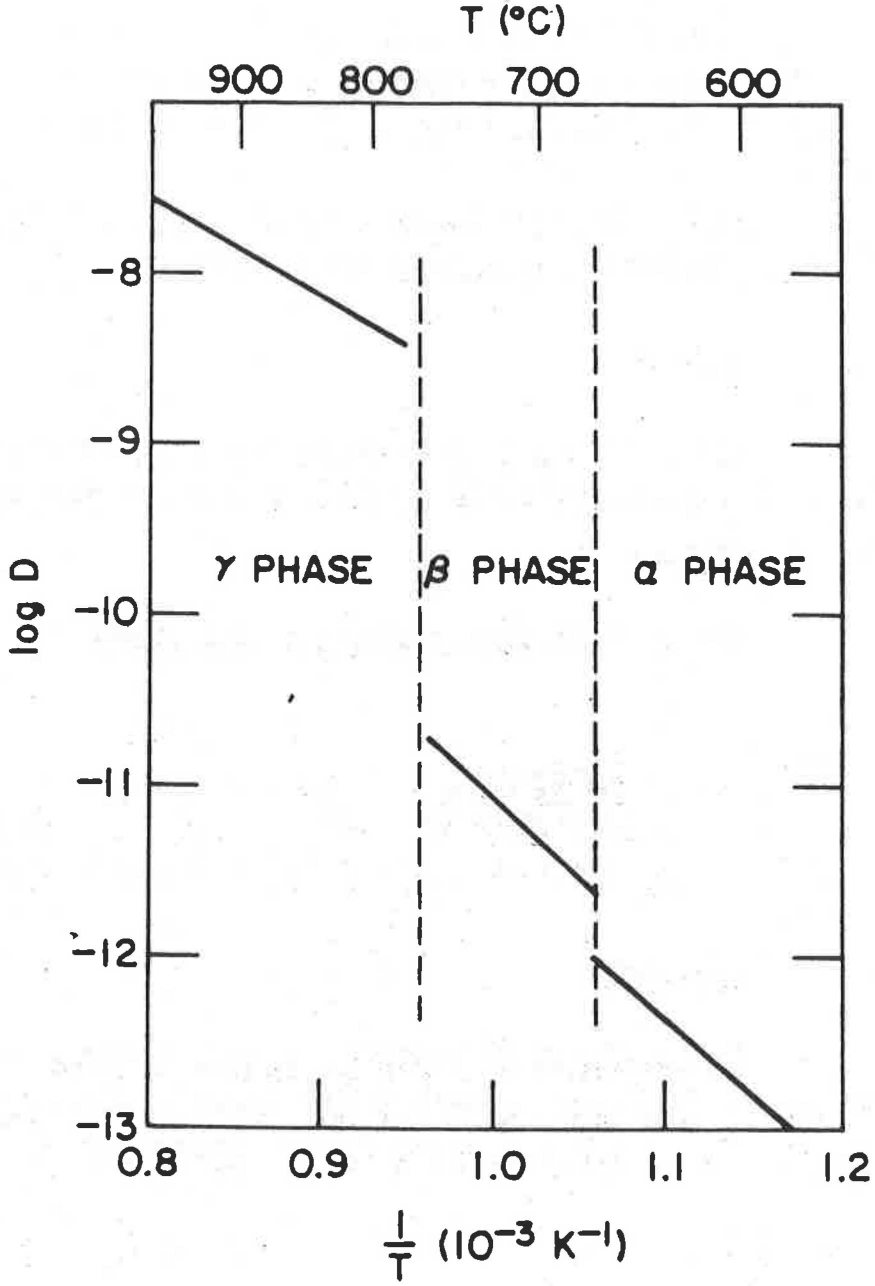

Fig. C.3.3-A Self-diffusion Coefficients of Uranium.
D is in cm^2/s.

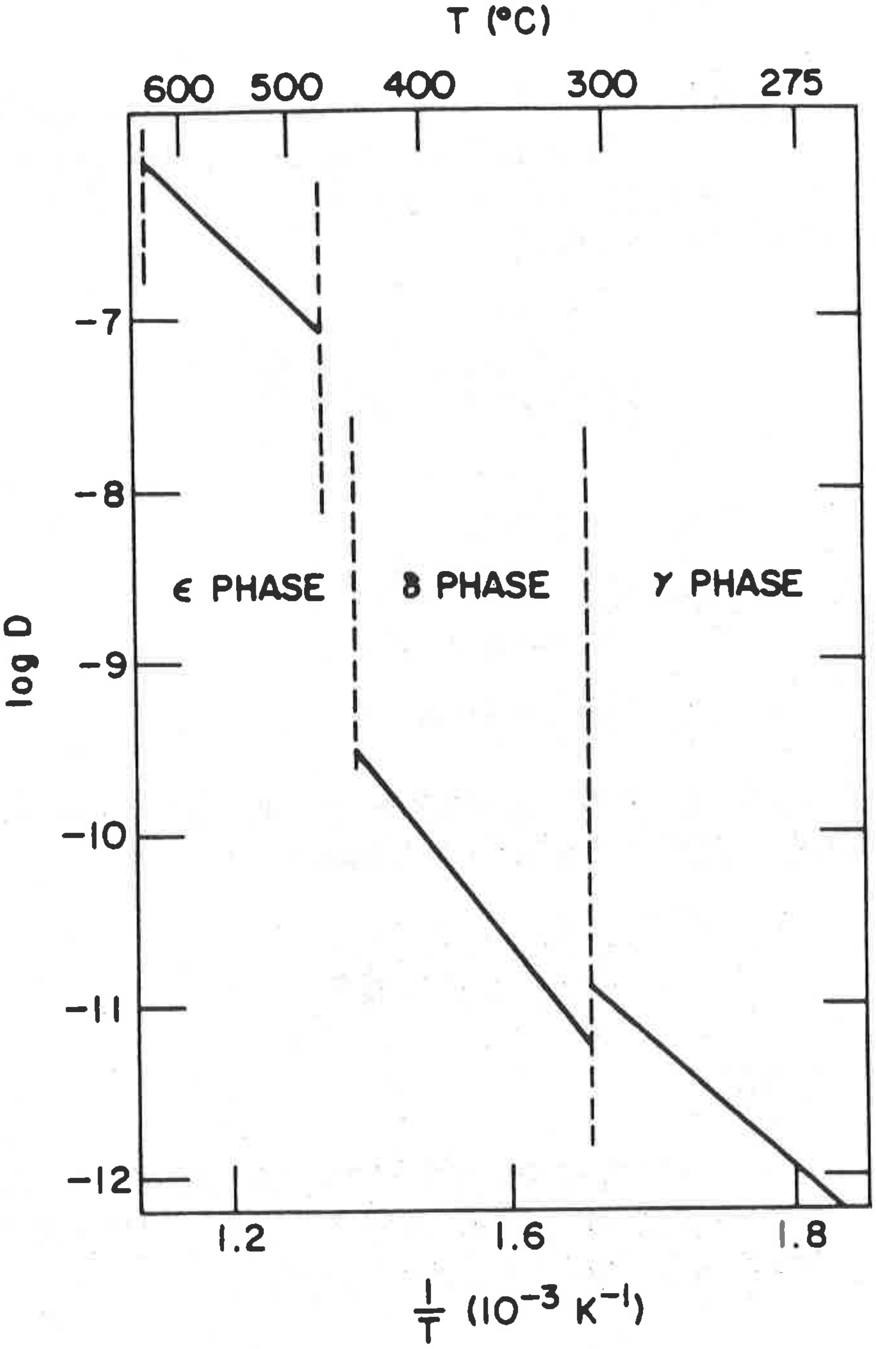

Fig. C.3.3-B Self-diffusion Coefficients in Plutonium. D is in cm^2/s.

Zirconium

Self-diffusion in zirconium (β) has been determined by several investigators.[23,24,25] The data show a curvature in the Arrhenius plot of log D vs. T^{-1}. Kidson [24] has suggested the following bilinear Arrhenius expression for D in the β-phase:

$$D = D_{o1}\exp\left(\frac{-Q_1}{RT}\right) + D_{o2}\exp\left(\frac{-Q_2}{RT}\right)$$

where $D_{o1} = 1.34\ \mathrm{cm^2 s^{-1}}$

$D_{o2} = 8.5 \times 10^{-5}\ \mathrm{cm^2 s^{-1}}$

$Q_1 = 65.2\ \mathrm{kcal\ mole^{-1}}$

$Q_2 = 27.2\ \mathrm{kcal\ mole^{-1}}$

Self-diffusion measurements in the α phase vary widely; however the most recent determination is recommended:

$$D_o = 2.1 \times 10^{-7}\ \mathrm{cm^{-2} s^{-1}}$$
$$Q = 27\ \mathrm{kcal\ mole^{-1}}$$

U-Pu

Chemical diffusion coefficients in U-Pu up to a concentration of 17.5% Pu over a temperature range of 400°C to 540°C have been measured by Dupuy [11]. The data are shown in Table C.3.3-1.

TABLE C.3.3-1 Diffusion Coefficients in Uranium-plutonium Alloys Between 400°C and 540°C

Pu (wt %)	D_o (10^{-7} cm^2/s)	Q (kcal/mole)
0.35	--	--
1.75	0.14	13.4
3.50	0.15	13.7
5.25	0.18	14.1
7.00	0.28	15.2
8.75	0.44	16.3
10.50	0.88	17.9
12.25	1.18	18.8
14.00	2.00	20.0
15.75	2.57	20.6
17.15	--	--

Pu-Zr

Plutonium self-diffusion was measured in a 40 at.% Zr alloy over a temperature range of 640°C to 600°C (ε-phase) [12]. The following coefficients were obtained:

$$D_o^{Pu} = 4 \times 10^{-2} \text{ cm}^2\text{s}^{-1}$$

$$Q = 30 \text{ kcal mole}^{-1}$$

Fission-gas Diffusion

Fission-gas diffusion data derived from Xe and Kr release, measured in out-of-pile annealing tests of irradiated uranium, have been reported by several experimenters. The results of the most thoroughly reported experiments are shown in Fig. C.3.3-C The data fall into two rather distinct groups. One group is characterized by higher diffusivities in the γ-phase and very high activation energies, e.g., 60 kcal mole^{-1} [14] to 98 kcal

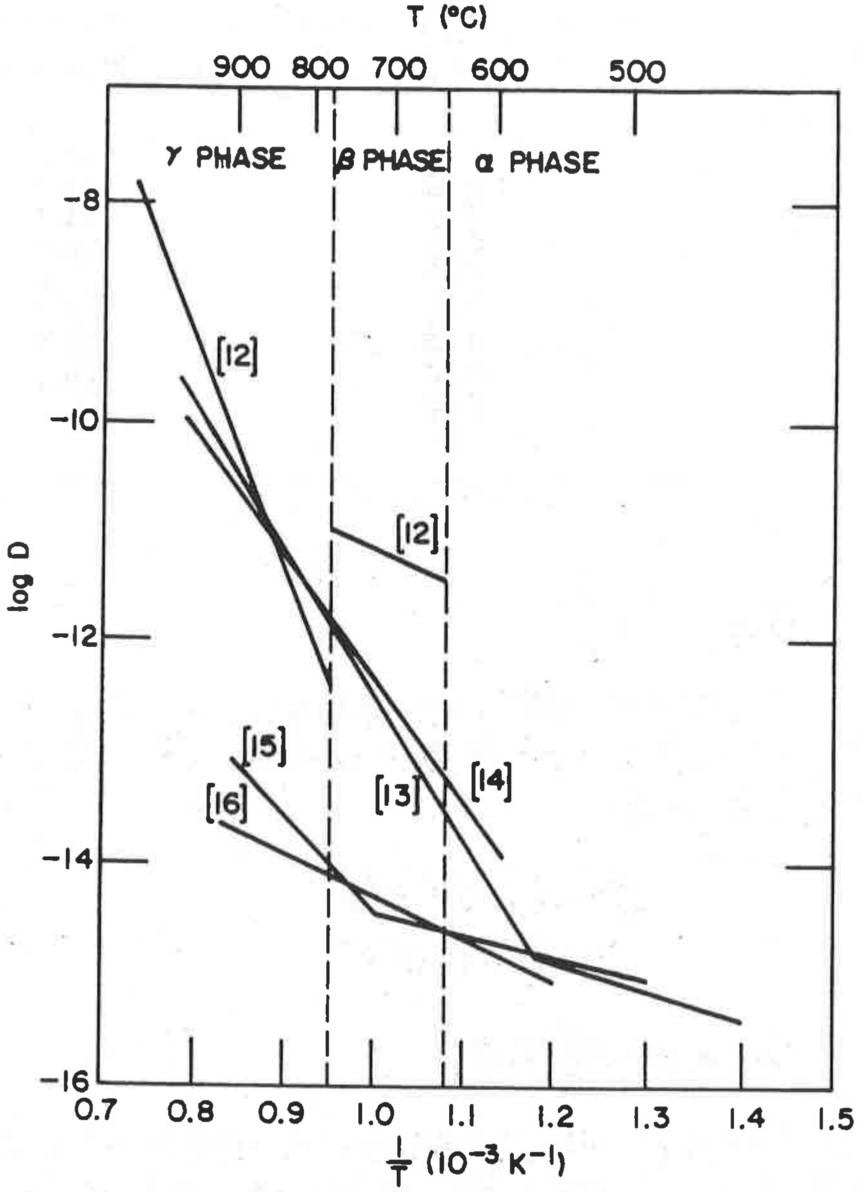

Fig. C.3.3-C Xenon-diffusion Coefficients in Uranium. D is in cm^2/s.

mole^{-1} [13]. This group is probably representative of diffusion of Xe in the U matrix, while the other group [14,15] that is characterized by a much lower activation energy and lower diffusivities is probably a reflection of primarily grain-boundary diffusion [17]. The different diffusion behavior in the β-phase reported by Perraillon [13] cannot be dismissed, as the experimental work appears to be of excellent quality.

Thermomigration

Redistribution of alloy constituents in a temperature gradient called thermomigration or sometimes thermotransport or Soret effect is characterized by a parameter called heat of transport, Q*.

Thermomigration experiments in U-Zr and U-Pu-Zr have not been done, and only very limited information is reported on pure uranium and zirconium.

D'Amico [18] reported a value for uranium (γ) of

$$Q^*/f = +4.7 \pm 0.5 \text{ kcal mole}^{-1}$$

where f is the tracer diffusion correlation factor. The positive value for Q* indicates that uranium migrates to the colder end of the sample.

Campbell [19] and Dubler [20] have reported data on zirconium (β). Campbell reports a value of

$$Q^*/f = -34 \pm 11 \text{ kcal mole}^{-1}$$

indicating transport to the hotter end of the sample.

Surface Diffusion

The recommended surface-diffusion coefficient is obtained from "homologous temperature" arguments by using the low-temperature correlation given by Gjostein [27], augmented by a high-temperature correlation from the data reported by Gjostein. The result is [28]

$$D_s = 1.66\text{x}10^5 \exp(-40T_m/RT) + (1.4 \times 10^{-2}) \exp(-13T_m/RT) \text{ cm}^2/\text{s}.$$

D. MECHANICAL

D.1 Elastic Constants

D.1.1 Unirradiated 100%-dense U-Zr

F. A. Rough [1] has reported the dynamic Young's modulus (E) for uranium-zirconium alloys as a function of composition and temperature ($20 < T < 500°C$). Figures D.1.1-A and -B summarize the data for induction-melted and arc-melted U-Zr alloys. The Young's modulus for the induction-melted samples is consistently higher than that for arc-melted, indicating the possible role of impurities (e.g., carbon) from the graphite crucibles used.

In order to develop a correlation to predict E as a function of temperature and Zr weight fraction (W_z), the temperature dependencies of pure uranium [2] and pure zirconium [2] were considered. The law of mixtures was used to derive

$$E = E_u[(1 + 0.17\ W_z)/(1 + 1.34\ W_z)][1 - 1.06\ (T - 588)/T_{mu}], \qquad (1)$$

where $E_u = 1.60 \times 10^5$ MPa is the Young's modulus of pure U at 588 K (315°C) and $T_{mu} = 1405$ K (1132°C) is the melting temperature of pure uranium. The temperature coefficient of 1.06 is consistent with the range of values for metals when the actual temperature is normalized with respect to the melting temperature [2]. The reference temperature of 588 K (315°C) was chosen over room temperature because it is the lowest in-reactor temperature for which there are data.

Table D.1.1-1 shows the comparison between the correlation and the data [1] for arc-melted U-Zr alloys. The Young's modulus varies inversely with both temperature and Zr weight fraction. The maximum deviation between

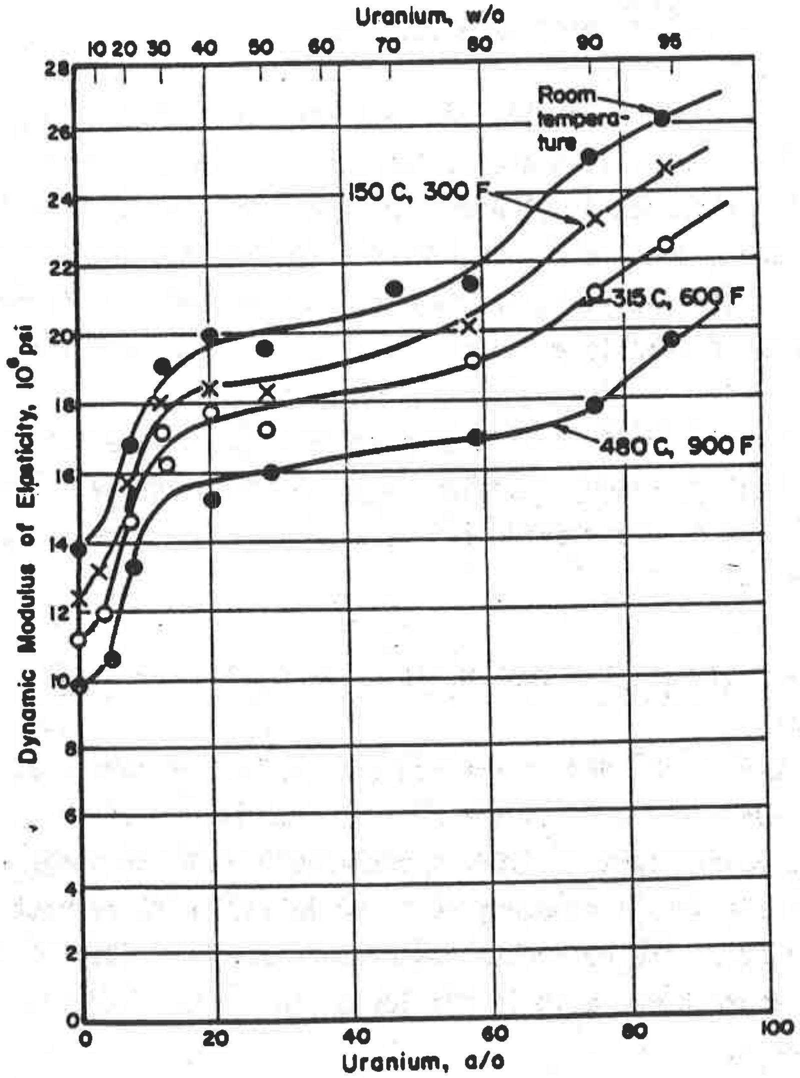

Fig. D.1.1-A. Variation of Dynamic Modulus of Elasticity at Various Temperatures With Uranium Content in Induction-melted U-Zr Alloys (from Ref. 1).

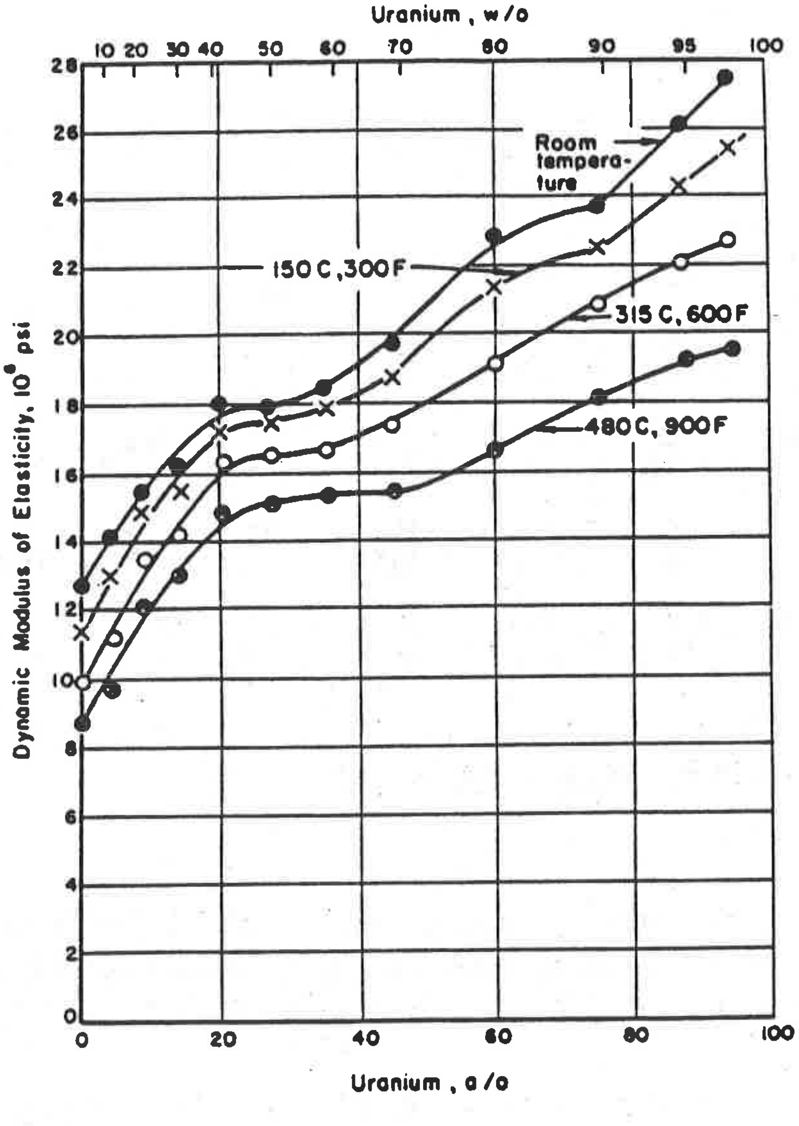

Fig. D.1.1-B. Variation of Dynamic Modulus of Elasticity at Various Temperatures With Uranium Content In Arc-melted U-Zr Alloys (from Ref. 1).

the correlation and the data is 9% for $W_z \le 0.4$ and $293 \le T \le 753$ K. No estimate is available on the accuracy of the data. The major uncertainty is associated with impurity content and fabrication procedures.

Table D.1.1-1. Comparison Between the Correlation Values and Experimental Data (from Fig. D.1.1-A) for U-Zr Alloys. Correlation values are in parentheses.

T (K)	T (°C)	0[a]	2.5	5	10	20	30	40
293	20	1.97 (1.98)	1.89 (1.90)	1.81 (1.85)	1.63 (1.75)	1.58 (1.61)	1.36 (1.47)	1.27 (1.27)
423	150	1.81 (1.80)	1.75 (1.75)	1.68 (1.70)	1.55 (1.61)	1.47 (1.47)	1.29 (1.35)	1.23 (1.25)
588	315	1.60 (1.60)	1.57 (1.56)	1.52 (1.51)	1.43 (1.43)	1.32 (1.30)	1.20 (1.20)	1.15 (1.11)
753	480	1.37 (1.40)	1.34 (1.36)	1.32 (1.32)	1.26 (1.26)	1.14 (1.14)	1.07 (1.05)	1.06 0.97

[a] Extrapolated values from curves in Fig. D.1.1-A

Equation 1 is recommended for the Young's modulus of 100%-dense U-Zr alloys for temperatures below the phase-change temperature (~650°C). The effects of the phase change and porosity will be discussed subsequently.

A similar approach was used to estimate Poisson's ratio (ν) for U-Zr alloys. Based on the ν values [3] for pure uranium and pure zirconium, the law of mixtures was used to derive

$$\nu = 0.24\ [(1 + 3.4\ W_z)/(1 + 1.9\ W_z)][1 + 1.2\ (T - 588)/T_{mu}] \qquad (2)$$

The Poisson's ratio for pure Zr varies from ~0.33 at room temperature to ~0.35 at the α-to-β phase-transition temperature of 862°C. The Poisson's ratio for pure U varies from ~0.19 at room temperature to ~0.29 at 300°C, which is the limit of the data base. Both of these results are dependent on the method of fabrication and, in turn, on the preferred orientation of these anisotropic materials.

No data for the Poisson's ratio of U-Zr alloys are available for comparison with Eq. 2. However, Eq. 2 is recommended for 100%-dense U-Zr alloys for temperatures below the phase-change temperature (e.g., ~650°C for U-10Zr). A maximum value of $\nu = 0.5$ should also be invoked. For U-10Zr at 650°C, Eq. 2 predicts $\nu = 0.35$ which is reasonable. The effects of phase change and porosity are discussed in the following.

The effective elastic properties (E, ν) generally decrease with increasing porosity. Correction factors of the form

$$f_e = E/E_{100} = 1 - \beta_e P \qquad (3)$$

and

$$f_\nu = \nu/\nu_{100} = 1 - \beta_\nu P \qquad (4)$$

have been used in the modeling of ceramic nuclear fuels [4,5]. The β_e values for UC, UN, and UO_2 (based on experimental data) are 1.54, 2.72, and 1.66, respectively. Similarly, the β_ν values are 0.21, 1.31, and 0.91 for UC, UN, and UO_2, respectively. Averaging these values gives $\beta_e = 1.2$ and $\beta_\nu = 0.8$. It is recommended that these f_e and f_ν factors be applied to Eqs. 1 and 2, respectively, in order to estimate the decrease in effective elastic properties with increasing fission-gas porosity.

The change in elastic properties with phase change is more complicated to unravel because of the sparsity of the data base. Zirconium exhibits a decrease of ~13% in Young's modulus from 862°C to 900°C [2]. No information was found on the change in shear modulus or Poisson's ratio beyond the phase-change temperature. In Fig. D.1.1-C the shear modulus of pure U is shown to change slope at the α-to-β transition temperature of ~670°C and the β-to-γ transition temperature of ~775°C [6]. If the β phase is ignored because it is suppressed in U-Zr alloys, then it appears that one would expect a decrease in shear modulus of ~30% if the α-to-γ phase change occurred at ~650°C. In the absence of more data, the preliminary recommendation is that E be decreased by 30% at the phase-change temperature and ν be held continuous through the phase change. This approach is consistent with the data for G, but it is certainly not a unique solution to the problem.

In summary, the following equations are recommended for the Young's modulus of U-Zr alloys:

$$E = E_u(1 - 1.2P)\left[\frac{1 + 0.17\ W_z}{1 + 1.34\ W_z}\right]\left[1 - 1.06\ (T - 588)/T_{mu}\right], \qquad (5a)$$

where T = temperature (< phase-change temperature) in K
P = porosity fraction
W_z = Zr weight fraction
T_{mu} = 1405 K, the melting temperature of pure U

and

$E_u = 1.6 \times 10^5$ MPa, the Young's modulus for pure U at the chosen reference temperature of 588 K.

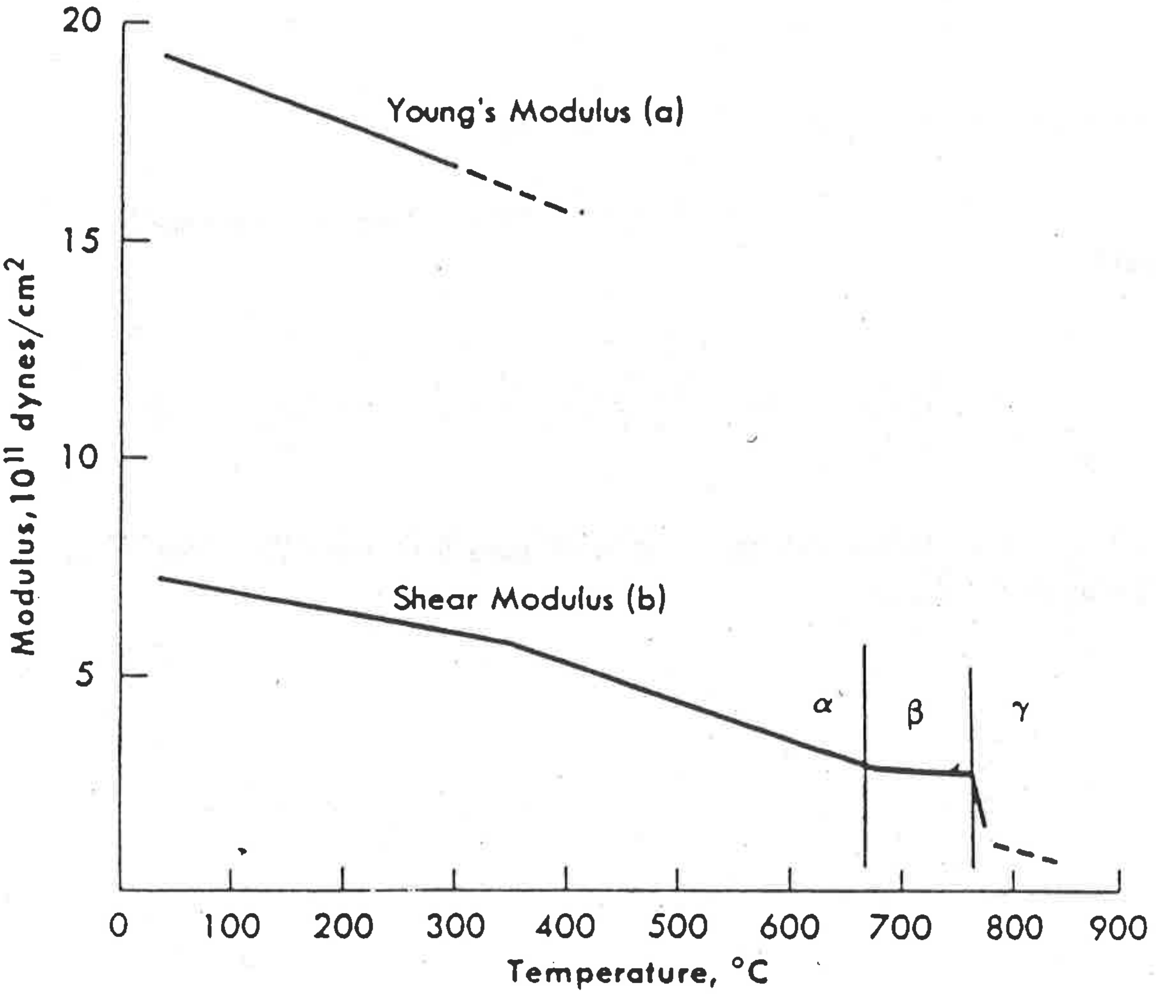

(A. N. Holden, Physical Metallurgy of Uranium, © 1952, Addison-Wesley Publishing Co., Inc., Reading, Massachusetts. Fig. 5.1. Reprinted with permission. Refer to Ref. 6.)

Fig. D.1.1-C. Effect of Temperature on Elastic Moduli of U

For $T>T_p$ where T_p is the α-to-γ phase-change temperature, the recommended Young's modulus (E_γ) for γ-phase U-Zr is

$$E_\gamma = E - 0.3E_p, \qquad (5b)$$

where $E_p = E(T_p)$ and E is defined by Eq. 5a.

For the Poisson's ratio of U-Zr alloys, the recommended equation is

$$\nu = \nu_u(1 - 0.8P)\left[\frac{1 + 3.4\ W_z}{1 + 1.9\ W_z}\right][1 + 1.2\ (T - 588)/T_{mu}], \qquad (6)$$

where $\nu_u = 0.24$ is the Poisson's ratio of pure U at the chosen reference temperature of 588 K.

D.1.2 Uranium-Plutonium-Zirconium Alloys

No dynamic data are available for the elastic properties of U-Pu-Zr alloys. The static (i.e., tensile-test) data are generally believed to be unreliable because of the effect of other deformation mechanisms which dominate even at room temperature. Even pure U does not have a well defined static modulus at room temperature [6]. The static data for Young's modulus of U-Pu-Zr alloys are summarized in Table D.1.2-1 [7]. Most of these data imply at least an order of magnitude decrease in Young's modulus for a Pu weight fraction of 15%.

The Young's modulus for pure Pu is less than that for U [3]. Based on a simple law of mixtures, it is reasonable to expect the Young's modulus of U-Pu-Zr alloys to vary inversely with Pu weight fraction (W_p). In order to attempt to quantify this dependency, the room-temperature data for cast U-11Pu-6.3Zr are used to estimate the decrease in E with W_p. This results in the following correlation for E:

$$E = E_u(1 - 1.2P)\left[\frac{1 + 0.17\,W_z}{1 + 1.34\,W_z} - W_p\right][1 - 1.06\,(T - 588)/T_{mu}], \quad (7)$$

where E_u, P, W_z, T, and T_{mu} have the same definition as in Eq. 5a and W_p is the Pu weight fraction. For temperatures above the $\alpha \rightarrow \gamma$ phase change temperature, Eq. 5b is recommended.

No data are available for the Poisson's ratio of U-Pu-Zr alloys. The room-temperature value for Pu(α) [3] is less than that for U(α). However, as Pu goes through so many phase changes between room temperature and typical U-Pu-Zr phase-change temperatures, it is difficult to use the law of mixtures in this application. Thus, Eq. 6 is recommended for U-Pu-Zr alloys.

TABLE D.1.2-1. Static Young's-modulus Values for Several U-Pu-Zr Compositions (from Ref. 7).

Alloy	Fabricated Method	T (K)	E (10^5 MPa)
U-15Pu-10Zr	Extruded	298	0.15
		573	0.14
		623	0.062
		673	0.028
U-15Pu-12.2Zr	Cast	298	0.097
U-11Pu-6.3Zr	Cast	298	1.70
		948	0.14

D.1.3 Others

Saller et al. [8] have reported some values of Young's modulus for U-5Fs alloys. For as-rolled flat-plate specimens tested statically at 563 K and 813 K, the respective values for E are 0.68×10^5 MPa and 0.63×10^5 MPa. Because static methods are not considered as reliable for determining the E values for uranium alloys, these data have not been used to guide the development of U-Zr and U-Pu-Zr correlations for elastic properties. It is recommended that Eqs. 5 and 6 be used to describe U-5Fs behavior with $W_z = 0.05$. This would probably give a more accurate representation of the U-5Fs elastic properties than the static U-5Fs data.

D. MECHANICAL

D.2 Creep

D.2.1 Uranium-Zirconium Alloys

Tensile-creep data for U-Zr alloys of various compositions have been reported by Battelle Memorial Institute [1,2]. Both secondary (minimum) creep rate and time to 1% creep were reported. Comparison of the minimum creep rates with a calculated average creep rate to 1% strain indicates that primary creep was not important in these tests. The strain-time curves given in Ref. 2 support this conclusion. Unfortunately, most of the data are for alloys containing greater than 45 wt % zirconium where at low temperatures the equilibrium phases consist of pure δ or δ plus α zirconium. Such high concentrations of zirconium are probably not relevant to fast-reactor fuel, even though zirconium migration is expected to increase the zirconium concentration in certain regions of the fuel during irradiation.

Because of the scarcity of data, correlations to estimate the thermal creep of uranium-zirconium alloys have been developed from theoretical models plus available data on uranium and uranium-plutonium-zirconium alloys. These correlations and their fit to the U-Zr data are given in Section D.2-3.

D.2.2 Uranium-Plutonium-Zirconium Alloys

The thermal creep of U-Pu-Zr alloys has been measured using cast [3] and extruded [4] tensile specimens. The results reported from these studies are the times to reach 2% strain at constant load (constant engineering stress) and constant temperature, as summarized in Table D.2.2-1. This table shows that, although the temperature ranges do not overlap, the data for the cast alloys and extruded alloys appear inconsistent, with the extruded samples creeping much more rapidly. Part of the difference may be due to the difference in fabrication methods, since uranium is known to work-harden considerably. However, hardness values for the as-cast material prior to extrusion were identical to the hardness values of the extruded material [4]. Furthermore, the effects of work hardening would be expected to be more important to the low-temperature, high-strain-rate tensile properties than to the high-temperature creep properties. A more likely explanation for the high creep rates of the extruded material is that these tests were performed at much higher stresses, lower temperatures, and shorter times, where primary and tertiary components of the creep strain dominate the lower-rate secondary creep strain.

Most of the times to 2% strain reported for creep of cast U-Pu-Zr [3] were extrapolated from tests terminated at about 1% strain. It was established that the strain-time relationship for this material was approximately linear on log-log coordinates to at least 5% strain so the extrapolation was meaningful. Data for times to creep to 1, 2, 3, 4 and 5% strain at 650°C given in Fig. 8 of Ref. 3 indicate that the slope is about 1, suggesting that most of the creep strain accumulated in the constant-rate secondary regime. As with U-Zr alloys, correlations for creep of U-Pu-Zr are included in the general discussion of creep of metallic fuels given in the following section.

TABLE D.2.2-1. Time (Minutes) to Attain 2% Strain in U-Pu-Zr Alloys

Alloy Composition (wt %)			Stress (MPa)	Temperature (°C)								
U	Pu	Zr		290	350	400	500	600	625	650	675	700
a												
82.6	11.1	6.3	4.9							15		
			9.8							5		
			19.6							3		
			39.2							1		
77.1	16.6	6.3	4.9						--		10	
			9.8						5000		1	
			19.6						210		--	
			39.2						10		--	
75.0	15.0	10.0	4.9						--	5000		
			9.8						5000	80		
			19.6						210	1		
			39.2						10	--		
67.4	18.5	14.1	4.9					100,000		5000	60	55
			9.8					10,000		80	10	10
			19.6					800		2	2	3
			39.2					70		--	--	--
b												
75.0	15.0	10.0	13.8				20					
			20.7				5					
			55.2			30						
			68.9			9						
			75.8			3						
			137.9		300							
			206.8		20							
			275.8		9							
72.5	15.0	12.5	13.8				8					
			20.7				4					
			103.4			15						
			117.2			8						
			131.0			4						
79.0	15.0	6.0	6.9				0.3					
			34.5	30								
			41.4	9								

a Cast Alloys, [3].

b Extruded Alloys, [4].

D.2.3 Others

In the α-uranium-rich regimes of U-Zr and U-Pu-Zr alloys, creep appears to be dominated by creep of the α uranium matrix. Data on creep of uranium is therefore included in the present discussion. As pointed out by Holden [5, Section 5-5] much of the early uranium creep data was extremely inconsistent due to poor control of grain size and grain orientation and control of temperature fluctuations during the tests. It is known in this regard that polycrystalline uranium samples elongate when repeatedly heated and cooled in the α temperature range [6] even without load.

More reliable data on creep of uranium have been measured by Shober, Marsh, and Manning [7]. Minimum creep rates were reported for temperatures ranging from 100 to 500°C and stresses yielding creep rates ranging from 2×10^{-5} to 2.5 h^{-1}. Secondary creep data at 500°C reported in the Reactor Materials Handbook [8] and the creep data of McIntosh and Heal [9] for tests at 400, 500 and 600°C appear consistent with the data of Shober et al.

The form of the secondary creep equation used here to correlate the data for all metallic fuels is the form used by Solomon, Routbort, and Voglewede to represent creep of UO_2 [10]. The total plastic strain rate $\dot{\epsilon}$ is given by

$$\dot{\epsilon} = C_1(d)\sigma \exp(-Q_1/RT) + C_2\sigma^n \exp(-Q_2/RT) \qquad (1)$$

where

$\dot{\epsilon}$ = secondary creep rate, s^{-1}
σ = equivalent stress, MPa
T = absolute temperature, K
R = universal gas constant = 1.987 cal g-mole^{-1} K^{-1}

Q_1, Q_2 = activation energies, cal g-mole^{-1}
d = grain size, μm
C_1, C_2 = material functions

In Eq. 1 the first term represents diffusional creep and the second term dislocation creep. In-reactor fission effects and low-temperature deformation mechanisms such as dislocation glide and twinning, which are important in α uranium at temperatures less than 400°C, are not considered here.

The temperature dependence of creep of uranium in the α regime has been determined by Shober et al. to obey an Arrhenius relationship with an activation energy Q of 52,000 cal g-mole^{-1}. This value of Q is approximately equal to the value of the activation energy for self-diffusion (55,000 cal g-mole^{-1} [11, p. 296]) in α uranium, as would be expected from theory. All of the low-temperature creep data for both uranium and the cast U-Pu-Zr have therefore been reduced using the Zener-Holloman parameter

$$Z = \dot{\varepsilon} \exp (52{,}000/RT)$$

as shown in Fig. D.2.3-A. The data are seen to follow the same curve with a slope of 1 at low stresses and a slope n = 4.5 at higher stresses, as predicted by Eq. 1. It is noted that the power-law slope of 4.5 has been frequently observed for other metals [12]. The constants C1 and C2 have been chosen here to minimize the least-squares error between the calculated and measured values of log Z. The final form of Eq. 1 for creep in the α regime,

$$\dot{\varepsilon} = 0.5 \times 10^4 \, \sigma \exp (-52{,}000/RT) + 6.0 \, \sigma^{4.5} \exp (-52{,}000/RT) \qquad (2)$$

is compared with the data in Fig. D.2.3-A. The root-mean-square error in log Z is 0.4 for the 47 data points.

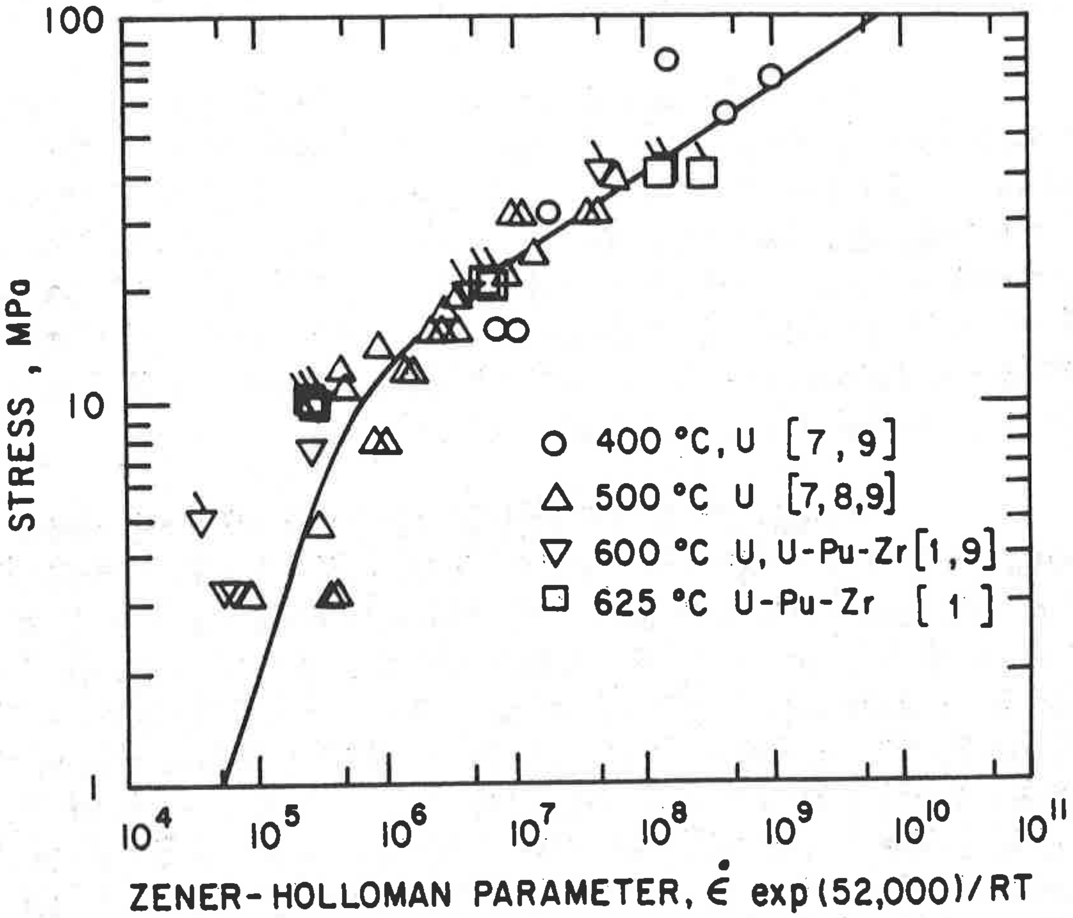

Fig. D.2.3-A. Secondary Creep of Metal Fuels. Open symbols are data for uranium. Symbols with flags were calculated for cast U-Pu-Zr alloys of various compositions using the reported times to 2% strain. References are given in the brackets. The curve is the least-squares fit to the data using Eq. 1.

The grain-size dependence of the linear diffusional creep term in Eq. 1 is expected to vary from d^{-2} to d^{-3} depending on whether Nabarro creep or Coble creep dominates. In addition, Harper-Dorn dislocation creep has the same linear stress dependence but is independent of grain size.

Most of the data in the low-stress range in Fig. D.2.3-A, where the creep rate is linear in stress, come from the experiments of McIntosh and Heal [9]. The grain size in these experiments was controlled to about 160 μm. Although small variations in grain size show the expected behavior of decreasing creep rate with increasing grain size, the variations are not sufficient to determine the power of the dependence. Other experiments on uranium and uranium alloys with larger variations in grain size gave powers that were intermediate between 1 and 2 [9].

Slattery and Miller [13] also measured the creep strength of α uranium and dilute alloys with different grain sizes at a test temperature of 500°C. The experiments used beams that were allowed to sag in a furnace under their own weight. Although these experiments are somewhat difficult to interpret, it is noted that at the low stress levels of the tests (0.75 MPa maximum) the strain rate was a linear function of stress, as predicted by Eq. 2. However, Slattery and Miller reported that there was no significant difference in creep strength after different heat treatments to refine the grain size. Compared to their data, Eq. 1 predicts creep rates that are about half an order of magnitude too high.

Most of the uranium and the U-Pu-Zr data appear to be fit reasonably well by Eq. 2. In the absence of more extensive data, it is recommended that Eq. 2 be used to estimate the thermal creep of IFR alloys in temperature regimes where the α phase is present.

At high temperatures, uranium, zirconium, and plutonium are mutually soluble and form a solid-solution γ phase. The only available data on creep of U-Pu-Zr alloys in the γ regime appear to be the measurements of Savage [3] as reproduced in Table D.2.2-1. Average creep rates calculated from these data by dividing the creep strain by the time are plotted in Fig. D.2.3-B. The 600°C and 625°C data are the same data that are plotted in Fig. D.2.3-A against the Zener-Holloman parameter for creep at lower temperatures. Note that in Fig. D.2.3-B there is a large increase in the creep rate between 625°C and 700°C. This is not surprising, because the creep mechanisms depend on diffusion and a large increase in the diffusion coefficient might be expected upon transformation to the BCC γ phase. A similar transformation from α to γ in pure uranium increases the diffusion coefficient by about 5 orders of magnitude [11, p. 299].

Although in pure metals the ratio of the creep rate on either side of a phase transformation is often directly proportional to the ratio of the self-diffusion coefficients [14, p. 93], the case is not so simple for solid solutions. Here the presence of solute atoms can hinder the rate of dislocation glide, making it possible that the creep rate is governed by dislocation glide rather than climb. Weertman [12] has shown that in this case the creep-rate power is 3. The temperature dependence of creep is again determined by diffusion, but the situation is more complicated in solid solutions than in pure metals because of the different species that are present. In many cases small alloy additions do not change the creep activation energy [14]. In other cases the activation energy is increased or decreased.

We have assumed here that creep of U-Pu-Zr and U-Zr alloys is governed by dislocation glide in the γ regime. The phenomenological creep equation is of the form

$$\dot{\varepsilon} = C_4 \sigma^3 \exp(-Q_4/RT) \qquad (3)$$

where Q_4 is the creep activation energy and C_4 may be a function of composition. In lieu of additional creep data we assume that Q_4 is the same as the

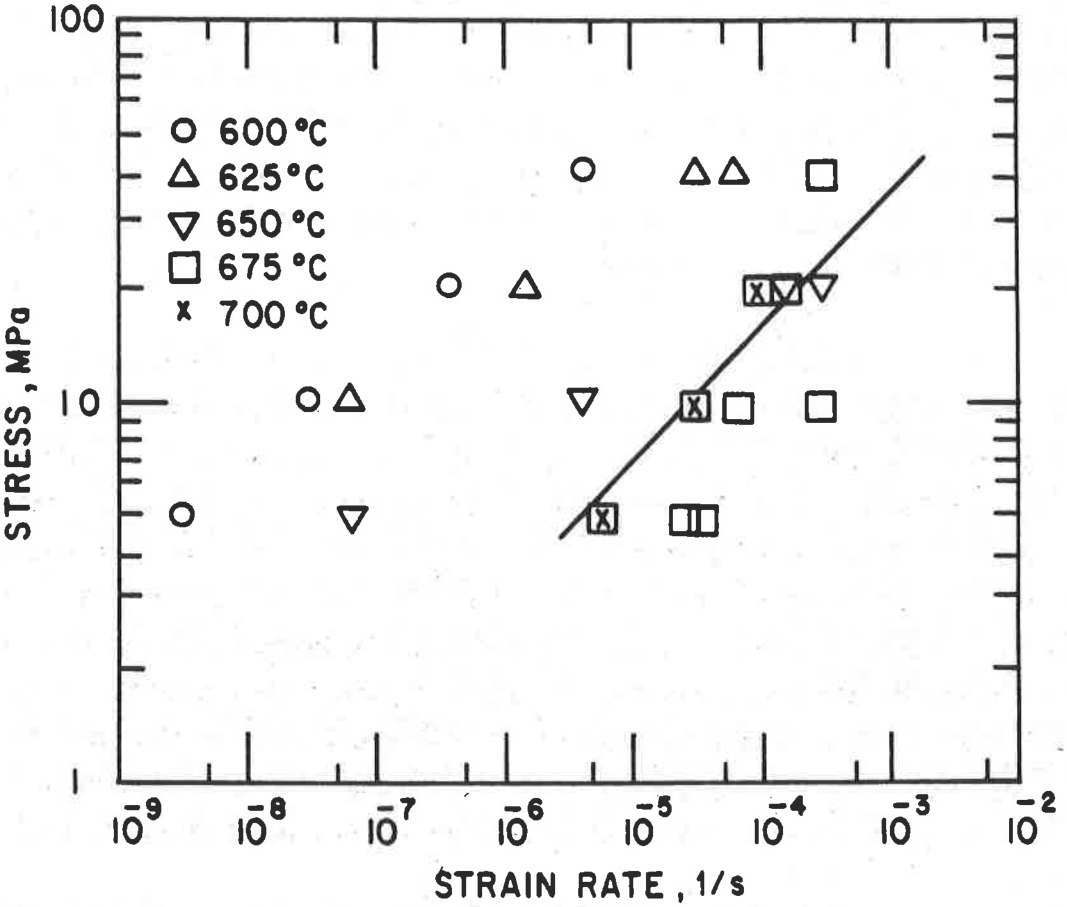

Fig. D.2.3-B Secondary Creep of U-Pu-Zr Alloys. Data are given by the symbols. Calculated creep rates at 700°C are represented by the curve.

activation energy for creep of the pure γ-uranium solvent, which in turn is the activation energy for self-diffusion in γ uranium. Thus,

$$Q_4 = 28{,}500 \text{ cal g-mole}^{-1} \text{ [11, p.296]}.$$

The constant

$$C_4 = 8.0 \times 10^{-2} \text{ MPa}^{-3}\text{s}^{-1}$$

is chosen to fit the 700°C data for U-18.5 wt % Pu-14.1 wt % Zr shown in Fig. D.2.3-B. Calculated values of strain-rate are compared with the 700°C data in Fig. D.2.3-B.

A correlation of the form of Eq. 3 was also developed by Walter, Golden, and Olson [15] in their study of U-Pu-Zr slumping in the high-temperature γ regime. The data [16] that were used in this correlation are the same data that were used for the extrapolations of U-18.5 wt % Pu-14.1 wt % Zr creep strain at 675 and 700°C given in Table D.2.2-1. The temperature above which the constituents are mutually soluble at this composition is about 660°C [17]. The creep tests at both 675 and 700°C were therefore probably performed on material in the γ phase, although some of the data given in Table D.2.2-1 and Fig. D.2.3-B do show anomalous behavior. Nevertheless, the creep power $n = 2.65$ and activation energy $Q = 27{,}000$ cal g-mole^{-1} (calculated using Fig. 9 of Ref. [15]) determined from these data are in very good agreement with the values of $n = 3.0$ and $Q = 28{,}500$ that were selected above on the basis of theoretical models.

As a further check on the activation energy and the importance of composition changes, we have also compared calculations using Eq. 3 with data [2] on creep of low-zirconium U-Zr binary alloys at 818°C. The results are shown in Table D.2.3-1. It would appear from this table that within the range of zirconium contents of interest, the creep rate is not a strong function of the composition. It should be noted, however, that very high zirconium alloys [2] show significantly reduced creep rates with a minimum at 46 wt % for tests at 818°C.

TABLE D.2.3-1. Measured and Calculated Minimum Creep Rates of Low-Zirconium Binary U-Zr Alloys at 818°C.

Alloy Composition (wt %)		Stress (MPa)	Measured Creep Rate (%/h)	Calculated Creep Rate (%/h)
U	Zr			
87.4	12.6	9.8	43.0	51.0
92.9	7.1	3.4	0.65	2.2
74.2	25.8	3.4	1.0	2.2

The structure of U-Pu-Zr and U-Zr between the α and γ regimes discussed here is very complex and depends strongly on composition [17]. The 650°C data and some of the 675°C data shown in Fig. D.2.3-B are for alloys in this regime. There is some indication of creep rates greater than would be calculated by extrapolating either the low-temperature or higher-temperature equations given here, although the data are closer to the creep rates for the pure γ phase. It is therefore recommended that Eq. 3 be used to estimate secondary thermal creep rates for U-Zr and U-Pu-Zr alloys at temperatures above which the α phase is no longer present.

Irradiation Effects

There are a number of in-reactor effects which could result in a dramatic change in the creep behavior of uranium and uranium-alloy fuels. The two effects which are considered in this section are: low temperature, fission-enhanced creep, and the influence of fission-gas porosity on the thermal creep rate. As no data are available for the materials (U-Zr, U-Pu-Zr, and U-5Fs) of interest, the recommendations presented are "best estimates" based on the behavior of U, other metals, and ceramics.

The thermal creep equation (Eq. 2) for the α-phase regime of U and U-Pu-Zr alloys applies to 100% dense materials tested out of the reactor. Let $\dot{\varepsilon}_{t\ell}$ be the thermal creep rate in Eq. 2 which is linear in stress and $\dot{\varepsilon}_{tn}$ be the thermal creep rate which is non-linear (stress exponent of 4.5) in stress. For the in-reactor effects of interest, it is assumed that the linear term is enhanced by a porosity-dependent factor $f_{p\ell}$, and the non-linear term is enhanced by f_{pn}. In addition, a fission-enhanced creep term, $\dot{\varepsilon}_i$, is assumed which is linear in stress. Equation 2 is modified to give the in-reactor creep rate of uranium alloy fuels as:

$$\dot{\varepsilon} = f_{p\ell}\,\dot{\varepsilon}_{t\ell} + f_{pn}\,\dot{\varepsilon}_{tn} + \dot{\varepsilon}_i \qquad (4)$$

The low temperature, in-reactor creep data of Roberts and Cottrell [18] (as reported by Gittus [19]) for α-U springs was used to generate are expression for $\dot{\varepsilon}_i$:

$$\dot{\varepsilon}_i = 7.7 \times 10^{-23}\,\dot{F}\,\sigma,\ s^{-1}, \qquad (5)$$

where σ is effective stress in MPa and $\dot{F}$ is fission rate in fissions/cm^3·s.

To gain some insight into the influence of porosity on fuel creep a literature search was conducted. Unfortunately, no information was found for metals and metal alloys. However, data are available for Al_2O_3, $(U,Pu)O_2$, UO_2, and UN ceramics. [20-25] Figure D.2.3-C shows the porosity-enhancement factor ($f_{p\ell}$) for the linear creep regime of these materials as deduced from data. These plots of $f_{p\ell}$ are compared to a simple analytical

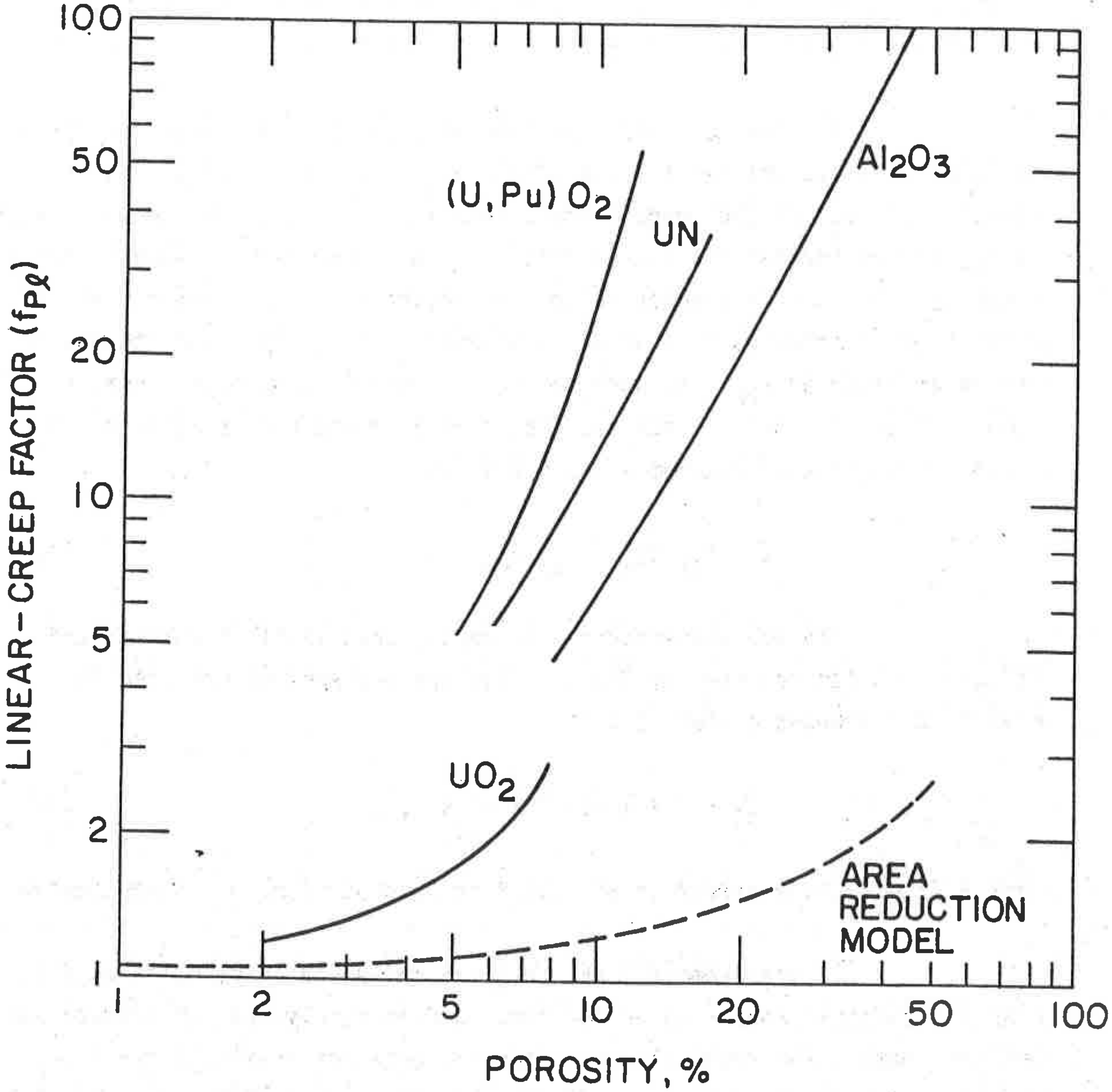

Fig. D.2.3-C Dependence of linear, secondary creep on porosity. Correlations are based on fits to data. All correlations have been re-normalized to give the enhancement in creep rate referenced to 100% dense material.

model (dashed line) which assumes that porosity reduces the effective load-bearing area of the material. Clearly, the data indicate a significantly higher enhancement than the area-reduction model.

An empirical correlation was developed to fit the Al_2O_3 data which cover the wide range of porosities expected for uranium-based alloy fuels:

$$f_{p\ell} = 1 + 7.9\ P + 470\ P^2, \qquad (6)$$

where P is porosity fraction referenced to 100% dense fuel volume. This correlation gives an enhancement factor of ~100 for P = 0.5 (50%).

Figure D.2.3-D shows the porosity-enhancement factor (f_{pn}) for the non-linear creep regime for UO_2, $(U,Pu)O_2$ and Al_2O_3. The dashed lines show what would be predicted from a simple area-reduction model. In this case, the model does a reasonable job of predicting creep-enhancement, at least for the $(U,Pu)O_2$ data. Thus, for the particular non-linear creep terms of interest, the recommended factors are:

$$f_{pn} = (1-P^{2/3})^{-4.5} \text{ for } \alpha\text{-phase (Eq. 2)} \qquad (7a)$$

and

$$f_{pn} = (1-P^{2/3})^{-3} \text{ for } \gamma\text{-phase (Eq. 3).} \qquad (7b)$$

In summary, the recommended in-reactor creep rate correlation for U-Zr, U-Pu-Zr, and U-5Fs alloys below the major phase change $(\alpha \leftrightarrow \gamma)$ temperature (T_p) is:

$$\begin{aligned}\dot{\varepsilon} = {} & 5.0 \times 10^3\ (1 + 7.9\ P + 470\ P^2)\ \exp\ (-52{,}000/RT)\sigma \\ & + 6.0\ (1-P^{2/3})^{-4.5}\ \exp\ (-52{,}000/RT)\sigma^{4.5} \\ & + 7.7 \times 10^{-23}\ \dot{F}\sigma,\ s^{-1}, \qquad (8a)\end{aligned}$$

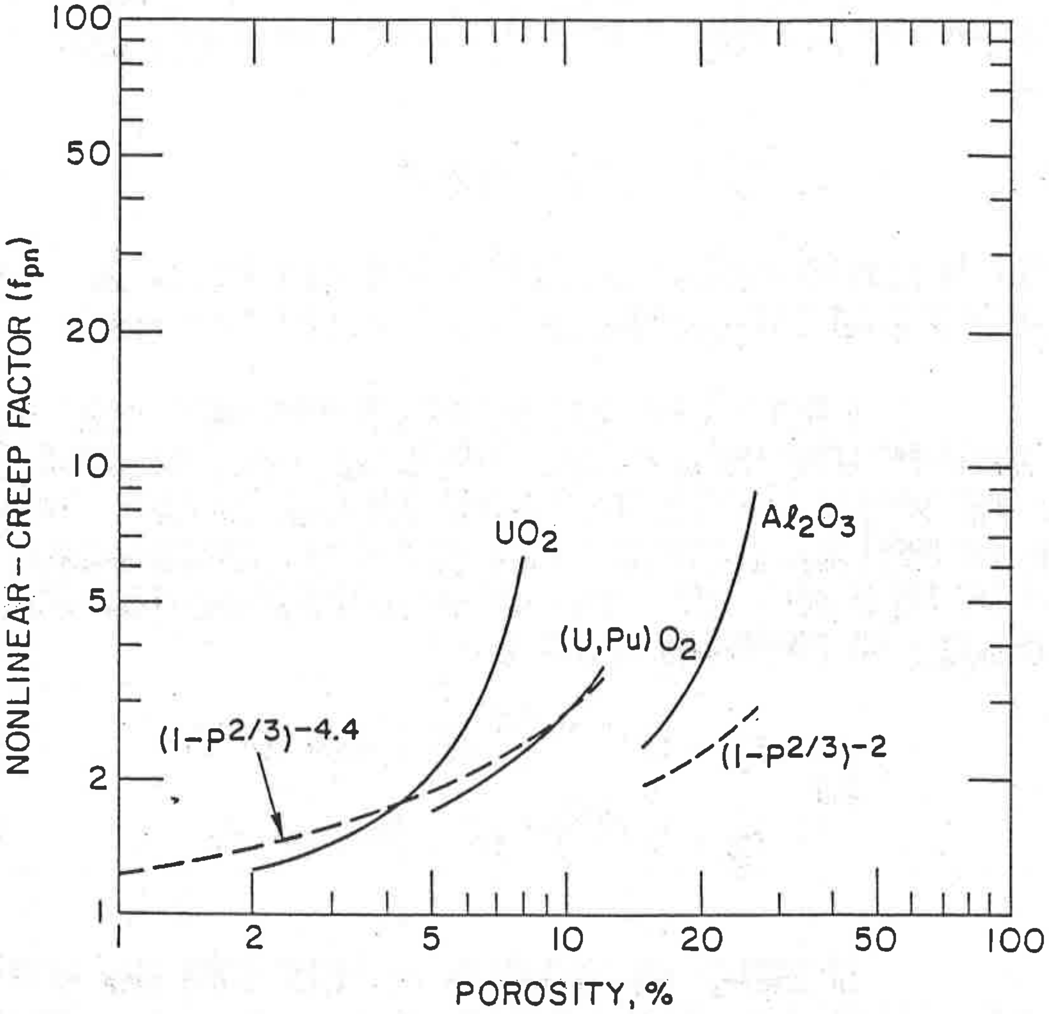

Fig. D.2.3-D Dependence of non-linear, secondary creep on porosity. Correlations are based on fits to data. All correlations are re-normalized to g[illegible] the enhancement in creep rate referenced to 100% dense material.

where P = porosity fraction referenced to initial fuel volume
$R = 1.987\ \mathrm{cal \cdot g\text{-}mole^{-1}}$
T = temperature in K
σ = stress in MPa

and
$\dot{F}$ = fission rate in fissions/$\mathrm{cm^3 \cdot s}$.

For $T > T_p$, the corresponding equation is

$$\dot{\varepsilon} = 8.0 \times 10^{-2}\,(1-P^{2/3})^{-3} \exp(-28{,}500/RT)\sigma^3 + 7.7 \times 10^{-23}\,\dot{F}\sigma,\ \mathrm{s^{-1}}. \quad (8b)$$

The creep regimes are represented graphically in Fig. D.2.3-E for an assumed fission rate of 8.6×10^{13} fissions/$\mathrm{cm^3 \cdot s}$. This corresponds to a 0.17-in. (4.3-mm) diameter fuel operating at 12 kW/ft (39 kW/m). The solid lines in the figure represent T-σ points for which the sum of the linear terms equals the power-law creep rate. The dashed line indicates the temperature for which the linear thermal creep rate equals the linear, fission-enhanced creep rate for 67% dense fuel. For 100% dense fuel, the fissioned-enhanced creep rate is always larger than the linear thermal creep rate.

As sophisticated as Eqs. 8a and 8b appear, the user is again reminded that these equations represent a "best estimate" based on the behavior of 100% U and trends observed in the creep behavior of other materials. Also, the dependence of grain size and alloy composition have not been included in these equations because of insufficient information. No reasonable uncertainty estimates can even be placed on Eqs. 8a and 8b at this time. Uncertainty estimates will become available in the future if creep tests are performed for the alloys of interest. An indirect way of verifying whether or not Eqs. 8a and 8b are of the correct order of magnitude is to use LIFE-METAL to try to predict cladding mechanical strain for those irradiated

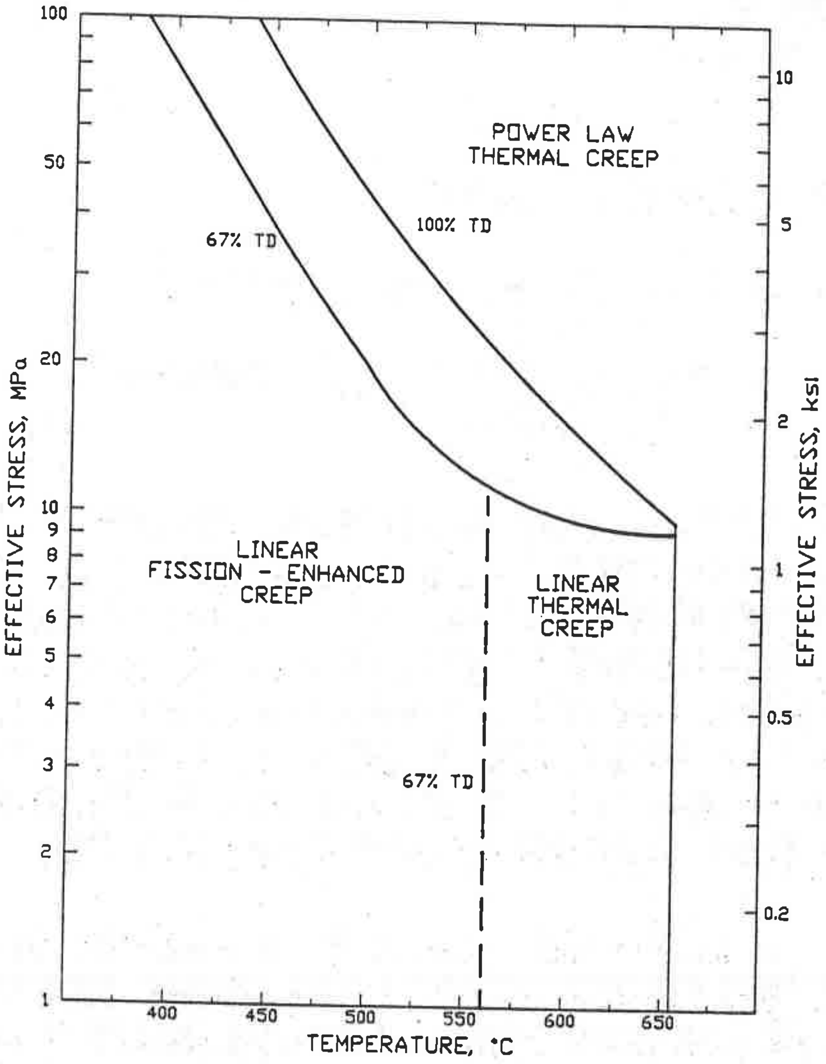

Fig. D.2.3-E Calculated creep-deformation regimes for U alloy fuels at 100% TD and 67% TD. The lines represent the stress and temperature conditions for which the power-low creep rate equals the linear (in stress) creep rate. A fission rate (8.6×10^{13} fissions/$cm^3 \cdot s$) corresponding to a linear heat rating of 12 kW/ft (39 kW/m) for 0.17-in. (4.3-mm) diameter fuel is assumed for these calculations.

fuel elements which show strains due to fuel-cladding mechanical interaction (FCMI). This was attempted for high-smear density (85% TD) U-5Fs elements which failed at low burnups (<5 at.%). [26,27] However, the results were inconclusive because of the rapid rise in gas pressure for these small-plenum elements and because of the uncertainty in cladding (annealed types 304 and 316 stainless steels) properties and other fuel models and properties. However, several high-smear density U-10Zr and U-19Pu-10Zr fueled experiments with D9 cladding are planned for the very purpose of gaining some insight into FCMI. Hopefully, some useful information, with respect to how "hard" (i.e. creep-resistant) or how "soft" the fuel is, can be gained from these tests.

E. PROPERTIES OF STAINLESS STEEL CLADDING ALLOYS

E.1 Cold-Worked D9 (CWD9)

D9 is an austenitic stainless steel developed under the former National Cladding and Duct (NCD) Program. In comparison to AISI 316 stainless steel, titanium has been added (0.2-0.3 wt.%) and the Ni/Cr increased to improve void swelling resistance. Nominal compositions for D9 as listed are Table E.1-1.

Through the development program molybdenum and silicon levels were changed slightly to control phase stability in reactor, resulting in variations in high-temperature strength, resistance to recrystallization, and creep rupture properties. The various heats of D9 (grouped as D9-C1 and D9-C1P Lot in Table E.1-1) which have been used in the LMFBR program, therefore, have property variations associated with them, some known and some which have not been measured. Those which are known will be identified in this Handbook. Note that D9-C1P is what has been used in the metal fuels irradiation program, and its properties should be used in performance predictions.

A more recent development in the D9 alloy, including specified quantities of boron and phosphorous, is designated D9i, and has improved creep rupture properties. This modification, however, is not included here because no use of it has been made, or is expected to be made, in the metal fuel development program.

D9 has been adopted in ASME code specifications as alloy S38660.

Table E.1-1 D9 Compositions, wt.%

Element	D9-C1 (nom)*	D9-C1P (nom.)**
C	0.05	0.05
Mn	2.00	2.00
Si	1.00	0.90
P	0.02 max.	0.01 max.
S	0.01 max.	0.007 max.
Cr	13.5	13.5
Ni	15.5	15.5
Mo	1.50	1.65
Cu	0.04 max.	0.02 max.
Nb	0.05 max.	0.01 max.
Al	0.05 max.	0.01 max.
Ti	0.25	0.25
As	0.03 max.	0.03 max.
Ta	0.02 max.	0.01 max.
V	0.02 max.	0.02 max.
Zr	--	0.001 max.
Co	0.050 max.	0.031 max.
O	--	0.005 max
B	0.001 max.	0.001 max.
N	0.01 max.	0.005 max.
Fe	Balance	Balance

---

*Identified heats include 2966 and N563

**Identified heats include 83508, 83509, and 83510

E.1.1 Mechanical Properties

E.1.1.1 Irradiation Creep

Irradiation creep correlation development has been largely based on measurements obtained on specimens made from early heats of D9, and the behavior of all D9 types is therefore assumed to be equivalent. Recent data from MOTA tests in FFTF have shown that creep strains for DP-C1P can be larger than those predicted with this equation, especially at high fluences. It is possible that D9-C1P creep rates are somewhat higher, or that stress-effected swelling is greater and can be confused with creep deformation. The equations below are those represented in Ref. 1 and the data base for the equation can therefore be located there. Note that similar equations have previously been used to represent D9 creep and one should check carefully to assure that the proper one is being used. For example, one previous equation was very similar, but improperly represented the thermal creep components, so that if used over a wide range of neutron fluxes inaccurate creep strains would result.

Equation Description

The recommended in-reactor creep equation for D9 is:

A. Integrated Form (Constant Stress - Constant Temperature)

$$\bar{\varepsilon} = A_1 \exp\left(-\frac{A_2}{T}\right) [1-\exp(-3\Phi)]\, \bar{\sigma} + A_3 \Phi \bar{\sigma} + A_6 t \left(\frac{\bar{\sigma}}{Y}\right)^4 \exp\left(-\frac{A_7}{T}\right) + 2.2\, R(T)\, (\Omega)^2 \bar{\sigma} \log_e \left[\cosh\left(\frac{\Phi}{\Omega}\right)\right] + A_4 t \bar{\sigma} \exp\left(-\frac{A_5}{T}\right) \qquad (1)$$

Note that the terms beginning with A_6 and A_4 represent the thermal creep (ε_{th}) and this component may underpredict D9-C1P creep somewhat, but the current data base is insufficient to recommend an alternative method for calculation.

B. Rate Form

$$\dot{\bar{\varepsilon}} = \{3A_1 \exp\left(-\frac{A_2}{T}\right) \exp(-3\,\Phi)\,\bar{\sigma} + A_3\,\bar{\sigma} + 2.2\,R(T)\,\Omega\,\bar{\sigma} \tanh\left(\frac{\Phi}{\Omega}\right)\}$$

$$\phi \times 10^{-7} + A_6 \left(\frac{\bar{\sigma}}{Y}\right)^4 \exp\left(-\frac{A_7}{T}\right) + A_4\,\bar{\sigma} \exp\left(-\frac{A_5}{T}\right) \qquad (2)$$

$R(T) = c_0 \exp[-c_1 (T - c_2)^2]$

t = time in units of s

T = temperature in units of K

$Y = 223000 - 79.29\,T$ = Young's Modulus in units of MPa

Φ = fluence in units of 10^{22} n/cm^2 [E > 0.1 MeV]

ϕ = flux in units of 10^{15} n/cm^2·s [E > 0.1 MeV]

$\bar{\sigma}$ = effective stress in units of MPa

$\bar{\varepsilon}$ = effective strain in units of %

$\dot{\bar{\varepsilon}}$ = effective strain rate in units of %/s

The constants in the equations have the following values:

$A_1 = 67$

$A_2 = 9461$

$A_3 = 1.0 \times 10^{-4}$

$A_4 = 3955$

$A_5 = 27680$

$A_6 = 6.14 \times 10^{13}$

$A_7 = 17111$

$\Omega = 9$, expressed in units of 10^{22} n/cm^2

$$c_0 = 1.9 \times 10^{-4}$$

$$c_1 = 3.0 \times 10^{-5}$$

and

$$c_2 = 823$$

Notes: Valid for temperature range of 350-700°C.
Valid for strain rates less than $10^{-5}\ s^{-1}$.
Valid for fluxes on the order of $2 \times 10^{15}\ n/cm^2 \cdot s^{-1}$.

Recommendations Regarding Stress and Temperature Changes

The in-reactor creep equations were developed from constant stress-constant temperature experimental data. Time hardening rules are recommended in the calculation of $\bar{\varepsilon}$ and $\dot{\bar{\varepsilon}}$ for temperatures less than 600°C. The user should investigate the effects of both strain and time hardening in his application of this equation to temperatures greater than 600°C and choose the result which yields the more conservative estimate of the creep strain for his application. These guidelines will be reviewed and updated when more data become available.

(1) Stress Changes: Use the local stress to calculate the incremental change in strain $\Delta\bar{\varepsilon}$ and the instantaneous strain rate $\dot{\bar{\varepsilon}}$ for a given time interval.

(2) Temperature Changes: Use the local temperature to calculate the incremental change in strain $\Delta\bar{\varepsilon}$ and the instantaneous strain rate $\dot{\bar{\varepsilon}}$ for a given time interval.

E.1.1.2 Stress Rupture

The following two equations represent the stress rupture properties of D9-C1 and D9-C1P, as measured for the materials in the unirradiated condition. Note that the equation for D9-C1P is identical to that for 20% CW 316 (Ref. 1) while D9-C1 is that listed in Ref. 1 for D9. The data base used to verify D9-C1P behavior appears in Ref. 2. In general, at 600°C and above, the D9-C1 has a longer rupture life than the D9-C1P. Figures E.1.1-A and E.1.1-B show typical behavior at given temperatures. The D9-C1 information is presented here only for comparison so that reference to previous LMR fuel element performance data which perhaps used D9-C1 cladding, could be compared with current data.

D9-C1P

$$\log_{10} t_r = A + B/T + C(\log_{10} \sigma)/T \qquad (3)$$

	A	B	C	SEE	
	-16.638	+34054	-7113	0.26	(High Stres)
or*	-12.637	+22219	-3591	0.18	(Low Stress)

*Use either the high stress or the low stress equation depending on which gives the shortest time-to-rupture

t_r = hours
T = K
σ = MPa
SEE = standard error of estimate

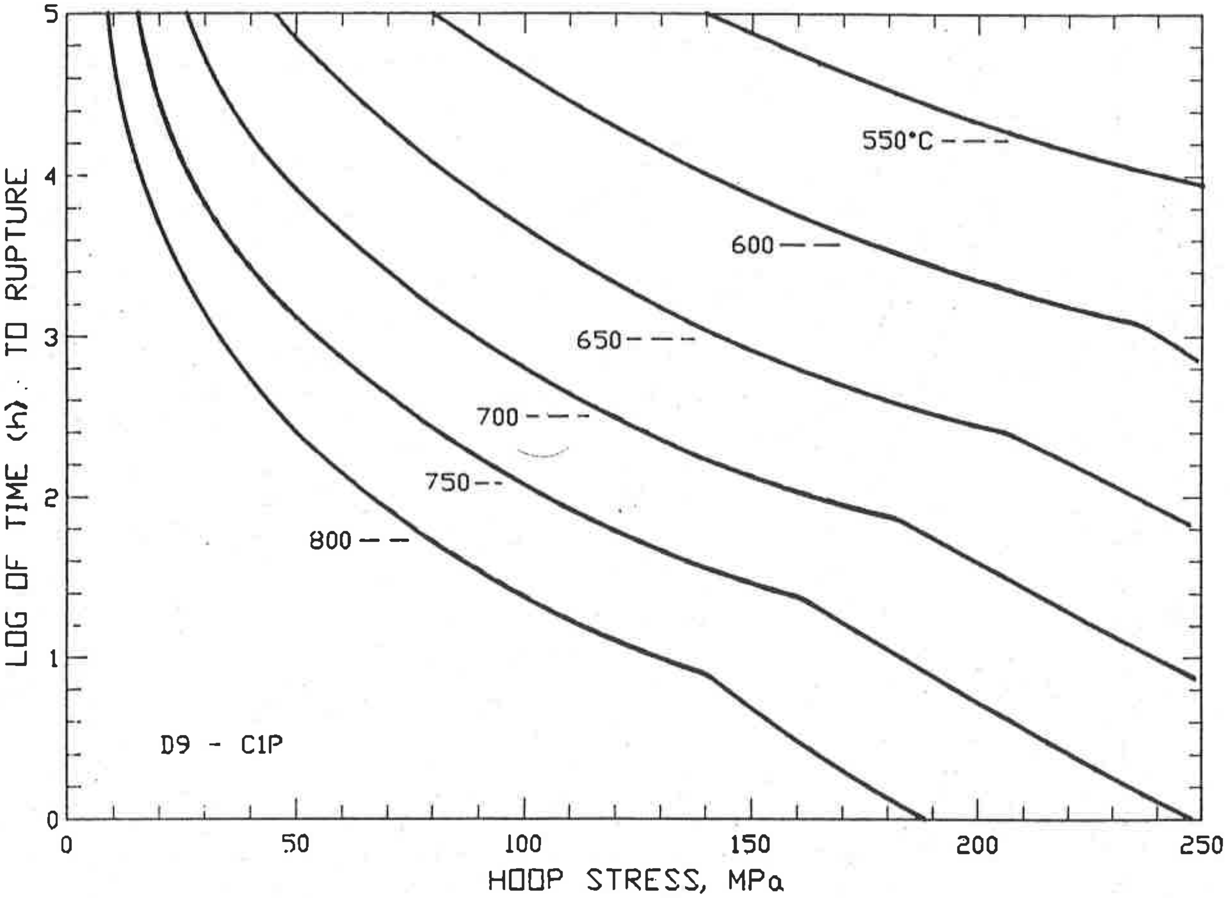

Fig. E.1.1-A Biaxial Stress Rupture Behavior of D9-C1P.

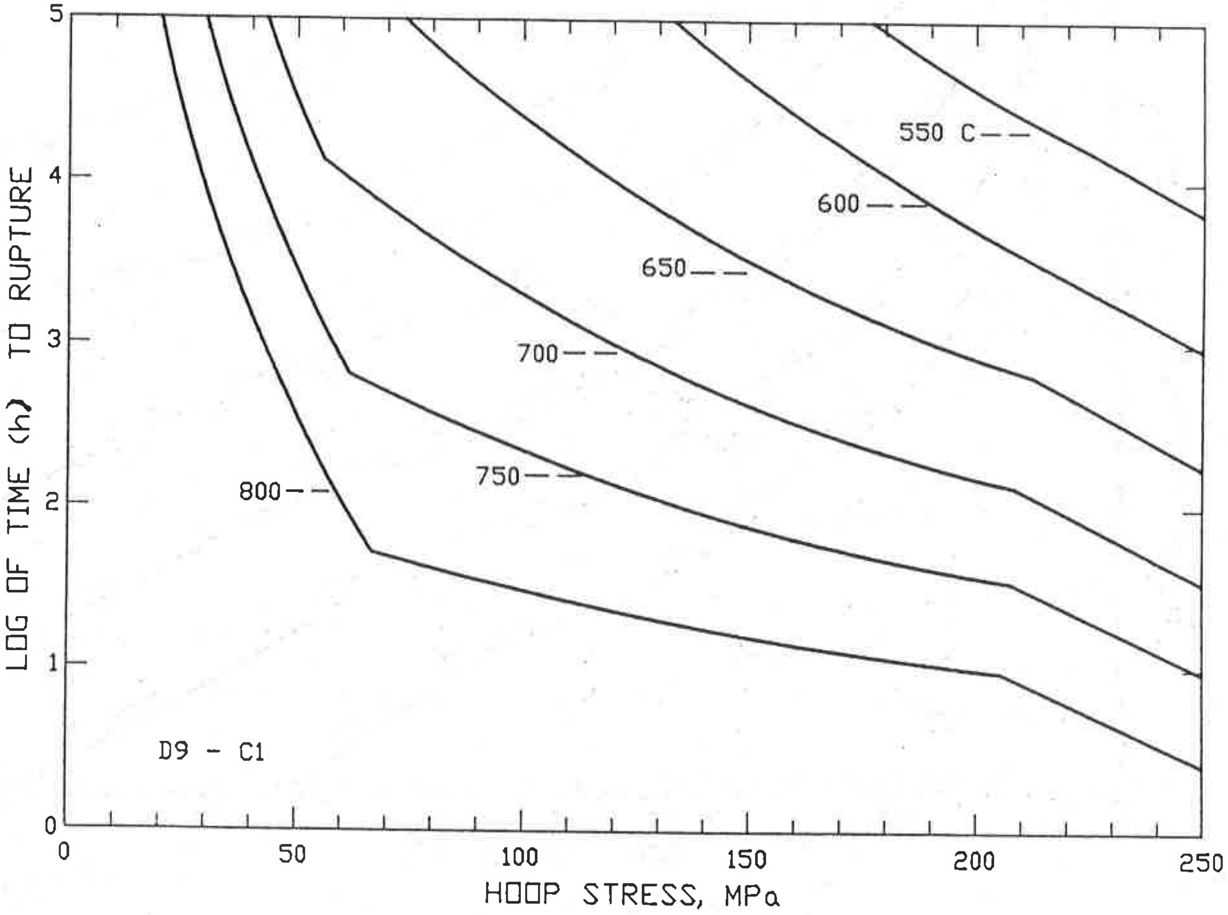

Fig. E.1.1-B Biaxial Stress Rupture Behavior of D9-C1.

Limitations

$770 < T < 1100$

$t_r \geq 2$ hours

Hoop Stress is calculated from the equation

$$\sigma = \frac{D_o^2 + D_i^2}{D_o^2 - D_i^2} \cdot P$$

where

D_o = the outside diameter,
D_i = the inside diameter, and
P = the internal gas pressure

Calculated stress rupture curves are shown in Fig. E.1.1-B.

D9-C1

The stress rupture behavior of unirradiated D9 is given by

$$\log_{10} t_r = A + \frac{B}{T} + \frac{C}{T} \log_{10} \sigma + D \log_{10} \sigma \qquad (4)$$

	A	B	C	D
High Stress	-10.727	29732	-7414.8	0
Medium Stress	-53.034	61542	-21246.8	18.361
Low Stress	-17.141	32605	-6803.5	0

where:

σ = Hoop stress, MPa
T = Temperature, K ($640 \leq T \leq 1100$)
t_r = Rupture time, hrs. ($t_r \geq 1$)

for $640 \le T \le 820$, use the high stress coefficients.

For $T > 820$, use the following criteria to determine the proper coefficients:

Valid Stress Range for Each Equation

High Stress $$\frac{42.306T - 31810}{18.361T - 13832.0} \le \log_{10} \sigma_H$$

Medium Stress $$\frac{35.893T - 28937}{18.361T - 14443.3} \le \log_{10} \sigma_M \le \frac{42.306T - 31810}{18.361T - 13832.0}$$

Low Stress $$\log_{10} \sigma_L \le \frac{35.893T - 28937}{18.361T - 14443.3}$$

Calculated stress rupture curves are shown in Fig. E.1.1-B.

E.1.1.3 Yield Strength

An equation taken from Ref. 1 is listed below for alloy D9-C1. The strength for D9-C1P is likely to vary slightly, particularly at very high temperatures, but these effects are now not known well enough to write a unique correlation for D9-C1P.

D9-C1

An interim correlation has been developed to describe the yield strength of D9-C1. It will be updated as more data become available. Heat-to-heat or lot-to-lot variations in strength exist for this alloy, including the D9-C1P material. A 10% margin on the nominal strength described here is probably adequate for estimation of minimum strength values.

The yield strength (0.2% offset) of unirradiated and irradiated D9 is given by the following "best fit" correlation:

$$\ln \frac{F\sigma^*}{\sigma_y} = A \left[\frac{\left(\frac{\sigma^*}{G}\right)^{M}}{\dot{\varepsilon}\,\exp\left(\frac{Q}{RT_k}\right)} \right]^{\lambda} \qquad \text{where:} \qquad (5)$$

$\sigma^* = 450 - 240 \tanh\left(\frac{T_T - 760}{300}\right)$

$G = 78600 - 38.41\ T_T$

$A = 30000$

$M = 5.5$

$\lambda = 0.22$

$Q = 70000$

$R = 1.98726$

$F = B - C \tanh\left(\frac{T_i - D}{170}\right) - E$

Note: To calculate the yield strength of unirradiated D9, set $F = 1$.

$B = 1.495 \pm 0.03\ \phi t$

$C = 0.776 + 0.046\ \phi t$

$D = 384 - 4.4\ \phi t$

$E = 0.15 + 0.15 \tanh\left(\frac{T_i - 630}{10}\right)$

σ_y = 0.2% offset yield strength, MPa

G = Shear modulus, MPa

$T_T = T_k - 273$

T_k = Test temperature, K
($273\ \text{K} \lesssim T_k \lesssim 1133\ \text{K}$)

$T_i = T_I - 273$

T_I = Irradiation temperature, K
($273\ \text{K} \lesssim T_I \lesssim 1023\ \text{K}$)

ϕt = Fast fluence, 10^{22} n/cm^2
($\phi t \lesssim 12 \times 10^{22}$ n/cm^2)

$\dot{\varepsilon}$ = Strain rate, s^{-1}
($10^{-5}\ \text{s}^{-1} \lesssim \dot{\varepsilon}\ 10^{-2}\ \text{s}^{-1}$)

E.1.1.4 Ultimate Tensile Strength

Below is an equation for the ultimate tensile strength of D9-C1 as a function temperature, irradiation temperature, and irradiation exposure. Note that the yield strength, given in Section E.1.1.3, must be used to calculate the tensile strength.

D9-C1

The average ultimate tensile strength of unirradiated and irradiated D9 is given by the following "best fit" equation:

$$\sigma_{UTS} = \sigma_{YS} \left[0.295 \left(1 - 0.9 \tanh \frac{\Delta T + 400}{150}\right) + 1.055\right] \qquad (6)$$

where:

σ_{UTS} = Ultimate tensile strength, MPa
σ_{YS} = Yield strength, MPa, [see E.1.1.3]
$\Delta T = T_T - T_i$
T_T = Test temperature, K
T_i = Irradiation temperature, K

The effects of fluence, temperature and strain rate are provided through the correlation for the yield strength. To calculate the ultimate strength of unirradiated D9, set F = 1 in the equation used to calculate yield strength, and $\Delta T = 0$.

The correlation is valid for irradiation temperatures of 640 to 1010 K and strain rates $\geq 10^{-5}$/s.

E.1.1.5 Total Elongation

The total elongation to be expected for unirradiated and irradiated D9-C1 at strain rates greater than 10^{-5}/s is given by:

$$\varepsilon_t = -2.22 + 1.64 \times 10^{-2} T_i + 2.17 \times 10^{-4} \exp (T_i/100) - 6.3 \times 10^{-3} T_t \qquad (7)$$

where:

ϵ_t = total elongation, %
T_t = test temperature, K
T_i = irradiation temperature, K, $640 < T_i < 1010K$

Note, this equation can be used for conditions where $T_t = T_i$, or $T_t = T_i +$ 110K. Note further that radiation hardening, or softening, depends upon irradiation temperature, so conditions where other relationships between T_i and T_t apply should not be modelled by this equation. This equation is taken from Ref. 1.

E.1.1.6 Elastic Moduli and Poisson's Ratio

The Young's modulus (E), shear modulus (G), and Poisson's ratio (ν) for D9, as a function of temperature, are given by:

$$E = 2.01 \times 10^5 - 79.29T \tag{8}$$

$$G = 7.86 \times 10^4 - 38.41T \tag{9}$$

$$\nu = (E/2G) - 1 \tag{10}$$

where, E, G are given in MPa
and, T is given in °C.

the equations are to be used for temperatures of $0 < T \leq 800°C$. These equations are those given in Ref. 3.

E.1.2 Physical Properties (D9)

Contained in this section are equations designed to be used to predict the void swelling behavior, thermal expansion, thermal conductivity, and density of cold-worked D9 stainless steel. No distinctions are made for heat-to-heat variations represented by D9-C1 and D9-C1P Types.

E.1.2.1 Void Swelling

The void swelling behavior of D9 has been developed using data accumulated using a number of D9 heats and thermal/mechanical treatments. Data of higher irradiation exposures are forthcoming. Note also that there may be stress enhancement of swelling by way of reductions in the incubation parameter, τ. Likewise temperature changes during irradiation may alter behavior through integrated effects on τ or α parameters . Neutron flux magnitude or energy spectrum may also cause variations in behavior. These effects have not been well quantified for D9 material and could only be qualitatively modelled. Applications involving stress, stress changes, or temperature changes (as in fuel element behavior) should therefore not be expected to be predicted exactly.

There has been a progression of swelling equations developed for D-9. The TC-293, Rev. 4 (Ref. 3) equation was the first published and still fits the known data nearly as well as any others. An improvement based on this form was subsequently made in 1981 [4] but is probably the worst-fit to the current data base. The first equation proposed for inclusion in the NSMH included some "engineering judgment" in which the swelling rate at high neutron fluences was expected to be large for $400 < T < 600°C$, based upon the behavior of similar alloy systems (austenitic stainless steels). This equation has been subsequently modified to provide that the high swelling rates do not begin with higher fluences (16.1 x 10^{22} n/cm^2, E > 0.1 MeV) as the data base progressed to higher fluences without showing the behavior as yet.

Thus, there are four equations which have been used, the first (TC-293) and most recent NSMH proposal being currently the most accurate. The TC-293 equation shows a small amount of swelling to fluences of 15 x 10^{22} n/cm^2, while the most recent equation shows almost none. At fluences greater than 20 x 10^{22} n/cm^2 the deviations between equations are dramatic, the TC-293 equation predicting much less swelling, at least for temperatures greater than 400-450°C. Since the data base does not support the choice of one over the other, either could be used to 20 x 10^{22} n/cm^2, while beyond this fluence the most recent equation, included in this document, should be used for conservative estimates of swelling behavior. Figures E.1.2-A and E.1.2-B show plots of the two equations for comparison.

Void Swelling of CWD9 - "NSMH Proposal"

Swelling is defined as volume change,

$$\frac{\Delta V}{V_o} = S_o - D \qquad (1)$$

where S_o is the fractional volume change due to void formation and D is the fractional volume decrease due to solid state reactions.

$$S_o = (0.01)\ R\ \{\phi t + \frac{1}{\alpha} \ln \{\frac{1 + \exp\ [\alpha(\tau - \phi t)]}{1 + \exp\ (\alpha\tau)}\}\} \qquad (2)$$

and:

$$D = (0.01)\ [1 - \exp\ (-3\ \phi t)]\ [0.178] \qquad (3)$$

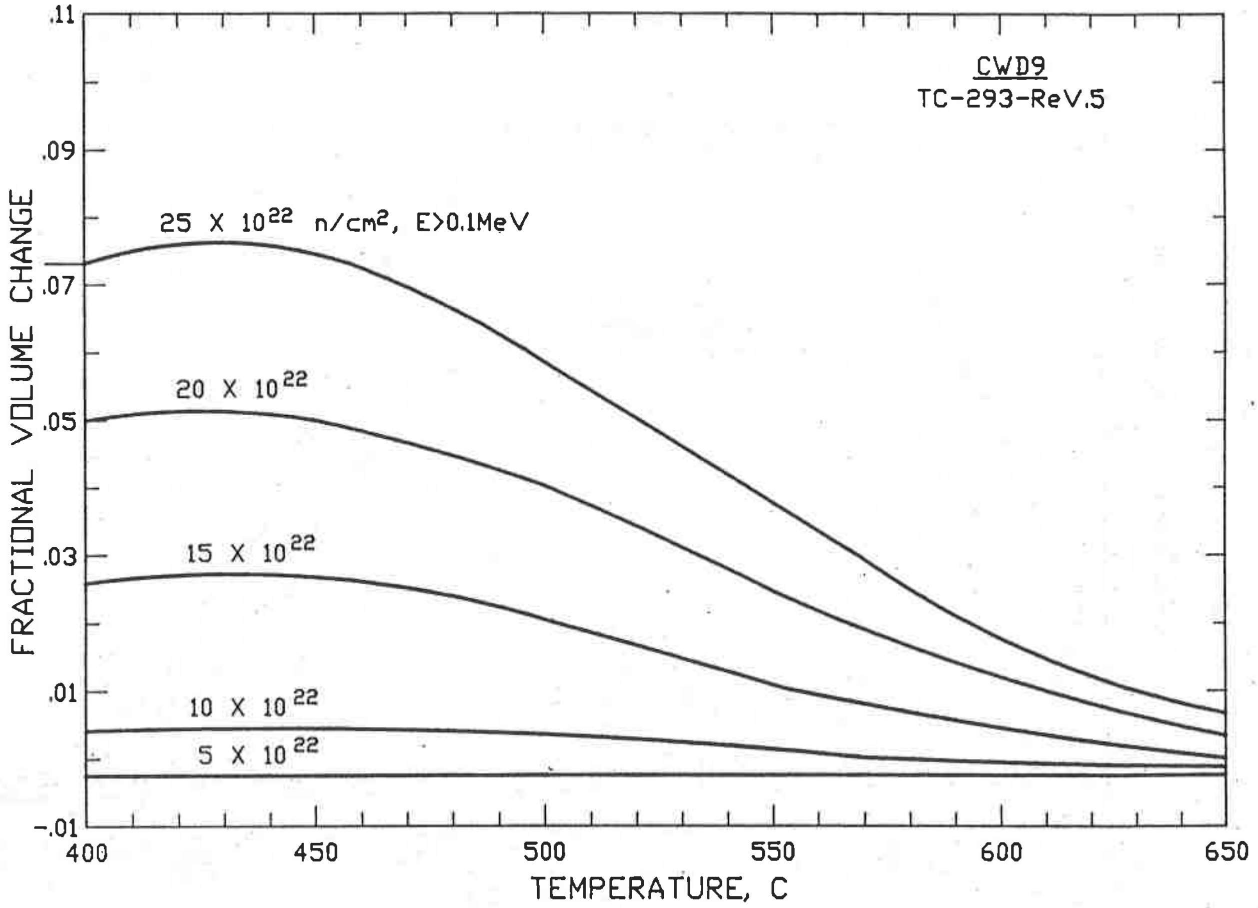

Fig. E.1.2-A Void Swelling Behavior of CWD9 As Predicted By The Equation From TC-293.

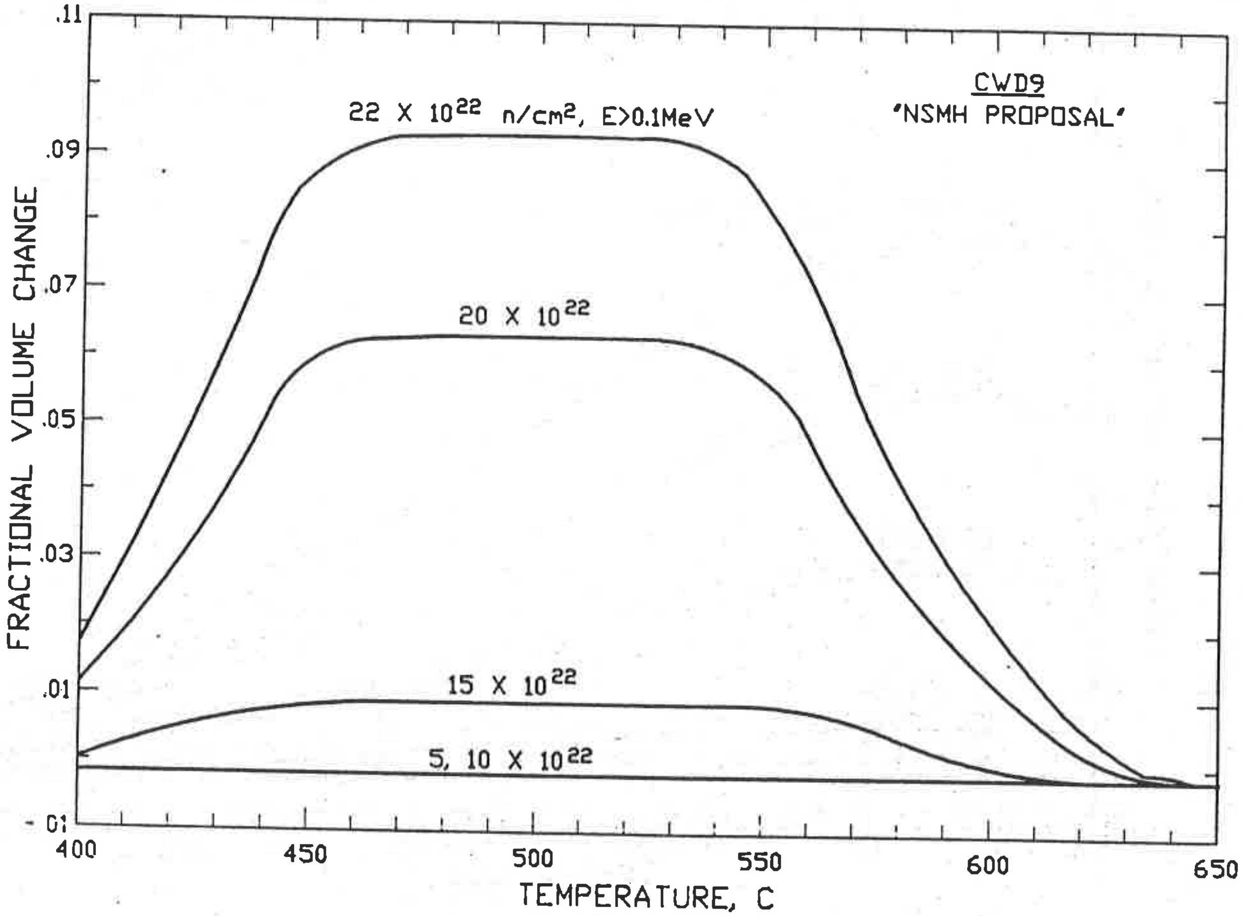

Fig. E.1.2-B Void Swelling Behavior of CWD9 As Predicted By A Correlation Based On The NSMH.

where:

$\beta = (T - 773)/100$,

$R = \exp\,(0.471 - 0.003\beta + 0.179\beta^2 - 0.077\beta^3 - 1.78\beta^4)$,

$\tau = 16.1$,

$\alpha = 0.6$,

ϕt = neutron fluence in units of 10^{22} n/cm^2 ($E > 0.1$ MeV),

α = curvature parameter in units of $(10^{22}$ n/cm$^2)^{-1}$,

τ = incubation parameter in units of 10^{22} n/cm^2 ($E > 0.1$ MeV),

T = temperature in units of K,

R = swelling rate parameter in units of % per 10^{22} n/cm^2 ($E > 0.1$ MeV)

E.1.2.2 Thermal Expansion

The thermal expansion behavior for D9 is depicted in Fig. E.1.2-C A corresponding equation to be used to model this behavior is:

$$\Delta L/L_0 = 0.72549 - 0.12875T^{\frac{1}{2}} + 5.1890 \times 10^{-3}T - 5.0431 \times 10^{-7}T^2, \quad (293 < T < 1200\text{K}) \qquad (4)$$

$$= -1.273 \times 10^{-3} \text{ at } 293\text{K}$$
$$= 1.76\% \text{ at } 1200\text{K}$$

where $\Delta L/L_0$ (%) is defined as the percentage length change from room temperature (293K) to T (K). The data base and corresponding equation are provided by ANL-CMT Division. The tests were performed by averaging data obtained from six consecutive heating/cooling cycles. The equation fits the overall data base with a standard deviation of 1.2%. D9 material corresponding to a D9-C1P Heat composition was used for the analysis.

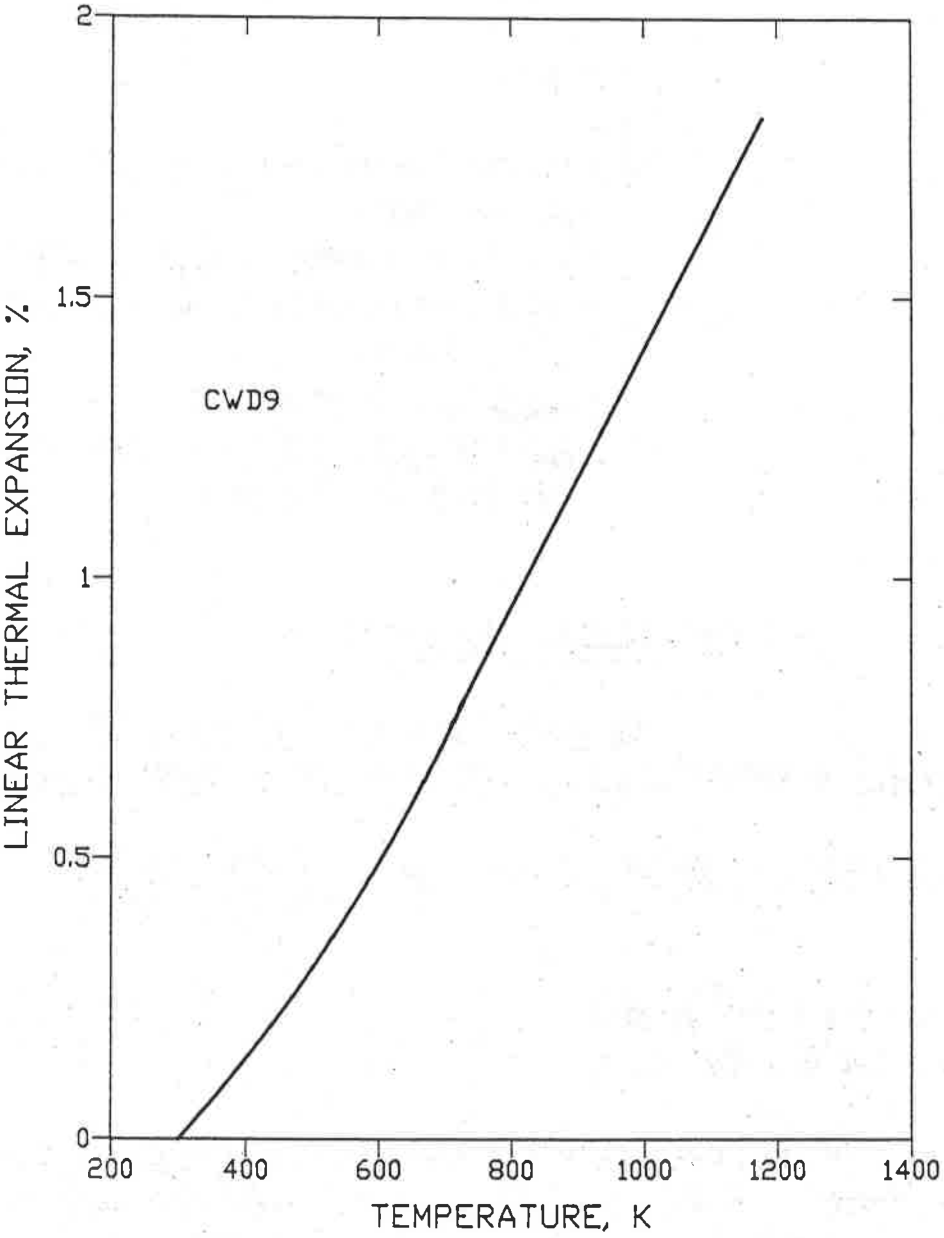

Fig. E.1.2-C Thermal Expansion Behavior of CWD9.

E.1.2.3 Thermal Conductivity

Thermal conductivity behavior of D9 is taken from Ref. 1 and is represented by the equation:

$$\lambda = 7.51213 + 5.70032 \times 10^{-3}T - 5.77849 \times 10^{-7}T^2 \qquad (5)$$

where:

λ = thermal conductivity, Btu/hr·ft·F
T = Temperature, $70 < T < 1500°F$

or:

$$\lambda = 8.25795 + 1.94121 \times 10^{-2}T - 3.24027 \times 10^{-6}T^2, \qquad (6)$$

$294 < T < 1088K$ for λ in W/m·K and T in K.

E.1.2.4 Density

The density of CWD9 (unirradiated) has been given as,

$$\rho = 7.98 - 4.30 \times 10^{-4}T \qquad (7)$$

for, ρ in g/cm^3, T in C ($300 < T < 800$).

This equation has been extracted from Ref. 3.

E. PROPERTIES OF STAINLESS STEEL CLADDING ALLOYS

E.2 Normalized-and-Tempered HT9

HT9 is a martensitic stainless steel based on Fe-12Cr-1Mo. The nominal composition is listed in Table E.2-1. Its time-temperature-transformation behavior is such that at least one hour at high temperatures (700-800°C) after austenitizing (>1000°C) is required to induce formation of ferrite/carbide mixtures. Therefore, heat treatment definition is less critical to create desired properties than with other heat treatable steels. Tempering is done following a normalization-and-cooling step to create desired ductility and is usually performed at 650-750°C to prevent formation and decomposition of austenite during the tempering process.

The properties listed in this section are largely derived from the Nuclear Systems Materials Handbook (Ref. 1), and some from the Alloy Properties Databook (Ref. 2) and those thermal properties determined under the IFR program by Argonne National Laboratory (Chemical Technology Division). HT9 has been adopted in ASME code specifications as alloy S42100.

Table E.2-1 HT9 Chemical Composition

Element	Weight, %
Carbon	0.17 - 0.23
Manganese	0.40 - 0.70
Phosphorus, max.	0.015*
Sulfur, max.	0.010
Silicon	0.20 - 0.30
Nickel	0.30 - 0.80
Chromium	11.0 - 12.5
Molybdenum	0.80 - 1.20
Niobium	0.05 - max.
Tungsten	0.40 - 0.60
Aluminum, max.	0.050
Vanadium	0.25 - 0.35

---

*Note that S42100 specifies 0.040, maximum; recent heats have been purchased to the specification listed above.

E.2.1 Mechanical Properties

E.2.1.1 Irradiation Creep

The in-reactor creep behavior of HT9 is of a simpler form than that exhibited by CWD9, largely because there are no transient terms caused by the presence of mobile dislocations from the as-fabricated cold-work levels. A creep equation based solely on ex-reactor thermal creep behavior has been developed for predictions above 600°C, where thermal creep often dominates (Ref. 3) and is effective to 750°C. This equation is represented by $\bar{\varepsilon}_T$. The purely irradiation-induced creep is represented as $\bar{\varepsilon}_I$ and has the form,

$$\bar{\varepsilon}_I = [B_o + A\exp\left(-\frac{Q}{RT}\right)]\ \Phi\ \bar{\sigma}^{1.3} \qquad (1)$$

where: $\bar{\varepsilon}_I$ = effective stain, %
$\bar{\sigma}$ = effective stress, MPa
B_o = 1.83×10^{-4}
Φ = neutron fluence 10^{22} n/cm^2 (E>0.1 MeV)
A = 2.59×10^{14}
Q = 73000
T = temperature, K
R = 1.987

Note that in the equation for the total creep strain, $\bar{\varepsilon}_C$ (pg. 3) that there are two terms, an irradiation-induced term and a purely thermal term. The second (thermal) term is small over this temperature range for low stresses (<250 MPa, 36 ksi). For high T (625-750°C), thermal creep becomes very important. The thermal creep component, $\bar{\varepsilon}_T$, can be calculated using the following equation (see Ref. 3)

$$\bar{\varepsilon}_T = \bar{\varepsilon}_{TP} \text{ (Primary)} + \bar{\varepsilon}_{TS} \text{ (Steady-State)} + \bar{\varepsilon}_{TT} \text{ (Tertiary)} \tag{2}$$

where

$$\bar{\varepsilon}_{TP} = [C_1 \exp(-\frac{Q_1}{RT})\,\bar{\sigma} + C_2 \exp(-\frac{Q_2}{RT})\,\bar{\sigma}^{\,4} + C_3 \exp(-\frac{Q_3}{RT})\,\bar{\sigma}^{\,0.5}] \times$$

$$(1 - \exp[-C_4 t])$$

$$\bar{\varepsilon}_{TS} = [C_5 \exp(-\frac{Q_4}{RT})\,\bar{\sigma}^{\,2} + C_6 \exp(-\frac{Q_5}{RT})\,\bar{\sigma}^{\,5}]t$$

and

$$\bar{\varepsilon}_{TT} = C_7 \exp(-\frac{Q_6}{RT})\,\bar{\sigma}^{\,10}\,t^4$$

Rate form: Constant temperature and stress

$$\dot{\bar{\varepsilon}}_T = \dot{\bar{\varepsilon}}_{TP} + \dot{\bar{\varepsilon}}_{TS} + \dot{\bar{\varepsilon}}_{TT}$$

where:

$$\dot{\bar{\varepsilon}}_{TP} = [C_1 \exp(-\frac{Q_1}{RT})\,\bar{\sigma} + C_2 \exp(-\frac{Q_2}{RT})\,\bar{\sigma}^{\,4} + C_3 \exp(-\frac{Q_3}{RT})\,\bar{\sigma}^{\,0.5}]\; C_4 \exp(-C_4 t)$$

$$\dot{\bar{\varepsilon}}_{TS} = C_5 \exp(-\frac{Q_4}{RT})\,\bar{\sigma}^{\,2} + C_6 \exp(-\frac{Q_5}{RT})\,\bar{\sigma}^{\,5}$$

and

$$\dot{\bar{\varepsilon}}_{TT} = 4C_7 \exp(-\frac{Q_6}{RT})\,\bar{\sigma}^{\,10}\,t^3$$

The values for the constants in these equations are:

$C_1 = 13.4$
$C_2 = 8.43 \times 10^{-3}$
$C_3 = 4.08 \times 10^{18}$
$C_4 = 1.6 \times 10^{-6}$
$C_5 = 1.17 \times 10^{9}$
$C_6 = 8.33 \times 10^{9}$
$C_7 = 9.53 \times 10^{21}$
$Q_1 = 15027$
$Q_2 = 26451$
$Q_3 = 89167$
$Q_4 = 83142$
$Q_5 = 108276$
$Q_6 = 282700$

The definitions for the other terms in these correlations are:

$\bar{\varepsilon}_T$ = effective thermal creep strain, %
R = gas constant = 1.987
t = time in seconds
T = temperature, K
$\bar{\sigma}$ = effective stress, MPa
$\dot{\bar{\varepsilon}}_T$ = effective thermal creep strain rate, %/s

These equations are valid for the following environment:

temperature range: 350-750°C
stress range: 0-250 MPa

The total creep strain $\bar{\varepsilon}$ can be calculated using the summation, $\bar{\varepsilon} = \bar{\varepsilon}_I + \bar{\varepsilon}_T$.

E.2.1.2 Stress Rupture (biaxial loading)

Due to a lack of in-reactor stress rupture data, the stress rupture correlation is largely based upon ex-reactor furnace testing data assuming that in-and-ex-reactor behavior are similar. Recent MOTA (Materials Open Test Assembly) data have shown that this assumption is mostly correct. However, the in-reactor rupture data show that the rupture times are a little less, especially at low stress (Ref. 4), so that attempts to compute strain-to-failure using in-reactor creep and ex-reactor stress rupture correlations overpredict strains at low stresses. In general, 3% uniform strain can be used to predict failure.

The stress rupture correlation to be used for unirradiated HT9 comes from the NSMH (section 10), and is given by,

HT9 Stress Rupture

$$\log_{10} t_r = A + \frac{B}{T} + \frac{C}{T} \log_{10} \sigma \qquad (3)$$

	A	B	C
High Stress	-32.490	57781	-11800
Low Stress	-35.173	45858	-5563.1

where,

σ = hoop stress, MPa
t_r = time to rupture, hrs
T = temperature, $700 \leq T \leq 1100$ K

The choice of high stress coefficients or low stress coefficients should be made to correspond to the equation predicting the shortest time to rupture. A plot of typical values obtained using this equation is shown in Fig. E.2.1-A.

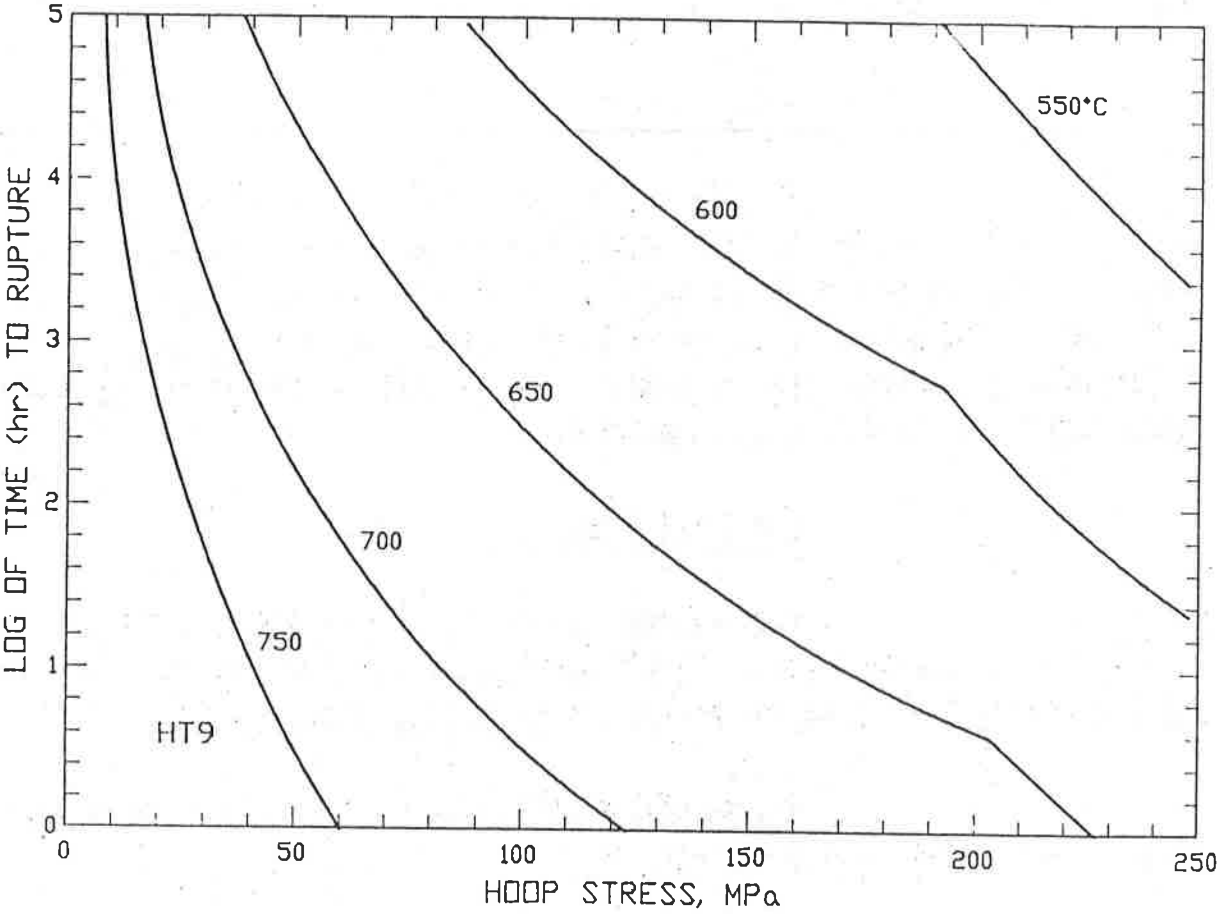

Fig. E.2.1-A Biaxial Stress Rupture Behavior of Normalized-and-Tempered HT9.

Stress rupture behavior at high temperature is not well-known and has not been characterized by a correlation. A plot of the limited data is shown in Fig. E.2.1-B. Failure strains can be large at these temperatures (10-30%). Note that a transient correlation for cladding rupture has been developed to cover a wide range of short-time, high-stress, high-temperature conditions. The correlation can be found in Ref. 5.

E.2.1.3 Yield Strength

The yield strength of HT9 (unirradiated and irradiated) is given by the NSMH equation below (Ref. 1). Note that the data base for irradiation-affected properties was limited to fast fluences of 11 x 10^{22} n/cm^2. The general behavior is to strengthen the material upon irradiation at temperatures below 600°C, and slightly weaken it for exposures about 600°C, likely due to overtempering.

HT9 Yield Strength

Heat-to-heat or lot-to-lot variations in strength are now well known for this alloy. A 10% margin on the nominal strength described here is probably adequate for estimation of minimum strength values.

The average yield strength of HT9 can be calculated from the following "best-fit" correlation:

$$\ln \frac{\sigma^* F}{\sigma_y} = A \left[\frac{\left(\frac{\sigma^*}{G}\right)^M}{\dot{\varepsilon} \exp \frac{Q}{RT_k}} \right]^{\lambda} \tag{4}$$

$$F = B \quad 1 - 0.5 \tanh\left(\frac{T_i - D}{90}\right)^{.5} + C$$

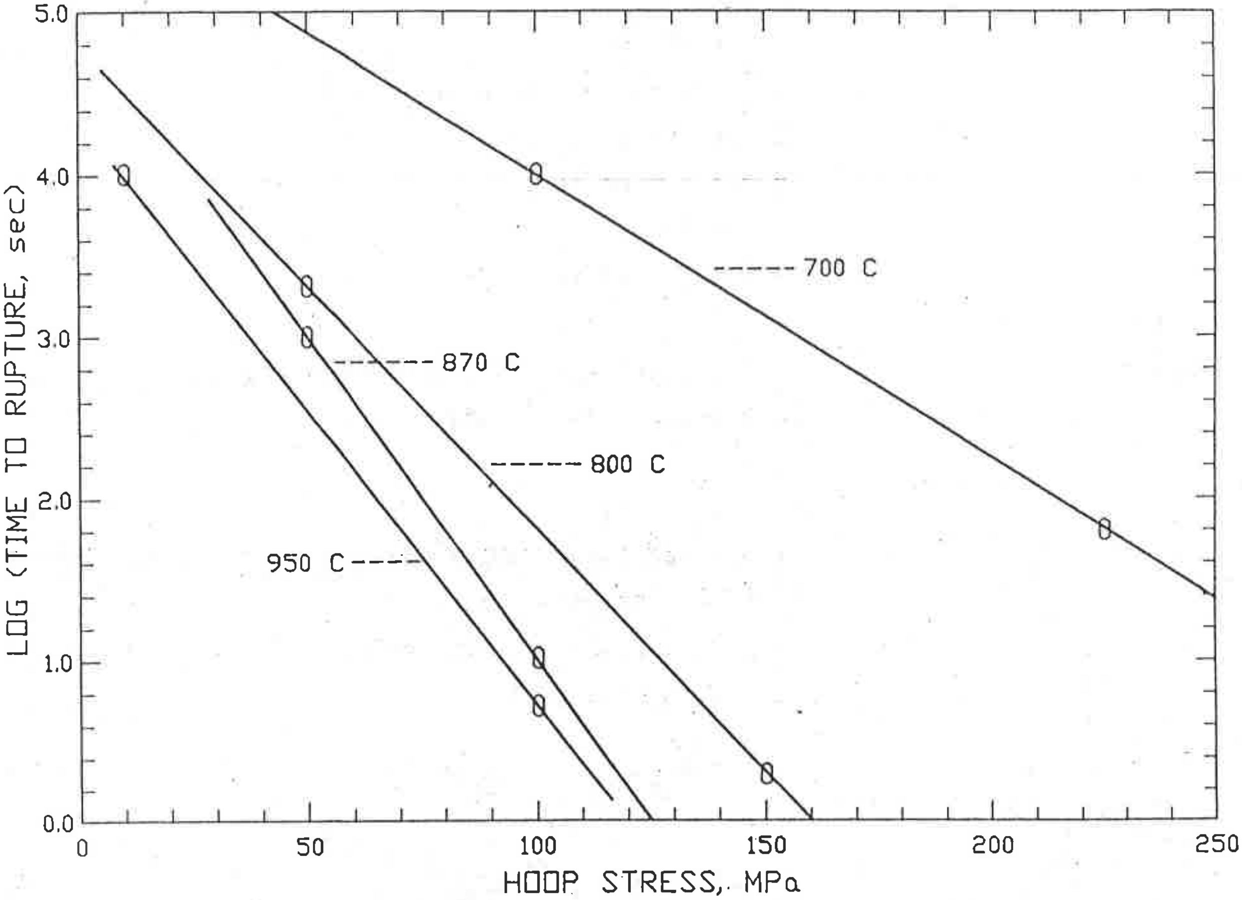

Fig. E.2.1-B Biaxial Stress Rupture Behavior of Normalized-and-Tempered HT9 at High Temperatures.

(For unirradiated properties set F = 1)

$A = 20000$

$M = 5$

$\lambda = 0.172$

$Q = 82000$

$R = 1.98726$

$$\sigma^* = 430 - 190 \tanh\left(\frac{T_t - 640}{225}\right)$$

$G = 89640 - 53.78\ T_t$

$B = 1 - 0.02\ \phi t$

$C = 0.02\ \phi t$

$D = 425 + 10\ \phi t$

where,

σ_y = 0.2% offset yield strength, MPa
G = Shear modulus, MPa
$T_t = T_k - 273$
$T_i = T_1 - 273$
T_1 = Irradiation temperature, K ($723\ K < T_1 < 933\ K$)
T_k = Test temperature, K
$\phi t = 10^{22}\ n/cm^2$, $E > 0.1$ MeV
$\dot{\varepsilon}$ = Strain rate, s^{-1}

$$10^{-5}\ s^{-1} < \dot{\varepsilon} < 10^{-2}\ s^{-1}$$

$$\phi t < 11 \times 10^{22}\ n/cm^2$$

E.2.1.4 Ultimate Tensile Strength

A correlation for the ultimate tensile strength of unirradiated or irradiated HT9 is given below based upon the yield strength calculated in E.2.1.3. Note that all limitations to the correlation such as strain rate, temperature, and neutron fluence, are the same as those given in E.2.1.3. The equation is taken from Ref. 1 (Section 10).

HT9 Ultimate Tensile Strength

$$\sigma_u = \sigma_y \left[1.1 - 0.1 \tanh \left(\frac{\Delta T - 200}{200}\right)\right], \text{ where} \qquad (5)$$

$\Delta T = T_t - T_i$
σ_u = Ultimate tensile strength, MPa
σ_y = Yield strength, MPa (see E.2.1.3)
T_t = Test temperature , K
T_i = Irradiation temperature, $723 < T_i < 933$ K.

To calculate the unirradiated properties set $\Delta T = T_t - 848$ and use the appropriate value of σ_y.

E.2.1.5 Total Elongation, minimum

The ductility of irradiated and unirradiated HT9 are very similar and as such the correlation for minimum total elongation does not contain an irradiation exposure term.

HT9 Minimum Total Elongation

The minimum total elongation of both unirradiated and irradiated HT9 is given by the equation:

$$\varepsilon_t = 9.97 + 1.34 \times 10^{-3} \exp \left(\frac{T_t}{100}\right) \qquad (6)$$

where,

ε_t = total elongation, %
T_t = Test temperature, $273 < T_t < 973$ K.

This equation for ductility was determined as a lower bound on the behavior of HT9. Total elongation is predicted to be a minimum of about 10% under any conditions.

E.2.1.6 Elastic Moduli and Poisson's Ratio

Young's modulus (E), shear modulus (G) and Poisson's ratio (ν) for HT9, as a function of temperature are given by:

$$E = 2.137 \times 10^5 - 102.74T \tag{7}$$

$$G = 8.964 \times 10^4 - 53.78T \tag{8}$$

$$\nu = (E/2G) - 1 \tag{9}$$

where, E and G are given in MPa

and, T is given in °C.

The equations are to be used for temperatures of $0 < T \leq 800°C$. These equations are those given in Ref. 2.

E.2.2 Physical Properties

E.2.2.1 Void Swelling

The correlation to be used for void swelling of HT9 is that given in the NSMH. Note that the data base suggests that HT9 may never show significant swelling, regardless of fluence, although transmission electron microscopy has revealed a few voids at low temperatures (~400°C). The equation form has been taken from the swelling behavior of austenitic alloys. It may be just as accurate to use $\Delta V/V_o = 0$ for all cases and omit the equation for swelling prediction.

HT9 Void Swelling

Swelling is defined as volume change, $\Delta V/V_o$,

$$\frac{\Delta V}{V_o} = S_o + D \qquad (1)$$

where S_o is the fractional volume change due to void formation and D is the fractional volume change due to solid state reactions.

$$S_o = (0.01)\, R\left[\phi t + \frac{1}{\alpha} \ln \left\{\frac{1 + \exp\left[\alpha(\tau - \phi t)\right]}{1 + \exp(\alpha\tau)}\right\}\right] \qquad (2)$$

and

$$D = (0.01)\,(0.15)\,[1 - \exp(-0.10\phi t)]$$

where:

$R = 0.085 \exp[-1 \times 10^{-4} (T - 400)^2]$ (3)
$\tau = 14.2$
$\alpha = 0.75$
ϕt = Neutron fluence, 10^{22} n/cm^2 (E > 0.1 MeV)
α = Curvature parameter, $(10^{22}$ n/cm$^2)^{-1}$
τ = Incubation parameter, 10^{22} n/cm^2 (E > 0.1 MeV)

T = Temperature, °C (applicable range is 380-700°C)

R = Steady state swelling rate, % per 10^{22} n/cm^2 (E > 0.1 MeV)

Note that the precipitation-induced volume change, D, is positive for HT9; it is a densification (negative D) for CWD9.

E.2.2.2 Thermal Expansion

NSMH (Ref. 1) thermal expansion correlations are given to describe the behavior at temperatures up to the ferrite (martensite-to-austenite transformation. Recently ANL-CMT (Chemical Technology Division) has extended measurement of the behavior to 1200K (Ref. 6); Fig. E.2.2-A shows a plot of the thermal expansion in the region of transformation.

An equation to describe thermal expansion up to the transformation temperature is given by:

$$\Delta L/L_0 = -0.16256 + 1.62307 \times 10^{-4}T + 1.42357 \times 10^{-6}T^2 - 5.50344 \times 10^{-10}T^3 \quad (4)$$

where,

$\Delta L/L_0$ = elongation, %

$293 < T < 1050$ K

E.2.2.3 Thermal Conductivity

Thermal conductivity of HT9 has been measured by ANL-CMT (Chemical Technology Division) to extend application to 1200 K. The correlation is given as plotted in Fig. E.2.2-B.

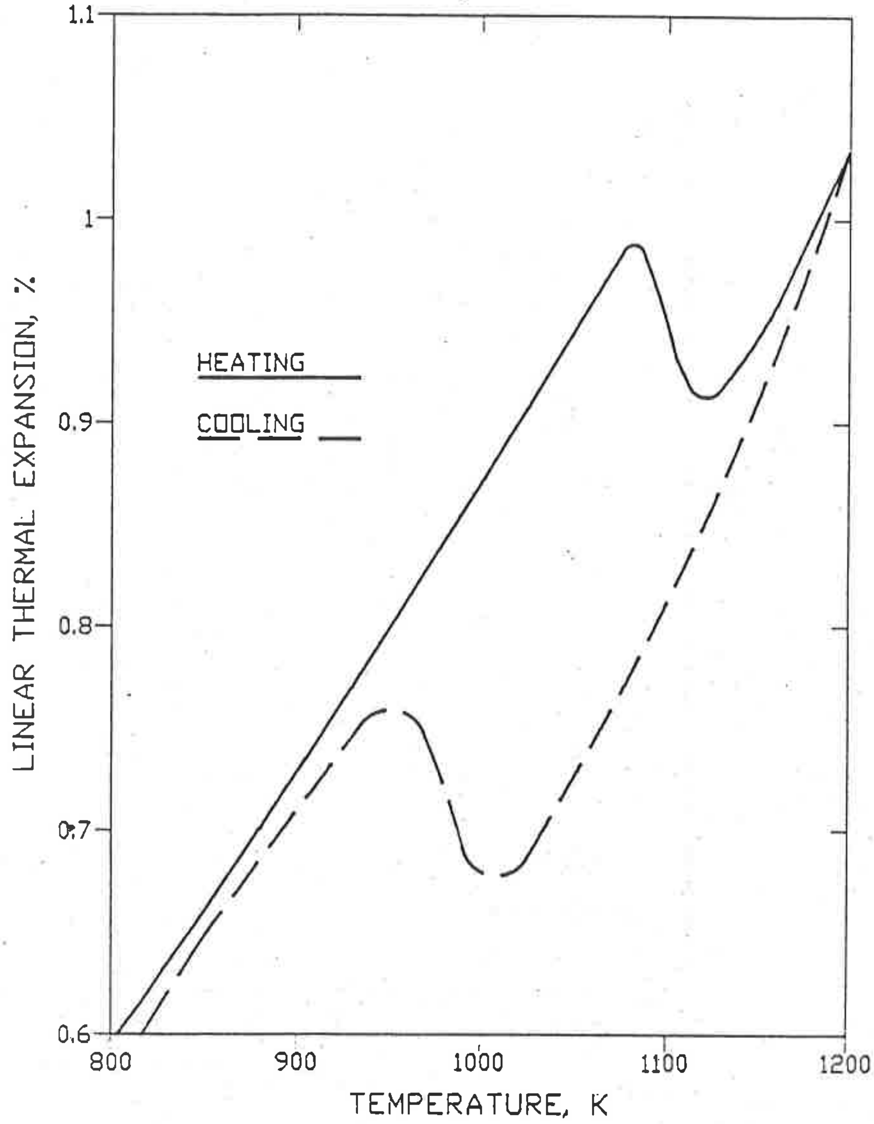

Fig. E.2.2-A Thermal Expansion of HT9.

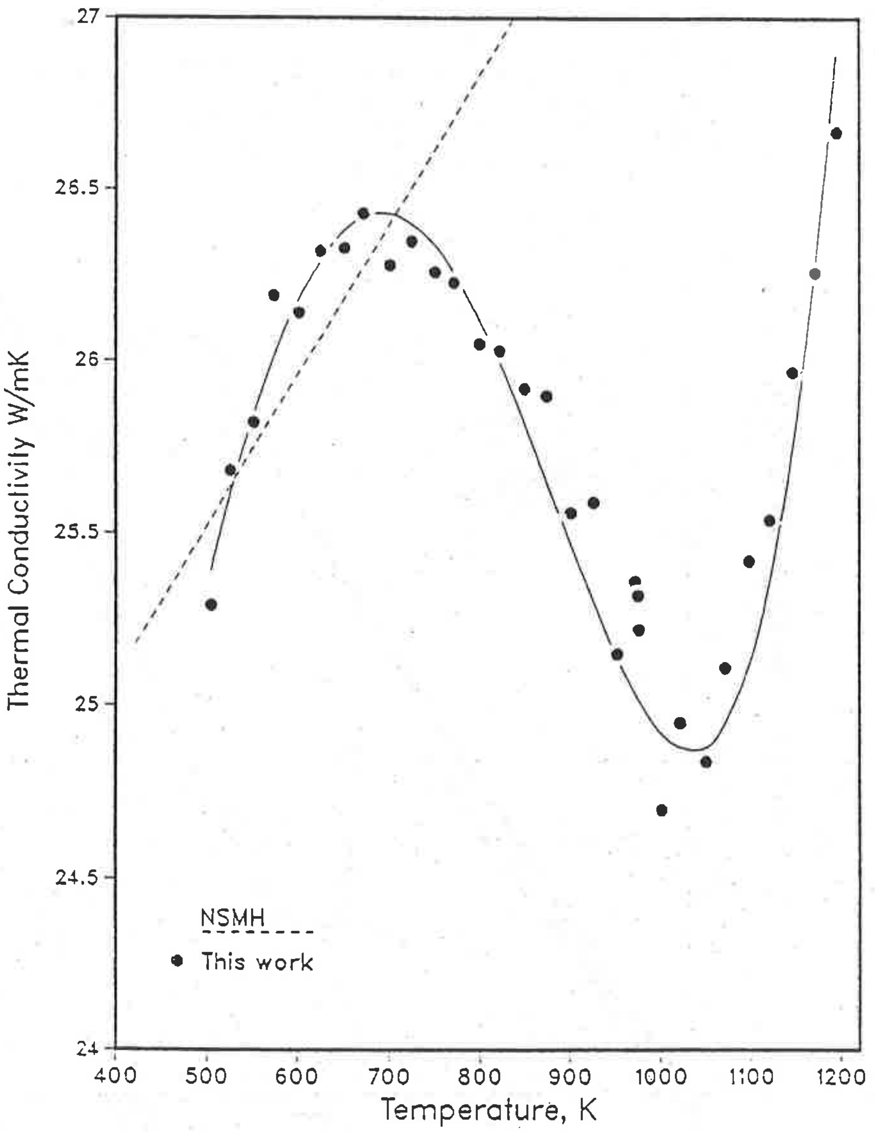

Figure E.2.2-B Thermal Conductivity
HT9 Cladding Alloy

$$\lambda = 29.65 - 6.668 \times 10^{-2}T + 2.184 \times 10^{-4}T^2 - 2.527 \times 10^{-7}T^3 + 9.621 \times 10^{-11}T^4 \quad (5)$$

The thermal conductivity, λ, is in W/m·K and the temperature, T, is in K.

The actual variation in thermal conductivity is fairly small over the temperature range studied. Of more significance could be the structural changes resulting from the indicated phase transition. It should be emphasized that the transition is fairly rapid on increasing temperature, but very slow when the temperature is decreased. We plan to explore this effect further by performing thermal expansion measurements at various heating/cooling rates.

E.2.2.4 Density

The correlation for density of HT9 as a function of temperature has been extracted from Ref. 2. The equation is:

$$\rho = a + bT \quad (6)$$

where,

ρ = Density, g/cm^3
T = Temperature, °C
a = 7.778
b = -3.07×10^{-4}
($0 \le T \le 800$°C)

Note that density calculations beyond the 800°C limit cannot be made with this equation as the ferrite-to-austenite transition creates volumetric strain which should be factored in.

References for Section B.1

1. G. B. Fedorov and E. A. Smirnov, *Thermodynamic Properties of Uranium-Zirconium Alloys*, At. Ehnerg. 25, 54 (1968); English translation: Sov. J. At. Energy 25, 795 (1968).

2. P. Chiotti, V. Akhachinskij, I. Ansara, and M. H. Rand, *The Chemical Thermodynamics of Actinide Elements and Compounds, Part 5, The Actinide Binary Alloys*, International Atomic Energy Agency, Vienna (1981).

3. F. K, Oetting, M. H. Rand, and R. J. Ackermann, *The Chemical Thermodynamics of Actinide Elements and Compounds, Part 1, The Actinide Elements*, International Atomic Energy Agency, Vienna (1976).

4. R. Hultgren, P. D. Desai, D. T. Hawkins, M. Gleiser, K. K. Kelley, and D. D. Wagman, *Selected Values of the Thermodynamic Properties of the Elements*, Wiley, New York (1973).

5. G. B. Federov, E. A. Smirnov, N. A. Makhlin, and P. I. Kalinin, Moscow Engineering-Physics Institute, *Thermodynamic Properties of Alloys of the Zirconium-Niobium System*, At. Ehnerg. 21, 189 (1966), English translation: Sov. J. At. Energy 21, 837 (1966).

6. A. D. Pelton, *Calculations of the Liquidus in the Plutonium-Uranium-Zirconium System*, Argonne National Laboratory Report ANL-IFR-12 (1985).

7. H. Savage, *Heat Content and Heat Capacity of U-15w/oPu-10w/oZr and U-15w/oPu-6w/oTi Alloys*, Annual Progress Report for 1966, Metallurgy Division, Argonne National Laboratory Report, ANL-7299, 21-22 (1967).

8. R. J. Dunworth, B. Blumenthal, and O. L. Kruger, *Plutonium Physical Properties Laboratory - DL208*, Annual Progress Report for 1961, Metallurgy Division, Argonne National Laboratory Report, ANL-6516, 403-407 (1962).

9. G. E. Moore and K. K. Kelley, *High Temperature Heat Content of Uranium, Uranium Oxide and Uranium Trioxide*, J. Am. Chem. Soc. 69, 2105-7 (1947).

10. D. C. Ginnings and R. J. Corruccini, *Enthalpy, Specific Heat and Entropy of Aluminimum Oxide from 0° to 900C°*, J. Research Nat'l. Bur. Standards 39, 309 (1946).

11. J. M. North, *Skull Melting and Centrifugal Casting Experiments on Monocarbide Produced by the Carbothermic Reduction of Uranium Oxide, Carbides in Nuclear Energy* 2, Atomic Energy Research Establishment Report, Harwell, Eng., M/R 1016 (1956).

12. H. Savage and R. D. Seibel, *Heat Capacity Studies of Uranium and Uranium-Fissium Alloys*, Argonne National Laboratory Report, ANL-6702, 27 (1963).

13. E.A. Mit'kina, *Experimental Determination of True Specific Heats of Uranium, Thorium, and of Other Metals*, Atomnaya Energy 7.5, 163 (1959).

14. L. S. Levinson, *Heat Content of Molten Uranium*, J. Chem. Phy. 40, 3584 (1964).

15. B. J. Blumenthal, *The Transformation Temperatures of High Purity Uranium*, J. Nucl. Mat. 2, 23-30 (1960).

16. R. W. Buzzard, R. B. Liss, and D. P. Fickle, *Titanium-Uranium System in the Region 0 to 30 Atomic Percent of Titanium*, J. Research Nat'l Bur. Standards 50, 209 (1953).

17. M. C. Udy and F. W. Boulger, *Uranium-Titanium Alloy System*, J. Met. 6, 207-210 (1954).

18. A. I. Dahl and H. E. Cleaves, *The Freezing Point of Uranium*, J. Research Nat'l. Bur. Standards 43, 513 (1949).

19. R. J. Ackermann and E. G. Rauh, *Determination of Liquidus Curves for the Th--W, Th--Ta, Zr--W, and Hf--W Systems: The Anomalous Behavior of Metallic Thorium*, High Temp. Sci. 4, 272 (1972).

20. R. J. Ackermann and E. G. Rauh, *Measurements of the Solubilities and Derived Thermodynamic Properties of Tungsten and Tantalum in Liquid Thorium and Uranium*, High Temp. Sci. 4, 496 (1972).

21. H. P. Stephens, *Determination of the Enthalpy of Liquid Copper and Uranium with a Liquid Argon Calorimeter*, High Temp. Sci. 6, 156 (1974).

22. W. L. Thayer and J. L. Robbins, *Enthalpy and Heat Capacity of Liquid Plutonium and Uranium*, Proc. 5th Int. Conf. on Plutonium and Other Actinides, Baden-Baden, Karlsruhe, Germany, (1975).

23. T. K. Engel, *Reactor Fuels and Materials Development Plutonium Research*, Mound Laboratory Report MLM01347, Miamisburg, Ohio (1967).

24. A. E. Kay and R. G. Loasby, *The Specific Heat of Plutonium at High Temperatures*, Phil. Mag. 9, 37-49 (1964).

25. T. A. Sandenaw and R. B. Gibney, *Heat Capacity and Derived Thermodynamic Functions of* ^{242}*Pu*, J. Chemical Thermodynamics 3, 85 (1971).

26. J. C. Taylor, Atomics Weapons Research Establishment (British), Aldermaston, private communication to F. L. Oetting, M. H. Rand, and R. J. Ackermann (1966).

27. F. L. Oetting, *Half-life of ^{239}Pu by Calorimetry*, Proc. 4th Int. Conf. on Plutonium and Other Actinides, Sante Fe, NM, Met. Soc., New York, 154, (1970).

28. J. C. Taylor, P. F. T. Linford, and D. J. Dean, *Low-temperature Elastic Constants and Specific Heats of Some Delta-Phase Plutonium-Gallium Alloys*, J. Inst. Metals 96, 178-82 (1968).

29. R. L. Rose, J. L. Robbins, and T. B. Massalski, *Heat Content and Heat Capacity of a Pu/1 wt Percent Ga Delta-stabilized Alloy at Elevated Temperatures*, J. Nucl. Mater. 36, 99-107 (1970).

30. R. G. Loasby, *Discussion of Papers*, Proc. 2nd Int. Conf. Plutonium Metallurgy, Grenoble, 97 (1960).

31. A. Goldberg and T. B. Massalski, *Phase Transformation in the Actinides*, Proc. 4th Int. Conf. Plutonium and Other Actinides, Sante Fe, NM, Metallurgical Society, 875 (1970).

32. C. Prunier, C. Roux, and M. Rapin, *Compared Study of the Plutonium Transformation Heats as Determined by Enthalpic Analysis and by the Use of High Pressure*, Proc. 4th Int. Conf. Plutonium and Other Actinides, Santa Fe, NM, Met. Soc., New York, 1001 (1970).

33. J. W. Anderson, *Studies on the Equilibrium of Temperature for the Alpha-Beta Transformation*, 3rd Int. Conf. on Plutonium, London, Institute of Metals, (1967).

34. T. K. Engel, K.C. Jordan, D. M. Scott, and G. W. Otto, *A High Temperature Calorimeter for Thermal Property Measurements of Plutonium Metal*, US Atomic Energy Commission Report, TID-7641 (1962).

35. J. D. Hill, *Exploring the Transformation Behaviour of the Allotropes of Plutonium*, J. Less-Common Metals 4, 376 (1962).

36. E. M. Cramer, L. L. Hawes, W. N. Miner, and F. W. Schonfeld, *The Dilatometry and Thermal Analysis of Plutonium Metal*, The Metal Plutonium, A.S. Coffinberry and W. N. Miner, eds., University of Chicago Press, Chicago, IL, 112 (1961).

37. R. Abramson, *A Dilatometric Study of Plutonium*, The Metal Plutonium, A. S. Coffinberry and W. N. Miner, eds., University of Chicago Press, Chicago, IL, 123 (1961).

38. J. A. Lee and P. G. Mardon, *Some Physical Properties of Plutonium Metal Studied at Harwell*, The Metal Plutonium, A. S. Coffinberry and W. N. Miner, eds, University of Chicago Press, Chicago, IL, 133 (1961).

39. R. Pascard, *Study by Thermal Analysis of Allotropic Transformations of Plutonium*, Acta Metallurgica 7, 305 (1959).

40. T.A. Sandenaw and R. B. Gibney, *The Electrical Resistivity and Thermal Conductivity of Plutonium Metal*, J. Phys. Chem. Solids 6, 81 (1958).

41. S. T. Konobeevsky, et al., *Some Physical Properties of Uranium, Plutonium and Their Alloys*, Peaceful Uses of Atomic Energy, Proc. 2nd Int. Conf., Geneva, United Nations, 6 194-203, (1958).

42. D. J. Dean, A. E. Kay, and R.G. Loasby, *Note on the Specific Heat of Plutonium Metal*, J. Inst. Metals 86, 464 (1958)

43. E. R. Jette, *Some Physical Properties of Plutonium Metal*, J. Chem. Phys. 23, 365 (1955).

44. T. B. Douglas and A. C. Victor, *Heat Content of Zirconium and of Five Compositions of Zirconium Hydride from 0 to 900°C*, J. Research Nat'l Bur. Standards 61, 13 (1958).

45. F. M. Jaeger and W. A. Veenstra, Rec. Trav. Chim. 53, 13 (1958).

46. I. B. Fieldhouse and J. I. Lang, *Measurement of Thermal Properties*, WADD Tehcnical Report 60-904, Armour Research Foundation (1961).

47. R. F. Redmond and J. Lones, *Enthalpies and Heat Capacities of Stainless Steel (316), Zirconium, and Lithium at Elevated Temperatures*, Oak Ridge National Laboratory Report ORNL-1342 (1952).

48. G. B. Skinner, *Thermodynamic and Structural Properties of Zirconium* Ph. D. Thesis, Dissertation Abstracts International Chemistry, Physical, 18/05, Ohio State University, 1646 (1951).

49. J. P. Coughlin and E. G. King, *High-temperature Heat Contents of Some Zirconium-containing Substances*, J. Am. Chem. Society 72, 2262 (1950).

50. A. H. Klein and G. C. Danielson, *Specific Heat of Zirconium by a Pulse Heating Method*, Proc. Black Hills Summer Conf. on Transport Phenom., South Dakota School of Mines and Tech., Rapid City, A4, 47 (1962).

51. J. L. Scott, *A Calorimetric Investigation of Zirconium, Titanium, and Zirconium Alloys from 60 to 960°C*, Oak Ridge National Laboratory Report ORNL-2328, (1957).

52. S. D. Gertsriken and B. P. Ukrain, Fiz. Zhur. 7, 439 (1962).

References for for Section B.2

1. D. R. O'Boyle and A. E. Dwight, *The Uranium-Plutonium-Zirconium Alloy System*, Proc. 4th Int. Conf. on Plutonium and Other Actinides, Santa Fe, NM 970, Met. Soc., New York, 720-32 (1970).

2. D. R. O'Boyle, H. V. Rhude, and B. Blumenthal, *Progress in the Development of Fast-Reactor Fuels*, Trans. Am. Nuc. Soc. 9, 1 (1966).

3. (a) Mound Laboratory, Reactor Fuels and Materials Development, Plutonium Research: January-March 1066, MLM-1346 (1967).
   (b) Mound Laboratory, Reactor Fuels and Materials Development, Plutonium Research: 1966 Annual Report MLM-1402 (1967).
   (c) Mound Laboratory, Reactor Fuels and Materials Development, Plutonium Research: January-June 1967, MLM-1445 (1968).
   (d) P. O. Tucker, D. E. Etter, and J. M. Gebhart, *Phase Study of Uranium-Plutonium-Zirconium Alloys*, Trans. Am. Nuc. Soc. 11, 99 (1968).

4. F. L. Oetting, M. H. Rand, and R. J. Ackermann, *The Chemical Thermodynamics of Actinide Elements and Compounds, Part 1, The Actinide Elements*, International Atomic Energy Agency, Vienna (1976).

5. R. Hultgren, P. D. Densai, D. T. Hawkins, M. Gleiser, K. K. Kelley, and D. D. Wagman, *Selected Values of the Thermodynamic Properties of the Elements*, Am. Soc. Met., Metals Park, Ohio (1973).

6. C. S. Barrett and T. B. Massalski, *Structure of Metals*, Third Ed., McGraw-Hill, New York (1966).

7. B. J. Blumenthal, *Transformation Temperatures of High Purity Uranium*, J. Nucl. Mat. 2, 23 (1960).

8. A. D. Pelton, *Calculation of the Liquidus and Solidus in the Plutonium-Uranium-Zirconium System*, Argonne National Laboratory Report ANL-IFR-12 (1985).

9. T. B. Massalski, *Binary Alloy Phase Diagrams*, American Society of Metals, Metals Park, Ohio (1986).

10. R. Hultgren, P. D. Desai, D. T. Hawkins, M. Gleiser, K. K. Kelley, and D. D. Wagman, *Selected Values of the Thermodynamic Properties of Binary Alloys*, Am. Soc. Met., Metals Park, Ohio (1973).

11. R. P. Elliot, *Constitution of Binary Alloys, First Supplement*, McGraw-Hill, New York (1965).

12. R. Boucher and P. Barthelemy, *Comparison of the Alloys U-Pu-Mo, U-Pu-Nb, Ti, U-Pu, Zr*, Argonne National Laboratory ANL-Trans-138 (1964), translation by B. Blumenthlal of CEA-R-2531 (1964).

13. (a) L. R. Kelman et al., Annual Progress Report for 1965, Metallurgy Division, Argonne National Laboratory ANL-7155, 14-25 (1965).
(b) L. R. Kelman et al., *Status of Metallic Plutonium Fast Power-Breeder Fuels*, Int. Conf. on Plutonium 1965, A. E. Kay and M. B Waldron, eds., Chapman and Hall, London, 458 (1967).

14. D. R. Harbur, J. W. Anderson, and W. J. Maraman, *Studies on the U-Pu-Zr Alloy System for Fast Breeder Reactor Applications*, University of California, LA-4512 (1970).

15. W. F. Murphy, W. N. Beck, F. L. Brown, B. J. Koprowski, and L. A. Neimark, *Postirradiation Examination of U-Pu-Zr Fuel Elements Irradiated in EBR-II to 4.5 Atomic Percent Burnup*, Argonne National Laboratory ANL-7602 (1970).

16. F. H. Ellinger, W. N. Miner, D. R. O'Boyle, and F. W. Schonfeld, *Constitution of Plutonium Alloys*, Los Alamos Scientific Laboratory LA-3870 (1968).

17. Reactor Development Program Progress Report, September 1965, Argonne National Laboratory Report ANL-7105, 23 (1965).

18. P. Chiotti, V. Akhachinskij, I. Ansara, and M. H. Rand, *The Chemical Thermodynamics of Actinide Elements and Compounds, Part 5, The Actinide Binary Alloys*, International Atomic Energy Agency, Vienna (1976).

19. A. D. Pelton and L. Leibowitz, *Calculation of the Liquidus and Solidus in the Plutonium-Uranium-Zirconium System*, ANL-IFR-93, August 1988.

20. L. Leibowitz, *IFR Monthly Report for October 1987*, ANL-CMTI-9438, November 1, 1987.

References for Section B.3

1. Y. S. Touloukian, R. K. Kirby, R. E. Taylor, and P. D. Desai, *Thermophysical Properties Matter* 12, Thermal Expansion, Metallic Elements and Alloys, Plenum, New York (1965).

2. A. V. Grosse, J. A. Cahill, and A. D. Kirshenbaum, *Density of Liquid Uranium*, J. Am. Chem. Society 83, 4665-6 (1961).

3. W. G. Rohr and L. J. Wittenberg, *Reactor Fuels and Materials Development Plutonium Research, January--June 1967*, MLM-1445, 2-13, Mound Lab., Miamisburg, Ohio (1968).

4. J. W. Shaner, *Thermal Expansion of Metals Over the Entire Liquid Range*, Thermal Expansion 6 69, Proc. 6th Int. Symposium on Thermal Expansion, I. D. Peggs, ed., 69, August 29-31, 1977 (1977).

5. W. D. Drotning, *Density and Thermal Expansion of Liquid U-Nb Alloys*, High Temperatures - High Pressures, (England), 14, No. 3, 253-258 (1982).

6. C. L. Rosen, N. R. Chellew, and H. M. Feder, *The Melt Refining of Irradiated Uranium: Application to EBR-II Fast Reactor Fuel. IV.* Interaction of Uranium and Its Alloys with Refractory Oxides, Nuclear Sci. and Eng 6, 504-510, (1959).

7. N. Asami, M. Yamada, and S. Takahashi, *Pressure-temperature Phase Diagram of Uranium Metal*, Nippon Kinzoku Gakkaisi 31, No. 4, 389-94 (1967); Chem Abstract 67 84382V 1967.

8. D. B. Tracy, Argonne National Laboratory, private communication (1985).

9. H. A. Saller, R. F. Dickerson, and W. F. Murr, *Uranium Alloys for High-Temperature Application*, Battelle Memorial Inst. Ohio Report, BMI-1098 (1956).

10. F. A. Rough, *An Evaluation of Data on Zirconium-Uranium Alloys*, Battelle Memorial Inst., Columbus, Ohio Report BMI-1030, (1955)..

11. R. Boucher and P. Barthelemy, *Comparison of the Alloys U-Pu-Mo, U-Pu-Nb, U-Pu, Ti, U-Pu-Zr*, ANL-Trans-138 (1964), translation by B. Blumenthal, CEA-R-2531 (1964).

12. (a) Argonne National Laboratory, Metallurgy Division, Annual Progress Report for 1965, ANL-7155, 14-25 (1965).
(b) L. R. Kelman, H. Savage, C. M. Walter, B. Blumenthal, R. J. Dunworth, and H. V. Rhude, *Status of Metallic Plutonium Fast Power-Breeder Fuels*, Plutonium 1965, A. E. Kay and M. B. Waldron, eds., Chapman and Hall, London, 458 (1967).

13. D. R. Harbur, J. W. Anderson, W. J. Maraman, *Studies on the U-Pu-Zr Alloy System for Fast Breeder Reactor Applications*, Los Alamos, LA-4512 (1970).

References for Section C.1

1. Y. S. Touloukian, R. K. Kirby, R. E. Taylor, and P. D. Desai, *Thermophysical Properties of Matter*, Thermal Conductivity, Metallic Elements and Alloys I, IFI/Plenum, New York (1970).

2. J. H. Kittel et al., *Properties of Fuels for Alternate Breeder Fuel Cycles*, Argonne National Laboratory Report, ANL-AFP-38, 134 (1977).

3. H. A. Saller, R. F. Dickerson, A. A. Bauer, and N. E. Daniels, *Properties of a Fission-Type Alloy*, Battelle Memorial Inst. Report BMI-1123 (1956).

4. S. T. Zegler and M. V. Nevitt, *Structure and Properties of Uranium-Fission Alloys*, Argonne National Laboratory Report ANL-6116 (1961).

5. R. A. Di Novi, *Effect of Burnup, Swelling, and Irradiation Temperature on Thermal Diffusivity and Conductivity of Uranium-Fission Alloy*, Argonne National Laboratory Report ANL-7886 (1972).

6. W. N. Beck and R. J. Fousek, *In-Pile Measurement of Fission Gas Release and Change in Thermal Conductivity for U-5 wt.% Fs Alloy*, Trans. Am. Nuc. Soc. 23, 1-78 (1969).

7. P. R. Betten, *In-core Measurements of U-5 wt.% Fissium Alloy Thermal Conductivity*, Trans. Am. Nuc. Soc. 50, 239-240 (1985).

8. G. L. Hofman, *A Reexamination of the Role of Fission Products in Mk-II Fuel Behavior*, Argonne National Laboratory Memo (1979).

9. D. L. Porter, Argonne National Laboratory, personal communication (1985).

10. L. Leibowitz and E. Veleckis, *Thermal Conductivity Measurements*, internal ANL memo to L. C. Walters, April 30, 1987.

References for Section C.3

1. Y. Adda, J. Philibert and H. Faraggi, *Study of Intermetallic Diffusion Phenomena in the Uranium-Zirconium System*, Revue DeMetallurgie 54, 597-610 (1957).

2. N. Muller, *Diffusion Studies in the Uranium-Zirconium and Uranium-Nickel Systems*, Z. Metallk 50, 652-60 (1959).

3. A. D. Schope and L. R. Jackson, *Diffusion Studies of Zirconium-Uranium System*, Battelle Memorial Inst. Report BMI-T-24 (1950).

4. D. R. Mash and B. F. Disselhorst, *Uranium-Zirconium Diffusion Studies*, California Research and Development Co., Livermore Research Lab. LRL-143, AECD-3701 (1954).

5. Y. Adda and A. Kirianenko, *Reduction of Self-Diffusion Coefficients in λ Phase of Uranium by Additions of Molybdenum, Zirconium or Niobium*, J. Nucl. Mat. 6, 136-6 (1962).

6. S. J. Rothman, L. T. Lloyd, and A. L. Harkness, *Diffusion in Uranium*, Trans. Am. Inst. Mech. Eng. 218 (1960).

7. A. A. Bochvar et al., *Properties of Reactor Materials*, Peaceful Uses of Atomic Energy, Proc. 2nd Int. Conf., Geneva, United Nations 5 (1958).

8. G. Martin and B. Perraillon, *Grain-boundary, Structure and Kinetics*, American Society for Metals, Metals Park, Ohio, Papers, 239 (1980).

9. M. Dupuy and C. R. Head, *Study of the Self Diffusion of Plutonium in the ε Phase*, CEA-CEN/FAR, Fontenay-aux-Roses, France, Compt. Rend., Ser. C, 263, 35-8 (1964).

10. R. E. Tate and E. M. Cramer, *Self-Diffusion Studies of Delta Plutonium*, Trans. Amer. Inst. Met. Engr. 230, 639-44 (1964).

11. M. Dupuy and D. Calais, *Chemical Diffusion in the Plutonium-Uranium System*, Compt. Rend 260, 1412-15 (1965).

12. J. P. Zanghi and D. Calais, C. R. Head, *La Correlation Fusion-Diffusion Dans les Alliages Plutonium-Zirconium*, J. Nucl. Mat. 60, (2), 145-150 (1976).

13. B. Perraillon, J. Levy and Y. Adda, *Study of the Diffusion of Fission Gases in Metals*, Mem. Sci. Rev. Met., 63, 3 (1966).

14. K. E. Zimen and L. Dahl, *The Diffusion of Fission-Xe from U Metal*, Zeitschrift fuer Naturforschung (West Germany), 12a, 167-9 (Feb. 1957).

15. F. H. Spedding et al., *Thermal Diffusion of Fission Products from Uranium + Uranium Oxide*, University of Chicago Met. Lab., MUC-NS-3067 (1957).

16. J. C. Bates and A. C. Clark, *The Diffusion Xenon in Uranium*, United Kingdom Atomic Energy Authority, FRDC/P.-108, (March 1965).

17. C. E. Curtis, *Swelling and Inert Gas Diffusion of Irradiated Uranium*, Peacefuel Uses of Atomic Energy, Proc. 2nd Int. Conf., Geneva, United Nations, 15/P/81 Section 4.1 (1958).

18. J. F. D'Amico and H. B. Huntington, *Electromigration and Thermomigration in Gamma-Uranium*, J. Phys, Chem. Solids 30, 1607-21 (1969).

19. D. R. Campbell and H. B. Huntington, *Thermomigration and Electromigration in Zirconium*, Phys. Rev. 179, 601-12 (1969).

20. H. Dubler and H. Wever, *Thermo- and Electrotransport in β-Titanium and β-Zirconium*, Phys. Status Solidi 25, 109-18 (1968).

21. D. Calais and J. A. Cornet, *Self-Diffusion of the Fcc ε Pu Under Hydrostatic Pressure*, Mem. Sci. Rev. Met., 69, 493 (1972).

22. American Society for Metals, *Diffusion in Body Centered Cubic Metals*, International Conference on Diffusion in Body-Centered Cubic Materials, Gatlinburg, Tenn. (1965).

23. E. V. Borisov et al., *Metallic Metallov*, Izd-Vo AN SSSR, Moscow (1958).

24. C. Kidson and J. McGurn, *Self-Diffusion in Body-centered Cubic Zirconium*, Canadian Journal of Physics (Canada), 39, (AECL-1271), 1146-57 (1961).

25. J. I. Federer and T. S. Lundy, *Diffusion of Zr^{95} and Cb^{95} in Bcc Zirconium*, Trans. Am. Inst. of Met. Engr. 227, 592-7 (1963).

26. R.E. Tate and G. R. Edwards, *Self-diffusion Studies of Gamma-Plutonium*, Symposium on Thermodynamics with Emphasis on Nuclear Materials and Atomic Transport in Solids, International Atomic Energy Agency, Vienna (1965).

27. N. A. Gjostein, *Surface Self-diffusion in FCC and BCC Metals*, Surfaces and Interfaces, 13th Sagamore Army Materials Research Conf., eds. J. J. Burke, N. L. Reed, and V. Weiss, Syracuse University Press, New York 1, 271-304 (1967).

28. E. E. Gruber and J. M. Kramer, *Gas Bubble Growth Mechanisms in the Analysis of Metal Fuel Swelling*, Argonne National Laboratory ANL/RAS-85-18 (1985).

29. L. V. Pavlinov, *Diffusion of Uranium in Alpha Zirconium*, Izv. Akad. Nauk SSSR Metally, No. 6, pp. 65-65, (1986).

References for Section D.1

1. F. A. Rough, *An Evaluation of Data on Zirconium-Uranium Alloys*, Battelle Memorial Inst. Report BMI-1030 (1955).
2. V. W. Koester, *Die Temperaturabhangigkeit des Elastizitats Moduls Reiner Metalle*, Z. Fur Metallkunde 39 (1948).
3. Bernard G. Ryle et al, *Uranium*, Reactor Handbook, 2nd Ed., Materials, edited by C. R. Tipton, Jr., Interscience Publishers, New York, I, 123-124 (1960).
4. M. C. Billone, *UNCLE-T, A Computer Code for the Analysis of Steady-State and Transient Performance of (U,Pu)C and (U,Pu)N Fuels*, Argonne National Laboratory, Argonne National Laboratory, ANL-AFP-79 (1979).
5. M. C. Billone et al, *The LIFE-III Fuel-Element Performance Code*, US Energy Research and Development Admn. Report ERDA-77-56 (1977).
6. A. N. Holden, *Physical Metallurgy of Uranium*, Addison-Wesley, Reading, MA, 59-63 (1957).
7. D. R. Harbur et al., *Studies of the U-Pu-Zr System for Fast Breeder Reactor Applications*, Los Alamos Scientific Laboratory Report, LA-4512 (1970).
8. H. A. Saller et al., *Properties of a Fissium-Type Alloy*, Battelle Memorial Inst. Report BMI-1123, 31 (1956).

References for Section D.2

1. E. A. Rough, *An Evaluation of Data on Zirconium-Uranium Alloys*, Battelle Memorial Inst. Report BMI-1030 (1955).

2. H. A. Saller, J. T. Stacy, N. S. Eddy and H. L. Klebanow, *Creep Strengths of Uranium Alloys at 1500 and 1800F*, Battelle Memorial Inst. Report BMI-834 (1953).

3. H. Savage, *Mechanical Properties of U-Pu-Zr and U-Pu-Ti Alloys*, Argonne National Laboratory Report ANL-7155, 20 (1965).

4. D. R. Harbur, J. W. Anderson, and W. J. Maraman, *Studies on the U-Pu-Zr Alloy System for Fast Breeder Reactor Applications*, Los Alamos Scientific Laboratory Report LA-4512 (1970).

5. A. N. Holden, *Physical Metallurgy of Uranium*, Addison-Wesley, Reading, MA (1958).

6. R. M. Mayfield, *Effects of Cycling Variables upon Growth Rate of 300°C Rolled Uranium*, Trans. Am. Soc. Metals 50, 926 (1958).

7. F. R. Shober, L. L. Marsh and G. K. Manning, *The Mechanical Properties of Beta-Quenched Uranium at Elevated Temperatures*, Battelle Memorial Inst. Report BMI-1036 (1955).

8. United States Atomic Energy Commission, *Relative Work Hardening Rates of Uranium, Stainless Steel, Nickel and Aluminum*, Table 1.22.11, Creep of Uranium at 930°F, The Reactor Materials Handbook, 3, Materials. Section 1, General Properties, AECD-3647, 400 (1955).

9. A. B. McIntosh and T. J. Heal, *High Temperature Properties of Uranium and Its Alloys*, Peaceful Uses of Atomic Energy, Proc. of the 2nd Int. Conf., Geneva, United Nations, 6, P/49, 413 (1958).

10. A. A. Solomon, J. L. Routbort and J. C. Voglewede, *Fission-induced Creep of* UO_2 *and Its Significance to Fuel-element Performance*, Argonne National Laboratory Report ANL-7857 (1971).

11. A. R. Kaufman, *Nuclear Reactor Fuel Elements: Metallurgy and Fabrication*, Interscience Publishers, New York (1962).

12. J. Weertman, *Creep of Indium, Lead and Some of Their Alloys with Various Metals*, Trans. Met. Soc., Amer. Inst. of Met. Engr. 218, 207 (1960).

13. G. F. Slattery and W. N. Miller, *The Creep Strength of Uranium Containing Small Alloying Additions*, J. Nucl. Mat. 22, 320-331 (1967).

14. F. Garofalo, *Fundamentals of Creep and Creep-Rupture in Metals*, MacMillan Co., New York (1965).

15. C. M. Walter, G. H. Golden and N. J. Olson, *U-Pu-Zr Metal Alloy: A Potential Fuel for LMFBR's*, Argonne National Laboratory Report ANL-76-28 (1975).

16. L. R. Kelman, H. Savage, C. M. Walter, B. Blumenthal, R. J. Dunworth and H. V. Rhude, *Status of Metallic Plutonium Fast Power-Breeder Fuels*, Proc. 3rd Int. Conf. on Plutonium, A. E. Kay and M. B. Waldron, eds., Chapman and Hall, London 458-484 (1965)

17. D. R. O'Boyle and A. E. Dwight, *The Uranium-Plutonium-Zirconium Ternary Alloy System*, Nuc. Met., 17, Part II, 720-732, Plutonium 1970 and Other Actinides, William N. Miner, ed., Proc. 45th Int. Conf. on Plutonium and Other Actinides, Sante Fe, New Mexico, October 5-9, 1970 (1970).

18. A. C. Roberts and A. H. Cottrell, *Creep of Alpha-Uranium during Irradiation with Neutrons*, Phil. Mag. 1 (1978) 711-717.

19. J. Gittus, *Creep, Viscoelasticity, and Creep Fracture in Solids*, J. Wiley & Sons (1975), p. 204.

20. W. D. Kingery, H. K. Bowen, and D. R. Uhlmann, *Introduction to Ceramics*, 2nd ed., J. Wiley & Sons (1976), p. 745

21. R. L. Coble and W. D. Kingery, *Effect of Porosity on Physical Properties of Sintered Alumina*, J. Am. Ceram. Soc., 39 (1956) 377-386.

22. G. M. Fryer and P. Thompson, *Compressive Creep of Porous Polycrystalline Alumina*, Trans. Brit. Ceram. Soc. 71 (1972) 61-66.

23. S. K. Evans, P. F. Bohaboy, and R. A. Laskiewicz, *Compressive Creep of Urania-Plutonia Fuels*, General Electric Company, GCAP-13732 (1971), p. 9.

24. A. A. Solomon, J. L. Routbort, and J. C. Voglewede, *Fission Induced Creep of UO_2 and Its Significance to Fuel-Element Performance*, Argonne National Laboratory, ANL-7857 (1971), p. 11.

25. D. Brucklacher and W. Dienst, *Creep Behavior of Ceramic Nuclear Fuels under Neutron Irradiation*, J. Nucl. Matls. 42 (1972) 285-296.

26. M. C. Billone and W. T. Grayhack, *Fuel Creep Model for LIFE-METAL*, Argonne National Laboratory internal memo, March 19, 1987.

27. W. T. Grayhack, *Fuel Creep Model for LIFE-METAL: Comparison with U5Fs Mark-II Data*, Argonne National Laboratory internal memo, April 14, 1987.

References For Section E.1

1. *Nuclear Systems Materials Handboook*, Volume 1, Book 2 and Volume 2, Book 2; TD-2666.

2. M. L. Hamilton, *Status Report on the Stress Rupture Behavior of Various Heats of D9*, HEDL-TC-160-36, Jan.-March 1983, p. 263-281.

3. *Alloy Properties Databook*, HEDL-TC-293, Rev. 4.

References For Section E.2

1. *Nuclear Systems Materials Handboook*, Volume 1, Book 2 and Volume 2, Book 2; TD-2666.

2. *Alloy Properties Databook*, HEDL-TC-293, Rev. 4.

3. F. R. Shober, *Physical and Mechanical Properties of Alloy HT9 Used in the Design Analysis of the Core Demonstration Experiment*, HEDL-TC-2845, July, 1986.

4. R. J. Puigh, *In-Reactor Stress Rupture Data from MOTA after Peak Fluence of 9.6 x* 10^{22} *n/cm*^{2} *(Through Cycle 4 Irradiation)*, HEDL-TC-160-42, 1984.

5. M. L. Hamilton and N. S. Cannon, *HT-9 Transient Data Base and Failure Correlation*, HEDL-TC-2681, 1985.

6. L. Leibowitz and R. A. Blomquist, *Thermal Conductivity and Thermal Expansion of Stainless Steel D9 and HT9*, ANL-CMTI-9589.

Nuclear Science and Engineering Division
Argonne National Laboratory
9700 South Cass Avenue, Bldg. 208
Argonne, IL 60439-4842 www.anl.gov